UNIVERSITA' DEGLI STUDI DELL'INSUBRIA

DOTTORATO DI RICERCA IN BIOTECNOLOGIE, BIOSCIENZE E TECNOLOGIE CHIRURGICHE

Curriculum: Biologia Cellulare e Molecolare

XXIX CICLO

Ph.D. program in Biotechnology, Biosciences and Surgical Technologies

Curriculum: Cellular and Molecular Biology

# *Immune response induced by multi-wall carbon nanotubes: in vivo and in vitro studies on the medicinal leech*

## *Risposta immunitatia indotta da nanotubi di carbonio a parete multipla: studi in vivo e in vitro sulla sanguisuga medicinale*

Tutor: Dott.ssa **Annalisa Grimaldi**

Tesi di dottorato di:
**Rossana Girardello**
**Matr. 700463**

Dip. Biotecnologie e Scienze della Vita - Università degli Studi dell'Insubria

Anno accademico 2015-2016

# Table of Content

# List of Figures

## Abstract

Since the production and use of engineered nanomaterials (NMs) is steadily increasing, the development of new reliable methods to analyze NMs effects are critical.

Here we propose the medicinal leech as alternative animal model to study multi-walled carbon nanotubes (MWCNTs) effects by means of *in vivo* (environmental dispersion and MWCNT supplemented Matrigel injection) and *in vitro* studies on leeches macrophages.

Our results show that water dispersed MWCNTs evoke a massive migration of $CD45^+/CD68^+$ monocyte-macrophages cells and the production of molecules involved in innate immune response, such as the pro-inflammatory cytokine IL-18 and amyloid fibrils.

Ultrastructural analysis of MWCNTs-supplemented biomatrix revealed that in leech macrophages MWCNTs are internalized both actively (phagocytosis) and passively (membrane piercing).

Finally, MWCNT *in vitro* treatment cause the decrease of cell proliferation rate and the increase of both ROS production and apoptotic rate.

Moreover, in this study we identified and characterized in *Hirudo* two inflammatory markers striking similar to vertebrate's MIF and GMFG, showing that these molecules are involved in macrophage response to MWCNTs.

Our combined experimental approaches, not only attest the ability of MWCNTs in inducing a potent inflammatory response, but also confirm the medicinal leech as a good alternative model that can be successfully used to study, both *in vivo* and *in vitro*, the possible harmful effects of any nanomaterial.

# 1. Introduction

In the last decade, the rapid development of nanotechnology has brought to market a large variety of nanomaterials (NMs) with different properties and possible applications. As defined by European Commission in 2011, NMs are composed by particles with one or more external dimension comprised between 1 and 100 nm (2011/696/EU, 2011). The other characteristics depend on their composing material (Ag, Co, Fe, C, etc.) and on their shape (nanoparticle, nanofibre, nanotube, etc.). Given the extreme difference in composition and structure of the various NMs, it is impossible to draw up general guidelines on their use and disposal. For this reason, each NM, interacting with living organisms, may cause adverse effects that need to be assessed.

The widespread use of NMs is leading to an increased risk of their environmental dispersion. Due to their nanoscale dimensions, it is difficult to evidence their presence in the environment. NM environmental contamination may occur through accidental spills, sewage sludge application, deposition of airborne manufactured NM or soil remediation (Gottschalk et al., 2013; Handy et al., 2008; Nowack and Bucheli, 2007; Paterson et al., 2011).

NMs can be found mixed in the air, in the soil and more often being washed from the soil into the water (rivers and lakes) being harmful to the health of animals, including humans (Lam et al., 2006; Simate et al., 2012).

Among NMs, carbon-based materials have been extensively used in different fields, from industrial to biomedical, raising several issues about their safety. Currently, the scientific debate is still open and it is crucial to clarify NM health effects and their impact on the environment.

## 1.1 Carbon nanotubes

Since their discover in 1991 (Iijima, 1991), carbon nanotubes (CNTs) appeared a promising NM for different scopes, becoming a central subject for technological studies. Originating from the rolling up of a graphene sheet, CNTs are composed by covalently bound carbon atoms. According to the number of carbon layers, CNTs are divided in 2

categories: single-wall carbon nanotubes (SWCNTs), with diameters of 1-2nm, and multi-wall carbon nanotubes (MWCNTs), formed by multiple layer of graphene, measuring from 10 up to 100nm in diameter and from 50nm up to several hundred microns in length (Liu et al., 2009).
Given their structure, CNTs have high strength and flexibility. Other features that contribute to make them unique are the high thermal and good electrical conductivities.

### *1.1.1 Synthesis and functionalization of MWCNTs*

The main methods to synthesize MWCNTs included arc-discharge, laser ablation and chemical vapor deposition (CVD). The first two involve high-temperature carbon vaporization starting from a solid-state carbon precursor. Despite these sophisticated techniques producing materials of high quality, large amounts of by-products are generated. The advantage in CVD technique is the lower temperature process, which involve the use of hydrocarbon gases as carbon source and a metal catalyst for nanotube growth (Dai, 2002).
Raw MWCNTs present highly hydrophobic surfaces, resulting therefore insoluble in aqueous solutions. To overcome this problem, MWCNTs may undergo to a covalent or non covalent functionalization process. This process is fundamental to disperse MWCNTs and requires chemical treatments to obtain biocompatible and low toxic MWCNTs (Liu et al., 2009).

### *1.1.2 MWCNT applications*

MWCNTs for their physical and chemical properties, represent a class of NMs widely used for several different applications, from industrial to biomedical field. Their electrical properties made them a promising material in electronics, where they are used as nanoelectrodes or nanowires components. Due to their strength and thermal conductivity, MWCNTs have been used in association with polymers to produce light weight and high-performance composites for different applications such as sport gears, aircrafts and fire resistant coatings (Zhang et al., 2013). MWCNTs, because of their incredible resilience, have been also used as reinforcement in ceramic production. In biotechnological field they are widely employed as scaffold to immobilize molecules, for the production

of fine membranes and filters or to create nanoscale biosensors binding MWCNTs to different enzymes (Schnorr and Swager, 2011).
As far as concern biomedical field, MWCNTs are promising for various potential applications such as drug delivery systems, gene transfer or gene silencing, and *in vivo* imaging (Liu et al., 2009).

### *1.1.3 MWCNT toxicity*

In the past few years, another discipline related to nanotechnology raised: the nanotoxicology (Donaldson et al., 2004), considered as "the other side of the coin" of nanotechnology (Kagan et al., 2005). Their nanometric dimensions as well as the same unique properties that make NMs suitable for many different applications, may cause potentially adverse effects on living organisms. Several studies highlighted the potential toxic effects of NMs both in the context of occupational health risk (Albini et al., 2015; Lam et al., 2006) and in the light of their potential environmental impact (Du et al., 2013; Farré et al., 2011). As reported by different authors, NMs dissolved in water or dispersed in soil can be accumulated in the organism (Demir et al., 2011; Hayashi et al., 2012; Kawata et al., 2009; Park et al., 2011), inducing toxic effects in different animals, such as zooplankton (Alloy and Roberts, 2011; Edgington et al., 2010; Kennedy et al., 2009; Roberts et al., 2007), earthworms (Coutris et al., 2012; Shoults-Wilson et al., 2011a, 2011b) and gastropod molluscs (Ali et al., 2014). Several *in vivo* studies in rodents lead to the same evidence that MWCNTs are accumulated in organs inducing a severe inflammatory response. After MWCNT administration via inhalation, instillation and intravenous or intraperitoneal injection, the effects observed in different organs included interstitial fibrosis, infiltration of inflammatory cells and rapid generation of ROS (Poland et al., 2008; Poulsen et al., 2015; Rawat et al., 2016). The same effects were observed after *in vitro* treatments (Boyles et al., 2015; Wang et al., 2012). In murine macrophages and rat epithelial cells, MWCNT exposure causes an oxidative stress, leading to a reduction in cell viability and even inducing apoptosis (Ravichandran and Baluchamy, 2010; Wang et al., 2012). Other authors observed in human bronchial epithelial cells exposed to MWCNTs, reactive oxygen species (ROS) production in dose

and time-dependent manner (Hussain et al., 2014). Moreover, other authors reported granuloma and mesothelioma formation after MWCNT treatment, remarking the similarity of this NM with asbestos (Donaldson et al., 2010; Ma-Hock et al., 2009; Rittinghausen et al., 2014).

Humans may come into contact with nanomaterials not only by inhalation, injection, penetration but also by ingestion, thus the bioaccumulation of MWCNTs in aquatic animals may as well represent an indirect risk for people. Even if the literature abounds with studies on MWCNT toxicity, the existing toxicological data are still fragmentary and the interactions among nanomaterials and cells, proteins and tissues have not yet been fully understood (Du et al., 2013).

Since there is the impellent need to analyze and fully understand NM bioaccumulation and cytotoxicity, the development of standardized methods combining *in vivo* and *in vitro* studies is an overriding concern. Here we propose a freshwater invertebrate, the leech *Hirudo verbana* (often wrongly sold in Europe as *Hirudo medicinalis*), as a comprehensive model to assess MWCNT effects both on the whole organism, by means of *in vivo* assays, and at tissues and cellular level, utilising different *in vivo* and *in vitro* approaches.

## 1.2 Experimental model

The medicinal leech, is a protostome ectoparasite characterized by a coelomic space extremely reduced (de Eguileor et al., 2003; Mann, 1962).

The “parenchimatous” body is delimited by a musculo-cutaneous sac (**Scheme 1**) formed by epithelial cells (involved in the formation of the cutaneous sac, barrier against potentially harmful agents, in cuticle production, that preserve animal from drying and from sunlight, and in respiration, osmoregulation and excretion) and by muscles (Mann, 1962; Sawyer, 1986). Helicoidal muscle fibres, separated each other by extracellular matrix, are grouped in small bundles disposed to form circular, oblique and longitudinal layers. The body wall enwrap internal organs such as gut characterized by diverticula for the storage of blood (Mann, 1962), gonads, nervous system, reduced circulatory system.

Between the gut and the body wall, two characteristic tissues are present: the vaso-fibrous tissue, involved in tissue repair during wound healing (Grimaldi et al., 2011; Huguet and Molinas, 1996, 1994), and the botryoidal tissue with different functions, including hematopoiesis (Grimaldi, 2016; Grimaldi et al., 2006) and angiogenesis (de Eguileor et al., 2003; Grimaldi et al., 2013).

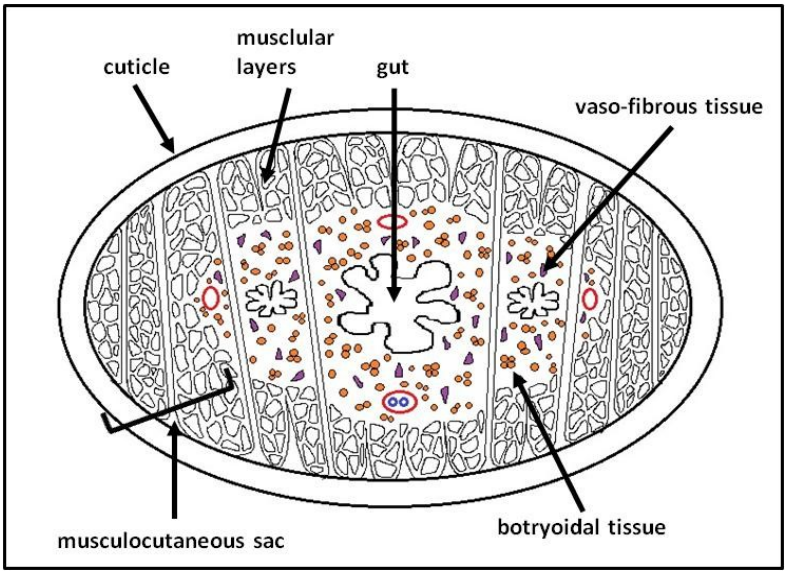


**Scheme 1.** Schematic representation of leech body wall in transversal section.

## 1.3 Innate Immune system

The immune system is arbitrarily divided into innate and adaptive immunity. Although the former was classically considered non-specific and primitive compared to the latter, this dogma has been recently challenged. Several authors, in fact, showed the complementarily and the overlap of these two systems during the immune response (van der Meer et al., 2015). Moreover, although the concept of immune memory has been for long associated to the adaptive immunity of vertebrate, in the recent literature diverse forms of innate immune memory have been observed in different invertebrate taxa (Milutinović and Kurtz, 2016), including Annelids (Cooper and Roch, 2003; Engelmann et al., 2005; Tettamanti et al., 2003a), but not yet fully clarified. For this reason the study of the mechanisms underlying the innate immune response is essential and the use of an invertebrate model, such as *Hirudo*, is an

excellent way to explore the molecular basis of innate immunity (Schikorski et al., 2008).

*1.3.1 Hirudo as model to study immune system and neuroimmunity*

The medicinal leech, as other invertebrates, is characterized by an innate immune system showing cellular and humoral responses. One of the advantages in using the leech as experimental model is due to its anatomical and physiological simplicity, making it suitable to study different events linked to bacterial infection, wound healing and tissue repair (de Eguileor et al., 2003; Grimaldi et al., 2011; Tettamanti et al., 2004). The entity of these responses, during the inflammatory phase, can be easily and unambiguously detected in leech's body wall. In unstimulated animals, a few immunocompetent cells (i.e. macrophages, granulocytes, NK cells), involved in phagocytosis and cytotoxicity, and low levels of humoral molecules, such as pro-inflammatory cytokines and growth factors, are constitutively present. However, after mechanical or bacteria challenge both the number of immunocompetent cells and the expression level of humoral factors increase (de Eguileor et al., 2000a, 2000b, 1999; Grimaldi et al., 2006; Tettamanti et al., 2006).

*Hirudo* reacts to a wide variety of stimuli with a massive angiogenesis and fibroplasia.

New vessels formation is due to a remodelling of botryoidal tissue that change from a solid cord of cells (in non stimulated animals), by means of a dehiscence process, to pre-vascular cavities (de Eguileor et al., 2001a; Grimaldi et al., 2013; Tettamanti et al., 2003a, 2003b).

The new vessels play an important role by conveying circulating precursors of immunocompetent cells to the stimulated area where extravasate and differentiate in mature leukocytes then mediating inflammatory responses (de Eguileor et al., 2001b; Grimaldi et al., 2013, 2006, Tettamanti et al., 2003a, 2003b).

In parallel with angiogenesis, fibroplasia occurs: fibroblasts increase numerically and synthesize a large amount of collagen that form a scaffold favouring immunocompetent cell migration through the affected site (Tettamanti et al., 2005, 2004).

The leech is an excellent model to study also neuroimmune processes. The leech central nervous system (CNS) responds to different stimuli (Le Marrec-Croq et al., 2013) and when the nerve cord of this annelid is crushed or partially cut, a rapid activation of microglial cells leads to their accumulation at the lesion site. The axons grow across the lesion and in the damaged region the conduction of signals is restored in a few weeks (Nicholls and Baylor, 1968).

The leech CNS is constituted by 6 head ganglia, 21 body ganglia, and 7 fused tail ganglia (**Scheme 2A**). Each segmental ganglion contains about 400 neurons, a neuropil giant glial cell, six packet-glial cells (macroglia) that unsheathe the cell bodies of neurons and a large population of resident microglial cells (**Scheme 2B**). Each ganglion is linked to its neighbours by thousands of axons that form longitudinal nerves known as connectives (Nicholls and Baylor, 1968).

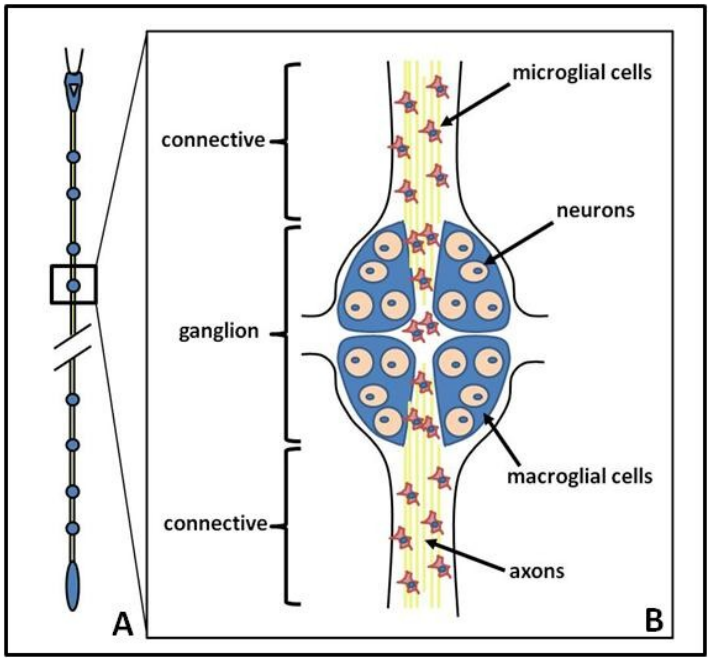


**Scheme 2.** Representation of the leech nervous system (**A**), with a detail of the ganglion (**B**). (modified from Le Marrec-Croq et al, 2013).

Numerous studies show the surprising similarity among leech and vertebrates with regard to both the cells involved in innate immune response such as macrophages, NK cells and granulocytes (de Eguileor et al., 2000a; Grimaldi et al., 2006; Schorn et al., 2015b), and the microglia,

involved in neuroimmune processes (Drago et al., 2014; Le Marrec-Croq et al., 2013; Macagno et al., 2010).

The response of the leech to a variety of treatments suggests that both surgical and biochemical stimuli may evoke in this model a signalling pathways analogous to those observed in vertebrates (de Eguileor et al., 2001b). These data are highly supported by recent studies showing that the majority of proteins known to participate in the vertebrate innate immune response are present in the medicinal leech transcriptome (Macagno et al., 2010).

All these evidences suggest that basic common features of fundamental biological events involved in innate immune response are conserved and extended across diverse species, supporting the general idea that an increasing number of early acquisitions during metazoan evolution are also common in higher vertebrates.

## 1.4 Molecules and mechanisms involved in leech innate immune and neuroimmune responses

### *1.4.1 Cluster of Differentiation Antigens (CDs)*

Leech immune cells not only display morphological features and behaviours similar to those found in vertebrates, but several authors provided also the evidences for the presence on leech immune cells surface of different cluster of differentiation antigens (CDs), commonly used as immune cells markers in Vertebrates (de Eguileor et al., 2000a, 2000b, Grimaldi et al., 2006, 2004; Macagno et al., 2010; Schorn et al., 2015a, 2015b). *Hirudo* macrophage-like cells express a panel of CDs typical of Vertebrate macrophages such as CD68 (de Eguileor et al., 2003), an intracytoplasmic molecule in human, and CD45 (Schorn et al., 2015a, 2015b), a cell surface glycoprotein implicated in integrin-mediated adhesion (Roach et al., 1997; St-Pierre et al., 2013; Zhu et al., 2011) and in regulation of cell responsiveness to chemoattractants (Mitchell et al., 1999; Roach et al., 1997). For these reasons several data concerning Hirudinea, Oligochaeta and Sipuncula (phylum closely related to annelids) support the use of antibodies raised against mammalian CDs

to detect invertebrates immune cells (Blanco et al., 1997; Cossarizza et al., 1996).

### *1.4.2 Allograft inflammatory factor-1 (AIF-1)*

*Hm*AIF-1, homolog to human AIF-1 is a molecule, recently identified and characterized in *H. medicinalis*.

*Hm*AIF-1, a 17 kDa cytoplasmic cytokine particularly expressed by leech microglial cells (Drago et al., 2014) and peripheral macrophages (Schorn et al., 2015b), is involved in the modulation of inflammatory response acting through autocrine and paracrine pathways. Moreover, recent studies proved *Hm*AIF-1 to be a potent angiogenic factor and a specific chemoattractant for macrophages during the early phases of immune response (Schorn et al., 2015b).

### *1.4.3 Phagocytosis and amyloidogenesis*

Phagocytosis is an essential event of immune system, highly conserved in all metazoan.

In the leech, if a small non-self crosses the external barriers, it is promptly recognized and phagocytozed by macrophage-like cells (de Eguileor et al., 2000a). On the other hand, when the foreign material is cumbersome, it is encapsulated by immunocompetent cells, that surround it and then produce and depose a thick layer of melanin close to the non-self. The synthesis of this pigment is always coupled, both in Vertebrate (Fowler et al., 2006) and in invertebrates (Falabella et al., 2012; Grimaldi et al., 2012b) with the physiological synthesis of amyloid fibrils, acting as a template for melanin deposition (Grimaldi et al., 2012a). Moreover, amyloidogenesis has also been proposed as a physiological detoxifying event in vertebrate and invertebrate cells to fight ROS increase (Falabella et al., 2012; Grimaldi et al., 2012b).

Amyloid fibrils are generally produced after the activation of a complex system of stress responses characterized by a cross-talk of molecules such as hormones, cytokines and neuromodulators. Among the intrinsic factors, closely related to amyloidogenesis, there is the over expression of Interleukin-18 (IL-18) (Grimaldi et al., 2012a, 2012b).

## 1.5 Inflammatory markers in the medicinal leech

Due to the striking similarities shared by vertebrates and invertebrates immune system, the research of new inflammatory factors is more than ever necessary to improve our knowledge on the basic principles of innate immunity. In this view, taking advantage of the establishment of databases such as Expressed Sequence Tag (EST) library from the leech CNS and the leech genome (Macagno et al., 2010), was possible to identify and select potential conserved chemotactic factors.

### *1.5.1 Macrophage migration inhibitory factor (MIF)*

Among the plethora of molecules involved in immune responses there is the Macrophage migration inhibitory factor (MIF). In mammals, MIF is constitutively expressed by macrophages and by tissues in direct contact with the environment. MIF is a 12.5 kDa protein composed of 115 amino acids. The secondary structure consists of 2 antiparallel α-helices and 6 β-pleated sheets and its active form is a homotrimer (Bach et al., 2009).
The Human gene MIF, composed of 3 exons separated by small introns, is highly conserved across species (>80% homology between mouse, rat, gerbil, chicken, calf and human) (Calandra, 2003).
Recently MIF has been defined as a mediator of inflammation and innate immunity. Unlike other cytokines, MIF is a pre-formed intracellular protein, stored in cytoplasmic pools and released by many cell types, including macrophages, and circulates in blood (Roger et al., 2003) in response to various stimuli such as microbial products, proliferative signals, and hypoxia (Grieb et al., 2010). The promoted action leads to differentiation of type I macrophages/microglia able in turn to mediate the production of TNF-a and iNOS.
It has been previously suggested that MIF may function to sustain inflammation by antagonizing the anti-inflammatory effects of glucocorticoids and preventing cellular apoptosis, but also through its chemotactic properties, retaining cells at sites of inflammation (Cox et al., 2013). MIF is constitutively present within both glial and neuronal cell types, and the CNS expression of MIF is regulated by inflammatory stimuli (Bacher et al., 1998). The injection of LPS in mice induces a

significant increase in the expression of mRNAs encoding MIF, IL-13, IL-6, and TNF-a.

### *1.5.2 Glia maturation factor (GMF)*

GMF is a highly conserved protein throughout the eukaryotes from yeast to mammals, with two isoforms being expressed in mammals: Glial maturation factor-β (GMFB) and Glia maturation factor-γ (GMFG). However, the two GMF isoforms exhibit distinct tissue distribution, suggesting a specific function in the respective tissues (Aerbajinai et al., 2011).

GMFB is a 17-kDa highly conserved 141-amino acid polypeptide isolated from the brain (Kaplan et al., 1991) with 99% homology between humans and rodents. This protein is expressed in glial cells (mainly astrocytes) and in some neurons while GMFB mRNA is predominantly expressed in the brain and spinal cord (Zaheer et al., 2007). GMFB is required in the production of pro-inflammatory cytokines and chemokines and is a prominent mediator of inflammation in the CNS and its expression is significantly upregulated under conditions of neurodegeneration (Zaheer et al., 2008, 2011).

A new gene, GMFG, highly homologous to human GMFB (82% identity), has been isolated (Asai et al., 1998). However despite the high sequence similarity, GMFG shows a different tissue distribution from GMFB, being present predominantly in proliferative and differentiative organs (Tsuiki et al., 2000). While GMFB acts as a growth and differentiation factor on neurons as well as glia in the vertebrate brain, GMFG show a very low expression in brain, neuronal cells and glial cells and it is involved in actin cytoskeleton reorganization in microvascular endothelial cells, inflammatory cells, and hematopoietic progenitor cells (Ikeda et al., 2006). In particular, it modulates actin-based cellular functions by interacting with Arp2/3 complex (Gandhi et al., 2010). Moreover, recent works show its role in TLR4 trafficking in endosomes in response to LPS (Aerbajinai et al., 2013).

## 2. Goals of the Research

Nowadays, is more than ever necessary to develop new and alternative assays to value possible toxic effects of NMs and to assess their presence in the environment. For this purpose, our work has been focused on the evaluation of the possible toxicity caused by MWCNT environmental dispersion, with regard to aquatic compartment. Since now, our studies has been centred on:

1) identification of new animal models to easily monitor and detect the diffusion of NMs in the water environment;

2) investigation about the mode of action of NMs on different levels of biological organisation from cells/tissue to individuals;

3) determination of the effects on organisms of NMs as stressors.

We selected as animal model the medicinal leech due to its anatomical and physiological features that allow the easy detection and monitoring of immunocompetent cell migration and of the angiogenic process.

Our combined experimental approaches, including morphological, immunocytochemical, histoenzymatic and Western blot analysis, aim to assess MWCNT effects both *in vivo* and *in vitro*, as a result of different treatments, such as MWCNT environmental dispersion, *in vivo* injection and *in vitro* treatment.

In the first part of our work, we evaluate the effects of multi-walled carbon nanotube (MWCNT) environmental dispersion on the leech, analysing both acute and chronic immune responses over a short (1, 3, 6 and 12 hours) and long time (from 1 to 5 weeks) exposure to MWCNTs.

Then, in order to better understand the interactions between MWCNTs and immunocompetent cells, we adopt an innovative procedure to inject MWCNTs in leeches and to study the subsequent immune response. This procedure involves the use of Matrigel (MG), a basement membrane extract, easily injectable without invasive surgical procedures. MG can be also used for an *in vivo* cell sorting approach permitting isolation and culture of specific cell populations by simply adding the appropriate chemoattractant (Girardello et al., 2015a; Grimaldi et al., 2011, 2009, 2008). As specific macrophage chemoattractant we use the cytokine Allograft inflammatory factor-1

(AIF-1) which is a well-established monocyte-macrophage marker and it is involved in the activation and migration of macrophages both in vertebrates (Tian et al., 2006; Utans et al., 1995; Yang et al., 2005) and in leeches (Drago et al., 2014; Girardello et al., 2015a; Schorn et al., 2015b). Isolated leech macrophages, has been cultured in order to obtain *in vitro* expansion of these cells. After morphological and immunocytochemical characterization, primary macrophage cultures were treated with different concentrations of MWCNTs in order to determine the direct effects of this nanomaterial.

Basing on rapid colorimetric tests, our experimental approaches could be used to evaluate NM presence in water and represent a quick sensitive tool for aquatic pollution bio-monitoring.

Moreover, another purpose of this study is to identify and characterize new inflammatory markers in *Hirudo* and to evaluate their expression after injury or infection in the CNS, in the body wall and in cultured macrophage cells.

Future research aims to extend our studies to other NMs in order to acquire new data and to develop new assays. The ultimate goal of our project is to obtain an alternative model and a set of techniques able to provide not only a rapid assessment of the presence of any NM in aquatic environment but also details about its interactions with the biotic compartment.

# 3. Materials and Methods

## 3.1 MWCNT characteristics and preparation

NANOCYL™ NC7000 carbon nanotubes were obtained from NANOCYL (Sambreville, Belgium). Their dimensions amounted at 9.5 nm external diameter by 1.5 µm mean length with a specific surface area ranging from 250 to 300 $m^2$/g. NC7000 were manufactured by a CCVD (catalytic carbon vapor deposition) process, presenting a purity of 90%. In these experiments, no chemical modification was applied to MWCNTs before use. Pristine MWCNT powder was weighed, dissolved in water or culture medium depending on the subsequent experimental plan, and then sonicated in an ultrasonic bath 15 min for two cycles to avoid aggregation of particles.

MWCNT concentrations were determined, according to the exposure type, basing on previous data in literature (Di Giorgio et al., 2011; Du et al., 2013; Zhang et al., 2014) reporting cytotoxic effects, oxidative responses and other biochemical parameter alterations after MWCNT exposure.

## 3.2 Animals treatment

Adult leeches (*H. verbana*, Annelida, Hirudinea, from Ricarimpex, Eysines, France) measuring 10 cm were kept in water at 19–20°C in aerated tanks. Animals were fed weekly with calf blood. According to the experimental protocol, leeches were anesthetized before dissection and/or injection procedures in a 10% ethanol solution.

### *3.2.1 Environmental exposure assay*

Leeches were exposed to MWCNTs (400mg/L) for 1, 3, 6 and 12 hours, to evaluate the acute response to treatment, and for 1, 2, 3, 4 and 5 weeks to value chronic response (5 animals for each time-point). Not treated (n.t.) animals were kept in freshwater without MWCNTs and used as control. At the planned time points, n.t. and MWCNT exposed leeches were sacrificed.

*3.2.2 Matrigel assay*

Animals were randomly divided into separate experimental groups according to different protocols and treatments. Each treatment was performed at the level of the 20th metamere.
Group 1: leeches injected with 300 µL of liquid MG (Corning Incorporated, Corning, NY, USA) (an extract of the murine Engelbreth–Holm–Swarm (EHS) tumor produced as described by Kibbey, 1994) served as controls.
Group 2: leeches injected with 300 µL of MG supplemented with 300ng of the recombinant protein rHmAif-1 (kindly donated by Jacopo Vizioli and Francesco Drago, University of Lille, France), were used to chemoattract macrophages.
Group 3: leeches injected with 300 µL of liquid MG supplemented with 20 µg of MWCNTs.
Group 4: leeches injected with 300 µL of liquid MG supplemented with 300ng rHmAif-1 and 20 µg of MWCNTs.
Animals were sacrificed after 1 week. MG implants were removed from the animal and processed in different ways depending on the type of experiment.

*3.2.3 MWCNT supplemented Matrigel*

Leeches were injected with 300 µL of MG supplemented with 300ng of r*Hm*Aif-1 and 2.5, 5, 10, 25, 50 and 100 µg/mL of MWCNTs. Leeches injected with 300 µL of MG supplemented only with r*Hm*Aif-1 were used as a not treated control (n.t.). MG implants were removed from the animal after 1 week and processed for cryofixation.

*3.2.4 primary macrophage cell culture*

After 1 week *in vivo* (corresponding to a suitable cell concentration for seeding) r*Hm*AIF-1 supplemented MG implants were harvested and cultured as previously described (Grimaldi et al., 2009, 2008). Each implant was minced in small pieces using sterilized razor blades and plated in wells of 60 mm in diameter in DMEM medium (Celbio, Milan, Italy) modified by dilution (1:4) to reach isoosmolality and supplemented with 1% glutamine, 10% fetal bovine serum and 1% gentamicin. Nor

growth factors nor cytokines were provided during the *in vitro* culture. Cells were maintained at 20°C and histologically and immunocytochemically examined 1 days and 1 week after seeding.

All cultures were performed in triplicate and scored at 1 week from seeding with an inverted microscope (Olympus, Tokyo, Japan). Data were recorded with a DS-5M-L1 digital camera system (Nikon, Tokyo, Japan).

*3.2.5 MWCNT in vitro treatment*

Cells were cultured on a round coverslip in 24 wells plate for 1 week before MWCNT treatment. MWCNT powder was weighed resuspended in culture medium and then sonicated 15 min for 2 cycles in an ultrasonic bath (starsonic 35, Liarre, Bologna, Italy) to avoid particles aggregation. MWCNTs were administrated at 2.5, 5, 10, 25, 50 and 100 µg/mL for 24 h. Particle exposure concentrations were chosen upon assessment of existing literature concerning exposure of vertebrate macrophages cell lines to MWCNTs and SWCNTs (Di Giorgio et al., 2011). Cells were then fixed with paraformaldehyde 3% for 10 minutes and washed in PBS before proceeding with immunocytochemical and colorimetric assays described above.

*3.2.6 Inflammatory markers in leeches*

Leech CNS were removed under sterile conditions and rinsed in Ringer solution. CNS used in the experiments were lesioned by forceps crushing at the connective level (**Scheme 3**) and then incubated at different times at 18°C in complete L-15 medium (85% Leibovitz's L-15 Medium, Gibco, Invitrogen, Carlsbad, CA) supplemented with 2mM L-glutamine, 10UI/mL penicillin, 10mg/mL streptomycin, 10mM Hepes, 0.6% glucose, and 10% fetal calf serum).

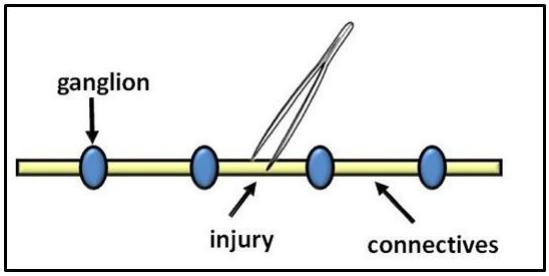


**Scheme 3.** Representation of the leech CNS indicating the connectives lesion site.

For peripheral tissues analyses, anaesthetized leeches were injected at the level of the 20th metamere with different sterile solutions: PBS, 100ng/mL LPS or 200ng/mL of the recombinant protein r*Hm*AIF-1, which has been previously demonstrated to be a specific chemoattractant for leech macrophage cells (Schorn et al., 2015b).
For macrophage isolation, anaesthetized leeches were injected with 300µl of liquid MG supplemented with 1 µg/mL r*Hm*AIF-1 and/or 100 ng/mL LPS. MG were extracted and cryofixed after 1 week *in vivo*.

## 3.3 Assessment of internalization of MWCNTs in leech tissues

Portions of tissue samples obtained after MWCNTs environmental exposure were excised and digested in 5 N potassium hydroxide (KOH) over night at room temperature. After repeated washes in distilled water ($dH_20$) to remove potassium salt, samples were resuspended in 100 µl of $dH_2O$ and dried on copper grids, (Formvar Carbon Film) for transmission electron (TEM) analysis (Jeol JEM 1010, Tokyo, Japan). Images were acquired with Morada, Olympus (Tokyo, Japan) digital camera. As control, KOH-treated and pristine MWCNTs were observed.

## 3.4 Scanning electron microscopy (SEM) and X-ray spectroscopy (EDS)

Leeches were then dissected and body wall tissues at the level of 20th metamere were fixed with paraformaldehyde 4% for 1h at room temperature. After standard ethanol dehydration, samples were embedded in paraffin (Bioptica, Milan, Italy) and then cut with a Leica Jung Multicut 2045 Microtome (Leica, Nussloch, Germany). Paraffin sections were deparaffinised with xylene and rehydrate. Slides were gold-sputtered and then observed with a SEM-FEG XL-30 microscope (Philips, Eindhoven, Netherlands). Samples were observed in backscattered electron mode with a scanning electron microscope coupled with an energy dispersive X-ray analyzer (EDAX Genesis 2000, EDAX, Mahwah, NJ, USA) to evaluate the presence of metal oxide associated to the crude MWCNT powder. Photographic maps of element distribution obtained on the image frames were processed by Image Analysis (Soft-Image Software; EDAX). These maps were then

superimposed to each source image with Adobe Photoshop (Adobe Systems).

## 3.5 Atomic Absorption Spectroscopy (AAS)

Chemicals used for the preparation of all standard and sample solutions were metal trace analysis grade: MilliQ water (Millipore, Darmstadt, Germany) and HCl (Baker 9530, 36.5–38%). The calibration standard solutions were prepared from a 1000 mg/L standard solutions (J.T. Baker Instra-Analyzed), and the blanks were prepared with 0.1M HCl. All measurements were performed on a Solaar M6 atomic absorption spectrometer (Thermo Fisher Scientific, Waltham, MA, USA): Al, Fe and Co were determined with a graphite furnace (GFAA) coupled with Zeeman background correction. Wavelength, bandpass and all others instrumental parameters were set according to manufacturers recommendations. The conventional instrumental detection limits (IDL, based on three standard deviations of the Blank signal) were calculated for each analytical run, typically ranging 1–3 ng/L. The reported results are the mean of three measurements.

## 3.6 Optical and Trasmission Electron Microscopy (TEM)

Leech body wall and MG samples were fixed for 1h in 2% glutaraldehyde/0.1 M cacodylate buffer at pH 7.4 and then washed in the same buffer and post-fixed for 1 h with 1% osmium tetroxide in cacodylate buffer, pH 7.4. After standard dehydration and embedding in Epon-Araldite 812, specimens were allowed to polymerize over night at 70°C and then sectioned with a Reichert Ultracut S ultratome (Leica, Wien, Austria). Semi-thin sections (0.75µm in thickness) were stained by crystal violet and basic fuchsin (Moore et al., 1960) and subsequently observed under a Nikon Eclipse Ni (Nikon, Tokyo, Japan) light microscope while data were recorded with a digital camera (DS-5M-L1, Nikon, Tokyo, Japan). Ultrathin sections (80nm in thickness), were stained by uranyl acetate and lead citrate, and observed with a transmission electron microscope (Jeol 1010 EX, Jeol, Tokyo, Japan). Data were recorded with a digital camera system (MORADA, Olympus, Tokyo, Japan).

## 3.7 Indirect immunofluorescence

Leech tissues and MG samples, embedded in polyfreeze tissue freezing medium (OCT, Tebu-Bio, Le Perray-en-Yvelines, France), were immediately frozen in liquid nitrogen. Slides were prepared with 7µm cryosections, obtained with cryotome a Leica CM 1850 and they were immediately used or stored at -20 °C. Cells, cultured on round coverslips, were fixed with 2% paraformaldehyde for 15 min at room temperature.
For indirect immunofluorescence experiments, samples were treated for 5 min at room temperature with phosphate buffer saline (PBS) and then incubated with a blocking solution with 2% Bovine Serum Albumin (BSA) and 0.1% Tween20 in PBS for 30 min.
Slides were then incubated for 1h at room temperature with different polyclonal primary antibodies:

- rabbit anti-human CD45 (Twin Helix, Milano, Italy), 1:200;
- rabbit anti-human CD68 (Santa Cruz Biotech., Dallas, TX, USA) (1:200);
- rabbit anti-human IL-18 (Abnova, Taipei, Taiwan) (1:200);
- rabbit anti-*Hm*AIF-1 (kindly donated by Jacopo Vizioli and Francesco Drago) (1:200);
- goat anti-MIF (R&D systems, Minneapolis, MN, USA) (1:1000);
- rabbit anti- human GMFG (Abcam, Cambridge, UK) (1:1000).

After PBS washing, slides were incubated for 1h at room temperature with the appropriate secondary antibody: donkey anti-rabbit (Jackson ImmunoResearch Laboratories, Inc., West Grove, PA, USA) or anti-goat (Biotium, Fremont, CA, USA), Cy3-conjugated, diluted 1:200 in BSA and then washed with PBS. Nuclei were counterstained with the nuclear marker DAPI (4',6-diamidino-2-phenylindole) (Sigma Aldrich, Saint Louis, MO, USA) diluted 1:5000, for 15 min at room temperature and slides were mounted with Citifluor (Citifluor, London, UK). In negative control experiments, primary antibodies were omitted and sections were incubated only with the secondary antibodies.

## 3.8 Whole mount immunolocalization on CNS

Dissected leech nerve cords were mechanically stressed and, after antibiotic treatment, incubated with a complete L15 medium for 0h, 24h, and 3 days. After incubation, nerve cords were fixed for 1h at RT in 4% paraformaldehyde. Membranes were permeabilized by incubating the samples in PBS-1% Triton X-100 O/N at 4°C. Non-specific background staining was blocked with a saturation buffer (PBS solution containing 1% Triton, 3% normal donkey serum, 1% BSA and 1% ovalbumin) for 4 h at 4°C. Samples were then incubated with different anti-human antibody: goat polyclonal anti-MIF (R&D systems, Minneapolis, MN, USA) and rabbit polyclonal anti-GMFG (Abcam, Cambridge, UK), diluted 1:1000 in the saturation buffer overnight at 4°C. Primary antibodies were removed and, after a rinsing step with PBS-1% Triton X-100, the samples were incubated with the appropriate secondary antibody conjugated to Alexa 488 (Invitrogen Corporation, Carlsbad, CA, USA) diluted 1:2000 in the saturation buffer. Slides were mounted in Vectashield (Vector, Burlingame, CA, USA).

## 3.9 Enzimatic hystochemistry and colorimetric staining.

For acid phosphatase (ACP) detection, after rehydration with PBS for 5 min, cryosections were incubated with 0.1M sodium acetate-acetic acid buffer for 5 min and then treated for 1 hour and 30 min at 37 °C with the reaction mixture (0.1 M sodium acetate-acetic acid buffer, 0.01% naphtol AS-BI phosphate, 2% NN-dimethylformamide, 0.06% Fast Red Violet LB and 0.5nM $MnCl_2$). After PBS washings, slides were mounted with PBS/glycerol 2:1.

MG cryosections were also treated with May Grunwald Giemsa differential staining (Bio Optica, Milan, Italy), which permits identification of hematopoietic cells based upon their cytoplasmic pH properties.

For thioflavine-T method for amyloid fibrils staining, cryosections were brought to distilled water and then stained for 2 minutes with Mayer's emallume. After washing in $dH_2O$, slides were incubated with 1%

Thioflavine and mounted with a non fluorescent medium (Eukitt, Bio Optica, Milan, Italy).
For double staining Thioflavin-T/CD68, the Thioflavin-T method was followed by anti-CD68 immunedetection with the same protocol described above.

## 3.10 Terminal deoxynucleotidyl transferase dUTP nick-end labeling (TUNEL) assay

The DeadEnd™ Fluorometric TUNEL System (Promega, Pittsburgh, PA, USA) was used to evaluate the presence of apoptotic cells in the different samples. For leech tissues, sections were deparaffinized and rehydrated, and tissues were then permeabilized with a 20µg/mL Proteinase K solution in PBS for 10 minutes at room temperature.
MG cryosections and *in vitro*-treated macrophages were fixed in paraformaldehyde 4% for 25 minutes at 4°C and then washed in PBS and permeabilized in 0.2% Triton X-100 in PBS for 5 minutes. According to the manufacturer's protocol, After an equilibration step, the incubation buffer, containing nucleotide mix and rTdT enzyme, was added. Slides were incubated at 37°C for 1 hour in the dark and then immersed in a 1x sodium chloride and sodium citrate buffer (SSC). Nuclei were counterstained with 1 µg/mL Propidium Iodide (Sigma Aldrich, Saint Louis, MO, USA) for 15 minutes at room temperature in the dark. Slides were mounted with a non fluorescent mounting medium Citifluor (Citifluor, London, UK). A negative control was performed by omitting the rTdT enzyme in the incubation buffer. A Positive control was performed by treating cells with DNaseI according to the manufacturer's protocol.

## 3.11 Cell proliferation assay

To assess the ability of cells to proliferate in MG and *in vitro* the 5-Bromo-2'-deoxy-uridine Labeling and Detection Kit I (Roche, Basel, Switzerland) was used.
Immediately after dissection, MG pellets were incubated with 5-Bromo-2'-deoxy-uridine (BrdU) 10 µM in cell culture medium for 1 hour at 20°C. After PBS washes, MG implants were embedded in a tissue freezing

medium (OCT, Tebu-Bio, Italy) and immediately frozen in liquid nitrogen and sectioned with a cryotome (CM 1850, Leica, Wetzlar, Germany). *In vitro* treated macrophages were incubated in the same conditions immediately after MWCNT treatment and then fixed with paraformaldehyde 4% for 15 minutes at room temperature.

Before the detection step, cryosections and cells were treated with acidic ethanol (50 mM glycine, absolute ethanol, pH 2.0), which allow the antibody to access to BrdU, as indicated in the data sheet.

For the immunofluorescence procedure, specimens were incubated with Anti-BrdU working solution (Roche, Basel, Switzerland) for 30 minutes at 37°C and then washed with the provided washing buffer. After that, an anti-mouse DyLight 549 conjugated antibody (KPL, Gaithersburg, MD, USA) was used for MG slides while an anti-mouse-Ig-fluorescein antibody (Roche, Basel, Switzerland) was used for macrophages. Specimens were incubated with the secondary antibody for 30 minutes at 37°C in the dark. After further washes, nuclei were counterstained with DAPI for 5 minutes at room temperature in the dark. Slides were mounted with Citifluor (Citifluor, London, UK).

## 3.12 Intracellular ROS evaluation

ROS production was evaluated after *in vitro* treatment by the use of 2',7'-dichlorodihydrofluorescein diacetate ($H_2$DCFDA) (Molecular Probes, Eugene, OR, USA), a fluorigenic probe commonly used to detect intracellular ROS. $H_2$DCFDA is a non-fluorescent compound, able to cross cell membranes. Once within the cell it is hydrolyzed to 2',7'-dichlorofluorescein (DCF), a compound which becomes fluorescent when it is oxidized by ROS. ROS level can be detected by monitoring the increase in fluorescence. Treated and not treated macrophages were washed with Hank's balanced salt (HBSS) solution (Sigma Aldrich, Saint Louis, MO, USA) and then incubated with 10 µM $H_2$DCFDA for 30 min at 20°C in the dark. Cells were then washed 3 times in HBSS and fixed with paraformaldehyde 4% for 15 minutes. Nuclei were stained with DAPI.

## 3.13 Images acquisition and recording

Slides were observed under a light/fluorescence microscope Nikon Eclipse Ni (Nikon, Tokyo, Japan) equipped with 3 different excitation/emission filters:

- 360/420nm, for DAPI nuclear staining;
- 488/525nm, for $H_2$DCFDA, fluorescein and Thioflavin-S staining;
- 550/580nm, for propidium iodide, Cy3 and DyLight 549 signals.

Data were recorded with Nikon Digital Sight DS-SM (Nikon, Tokyo, Japan) digital camera and images were combined with Adobe Photoshop (Adobe Systems, San Jose, CA, USA).
Whole mount immunolocalizations were examined with Zeiss LSM 510 confocal microscopy (Zeiss, Oberkochen, Germany).

## 3.14 Protein extracts preparation, SDS-PAGE and Western Blot

Immediately after dissection, portions of *Hirudo* tissues were frozen in liquid nitrogen. Tissues were then homogenized and suspended in extraction buffer (2X Laemmli's Buffer) with the addition of a protease inhibitor cocktail (Sigma, Milan, Italy). After centrifugation at 13000 rpm for 10 min at 4 °C, supernatants were collected and then proteins extracts were denatured at 100°C for 10 min. Equal amounts of protein extracts were separated in analytical SDS-PAGE using 10% acrylamide minigels. Broad range standards from Bio-Rad (Bio-Rad, Richmond, MA, USA) were used to determine molecular weights. Once separated by SDS-PAGE, proteins were then transferred onto Bio-Rad nitrocellulose filters. Membranes were saturated with 5% non fat dried milk in Tris buffered saline (TBS: 20 mM Tris-HCl buffer, 500 mM NaCl, pH 7.5) for 2 hours at room temperature, and then incubated for 90 min with rabbit polyclonal anti-CD45 antibody (1:500 dilution in 5% TBS-milk). After three washes, antigens were revealed with the secondary anti-rabbit IgG antibody HRP-conjugated (Jackson ImmunoResearch, West Grove, PA, USA), diluted 1:5000. After further washing, the membranes were incubated with luminol LiteAblot® PLUS Enhanced Chemiluminescent Substrate (EuroClone S.p.A., Pero, Italy) to reveal the immunocomplexes. In control experiments, anti-CD45 antibody was omitted. Bands were

normalized by using the ImageJ software package with the housekeeping protein GAPDH, which was detected with a rabbit polyclonal anti-human GAPDH IgG (Proteintech™, Chicago, IL, USA) diluted 1:2000. The expression level of CD45 in exposed leeches was reported relatively to control untreated animals. Experiments were performed in triplicate and data represent the mean values ± SEM. Statistical significance was assessed by an unpaired Student's t test (Statistica 7.0, StatSoft Inc., Tulsa, OK, USA).

## 3.15 RNA extraction from CNS

Dissected leech nerve cords were incubated in complete L15 medium for 0 h, 6h and 24 h and in complete L15 medium added with LPS (1:1000) for 6 h.

The nerve cords were put in 2mL standard tubes prefilled with 1.4mm ceramic (zirconium oxide) beads (Soft tissue homogenizing CK14, precellys lysing kit, Bertin, Montigny le Bretonneux, France) with 500µl Qiazol reagent (Qiagen, Hilden, Germany). The nerve cords were then homogenized by shaking twice for 45 sec at 6500 rpm in a Precellys®24 homogenizer (Bertin, Montigny le Bretonneux, France).

## 3.16 cDNA Cloning

Genes homologous to Vertebrate MIF and GMFG, so named *H*MIF and *H*GMFG for *Hirudo*, was identified in the EST database of *Hirudo* CNS (Hirudinea Genomics Consortium). The cDNA encoding *H*MIF and *H*GMFG were amplified by PCR from total leech CNS cDNA as template. Amplifications were performed using specific forward (*H*MIF: CATATGATGCCGTCTTACGTGCTGAA; *H*GMFG: ATGGGAGAAAACGTACGTG) and reverse (*H*MIF: GGATCCTCAGAAGGTTGAAGTACCATA; *H*GMFG: TCAACGGAAGAACTGCAGC) primers. PCR amplifications were carried out on a ThermalCycler (Mastercycler Gradient, Eppendorf, Hambourg,Germany) with 150ng of cDNA in a solution containing 2 U of PlatinumVRTaq DNA Polymerase (Invitrogen, Carlsbad, CA, USA), 10mM of each PCR primer, 10 mM dNTPs, 1.5 mM $MgCl_2$, and 13 of PCR buffer in a final volume of 50 µL. The reaction cycles were performed as

follows: 94°C for 1 min, followed by 35 cycles of 30 s at 94°C, 30 s at58°C, and 40 s at 72°C. A single PCR product was obtained and cloned into the pGEM T-easy vector (Promega, Madison, WI, USA) following the manufacturer's protocol.

## 3.17 Statistical analysis

Cells extracted from matrigel pellet were plated out in 60 mm diameter at a density of 1000 cells/well and counted after one week from seeding, using the Image J software package. Five fields for each time lapse (1 day and 1 week) were analyzed and the number of counted cells is referred to the total area of the well. Statistical significance was assessed by an unpaired Student's t test.

The percentages of positive and negative cells after BrdU and TUNEL assays, and the fluorescence intensity of Thioflavin-S and ROS assays were assessed by analysing 3 different slides for each time point/assay using the Image J software package. Statistical differences were calculated by Factorial ANOVA followed by Tukey's post-hoc test and $p<0.05$ was considered statistically significant.

Statistical analysis were performed using Statistica 7.0 software (StatSoft Inc., Tulsa, OK, USA).

# 4. Results

## 4.1 Environmental exposure assay

### *4.1.1 Determination of MWCNT presence in tissues*

MWCNT internalization has been validated by KOH digestion of tissues excised from exposed leeches. The particulates resulting after digestion were observed. TEM analysis confirmed MWCNT presence in exposed-animals tissues (**Fig. 1 A**). Moreover, their characteristics resulted identical to MWCNT crude powder, used as control (**Fig. 1 B**). To demonstrate that experimental procedures did not affect MWCNT morphology, pristine MWCNTs were subjected to sonication (**Fig. 1 C**) and KOH treatment (**Fig. 1 D**).

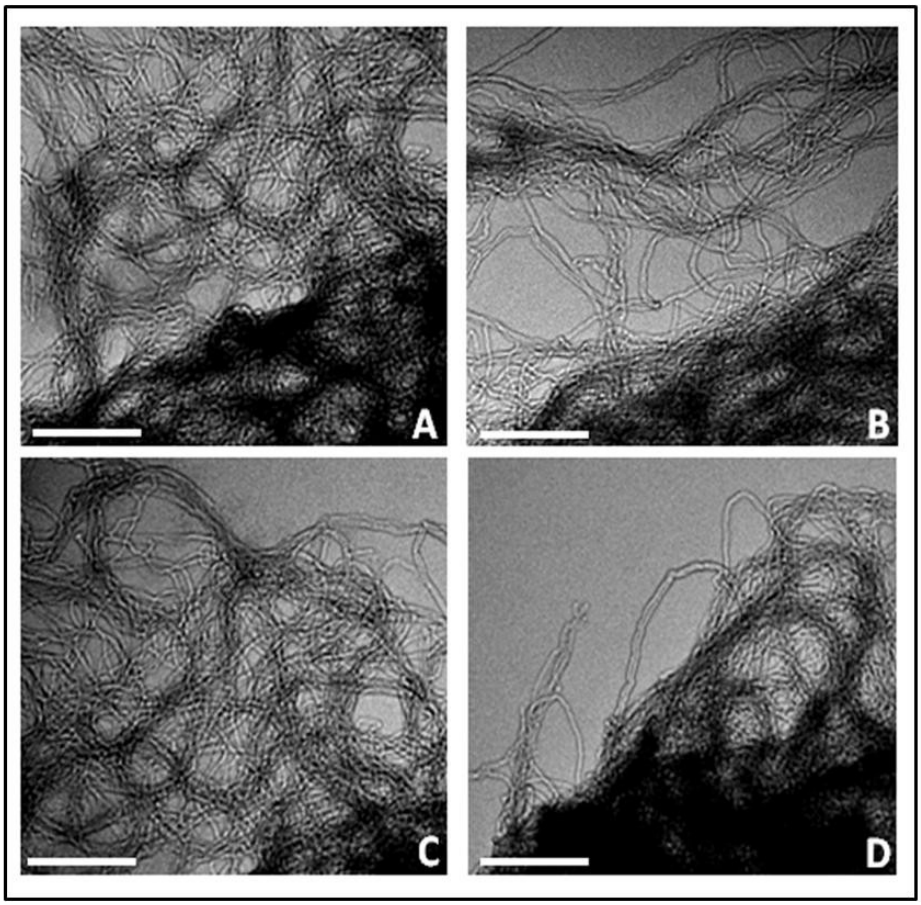


**Fig. 1.** Determination of MWCNT presence in tissues (**A-D**). (**A**) MWCNTs extracted by means of KOH digestion from exposed-animals tissues. (**B-D**) MWCNT crude powder (used as control) raw (**B**), after sonication (**C**) and after KOH treatment (**D**). Bars in A-D: 500 nm. (Girardello et al., 2015b).

### *4.1.2 EDS and AAS analyses*

In order to confirm the possible release of metal oxides impurities associated to MWCNTs in leech exposure water, EDS analysis were performed. Although microanalytical analysis have shown MWCNT aggregates to contain aluminum residues (**Fig. 2 A-C**), no evidence for this element in MWCNT exposed leech was detected (**Fig. 2 D-F**). As far as concern iron and cobalt, no picks were detected. AAS analyses were conducted on leech exposure water and the concentration of aluminum oxide was of 0.25 µg/L. Iron and cobalt concentrations were below the instrument detection limits.

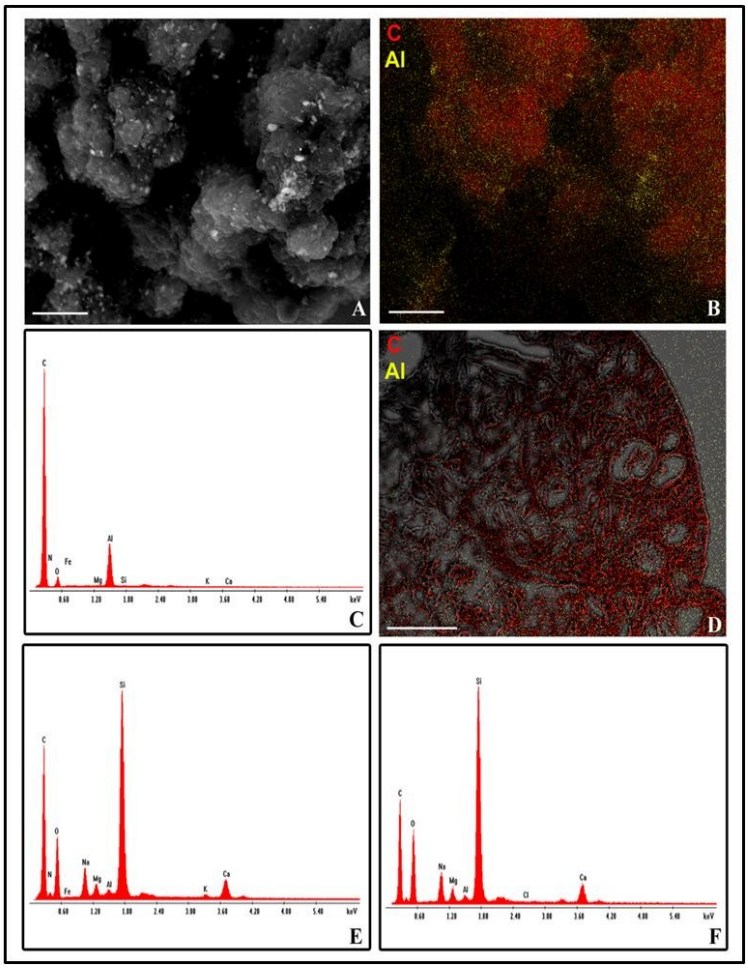


**Fig. 2.** SEM-EDAX (**A-F**). SEM (**A**) and Elemental mapping images (**B**) of MWCNTs crude powder (red: Carbonio; yellow: Aluminum). EDAX spectra for MWCNT crude powder (**C**) and aqueous suspension (**D**). Combined SEM-EDAX elemental mapping image of a section of leech body wall 5 weeks after treatment (**E**). EDAX spectra for treated (**F**) and untreated (**G**) tissue samples. Bars in A, B: 10 µm; bar in D: 100 µm. (Girardello et al., 2015b).

*4.1.3 Morphological analysis*

The leech body wall was made of an epithelium enwrapping thick layers of muscle fibers (**Fig. 3 A**). In the parenchyma between the muscular sac, virtually avascular, and the gut, was localized the botryoidal tissue (**Fig. 3 B**). After MWCNT treatment, from 1h up to 12 h, a network of blood vessels appeared in the thickness of musculocutaneous sac (**Fig. 3 C**). The formation of new vessels, typical of the inflammatory phase of innate immune response, was due to botryoidal tissue remodeling.

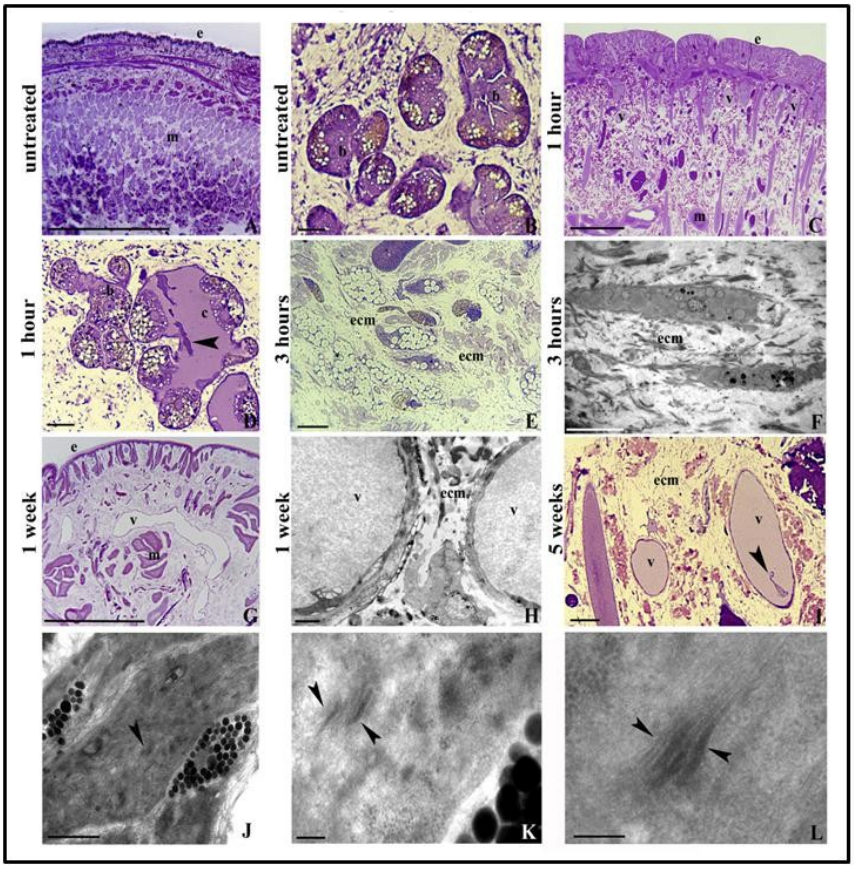


**Fig. 3.** Morphological at optical (**A-E, C, I**) and transmission electron microscopes (**F, H, J-L**) analyses of sections from *H. medicinalis* body wall. (b: botryoidal tissue; v: neo-vessels; m: muscles; e: epithelium; c: cavities; arrowhead in D: immunocompetent circulating precursors cell; ecm: extracellular matrix; arrowheads in J-L: MWCNTs). Bars in A, C, G: 100 µm; Bars in B, D-E, I: 10 µm; Bar in F: 5 µm; Bar in H: 2 µm; Bar in J: 500 nm; Bars in K-L: 200 nm. (Girardello et al., 2015b).

During this process, the lumen of the new vessels and circulating precursors of immunocompetent cells became visible (**Fig. 3 D**). At the same time, leech fibroblasts, easily recognizable thanks to their spindle

shape and the numerous lipid droplets in their cytoplasm, were involved in a strong remodeling process of the extracellular matrix (**Fig. 3 E, F**).

After a prolonged period of MWCNT exposure (from 1 up to 5 weeks), numerous infiltrating cells were visible in the musculocutaneous sac among the newly formed vessels (**Fig. 3 G-I**).

In the cytoplasm of these migrating cells, showing typical macrophage features, an engulfment of particles was evident (**Fig. 3 J-L**).

### *4.1.4 Characterization of circulating cells*

Immunofluorescence experiments with anti-CD45 antibody confirmed that circulating cells observed within the neo formed vessel lumen (**Fig. 4 A**) and in the peripheral vessels (**Fig. 4 B**) belonging to the leukocyte cell line (Grimaldi et al., 2006).

Western blot analysis confirmed CD45 expression in control and in MWCNT treated animals extracts showing the presence of two immunoreactive products of about 145 kDa and 180 kDa (**Fig 4. C**). These molecular weights of leech products were consistent with existing literature, reporting for vertebrates the presence of different CD45 isoforms with a molecular weight ranging from 140 kDa to 240 kDa (Trowbridge and Thomas, 1994).

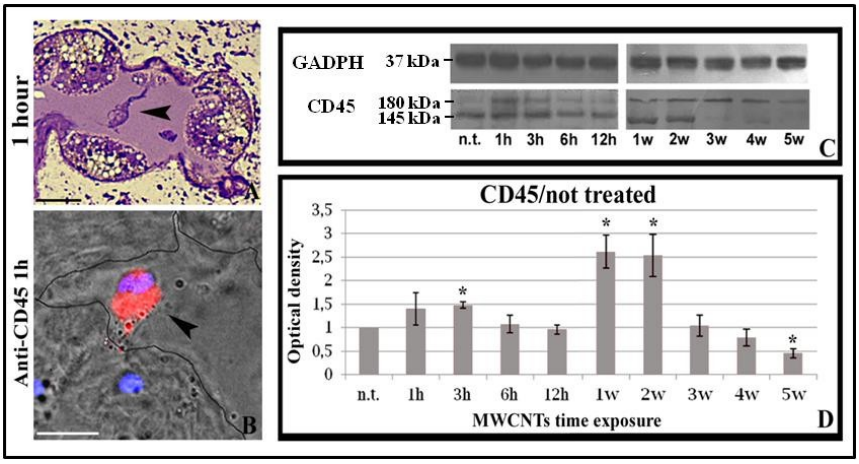


**Fig. 4.** Morphological (**A**) and immunohistochemical (**B**) characterization of circulating precursors cells (arrowhead). Western blot analysis (**C-D**) of untreated (n.t) and MWCNT treated leeches from 1 to 12 hours and from 1 to 5 weeks. A protein extracts from the body wall were probed with the anti-CD45 antibody. The housekeeping protein D-glyceraldehyde-3-phosphate dehydrogenase (GAPDH) was used as a loading control. In all samples, the anti-CD45 detected two specific immunoreactive bands of about 145 kDa and 180 kDa (**C**), according to the molecular weight ladder (kDa). CD45 protein was quantified by densitometry from three experiments. *P<0.05 compared with untreated leeches (**D**). Bars in A-B: 10 µm. (Girardello et al., 2015b).

Our data showed a variation in the expression profile of the two isoforms depending on the time of MWCNT administration (**Fig. 4 D**). In particular, in respect to the untreated leeches, the 180 kDa isoform increased significantly after 1h MWCNT exposure, while the 145 kDa isoform drastically decrease starting from 3 weeks MWCNTs treatment.

Summarizing, the total CD45 expression presented a cyclical pattern with 2 peaks of expression, 3 hours and 1 week after treatment. The loading samples were homogeneously distributed, as shown by GADPH, used as internal reference. In the negative control experiments, performed omitting the primary antibody, no signals were detected (data not shown).

### *4.1.5 Characterization of migrating cells*

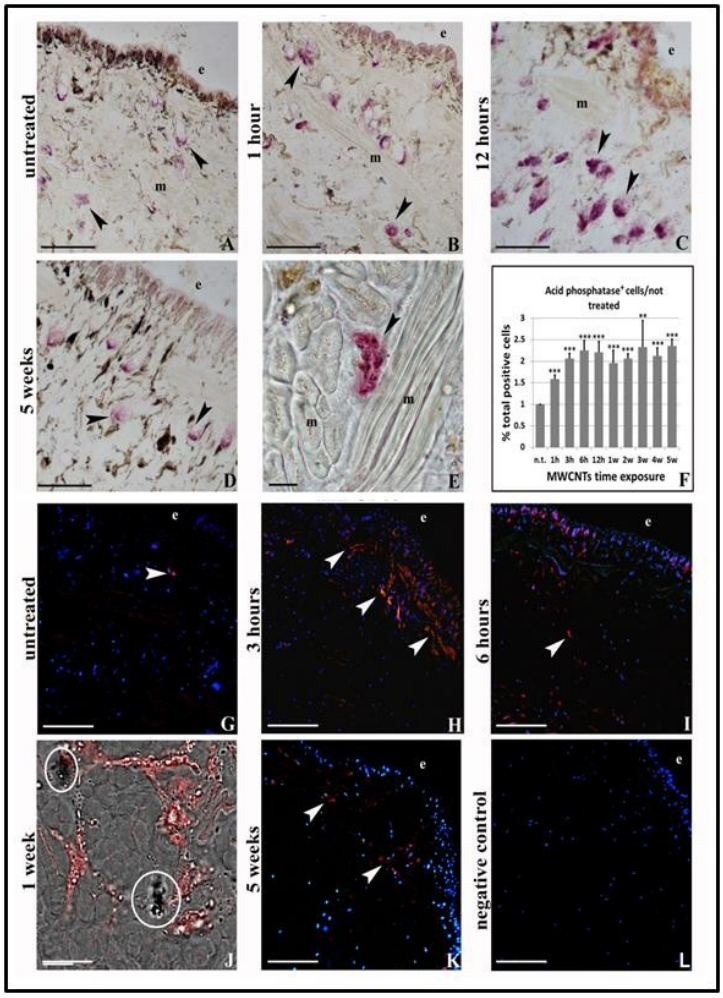


**Fig. 5.**
Acid phosphatase reaction (**A-F**) and anti CD68 immunofluorescence staining (**G-L**).
(e: epithelium; m: muscle; arrowheads: positive cells).
(**F**) Quantitative evaluation of cell numbers.
Column 1: number of cells in untreated sample, columns 2-10: number of cells in MWCNT treated sample from 1h up to 5 weeks. *p<0.01.
(**J**) Combined transmission and fluorescence images showing CD68+ cells (in red) in spatial association with MWCNTs aggregates (circled).
Bars in A-E, G-I, K-L: 100 µm; Bar in F, J: 10 µm. (Girardello et al., 2015b).

Cells infiltrating the extracellular matrix has been characterized by means of histo- and immuno-cytochemical approaches. Compared to not treated (n.t.) leeches, in MWCNT exposed animals a large number of infiltrating cells resulted positive for acid phosphatase reaction (**Fig. 5 A-E**), suggesting that these cells had a broad phagocytic activity. After 1 hour from MWCNTs exposure the number of migrating cells increased, the highest value was reached after 3 hours and persisted even after 5 weeks from treatment, as demonstrated by cell counting performed on 3 representative images for each time lapse, and was statistically significant (**Fig. 5 F**). Migrating cells resulted also positive for the typical macrophage marker CD68 (**Fig. 5 G-L**) and the evolutionarily conserved pro-inflammatory cytokine IL-18 (Alboni et al., 2010) (**Fig. 6 A-F**).

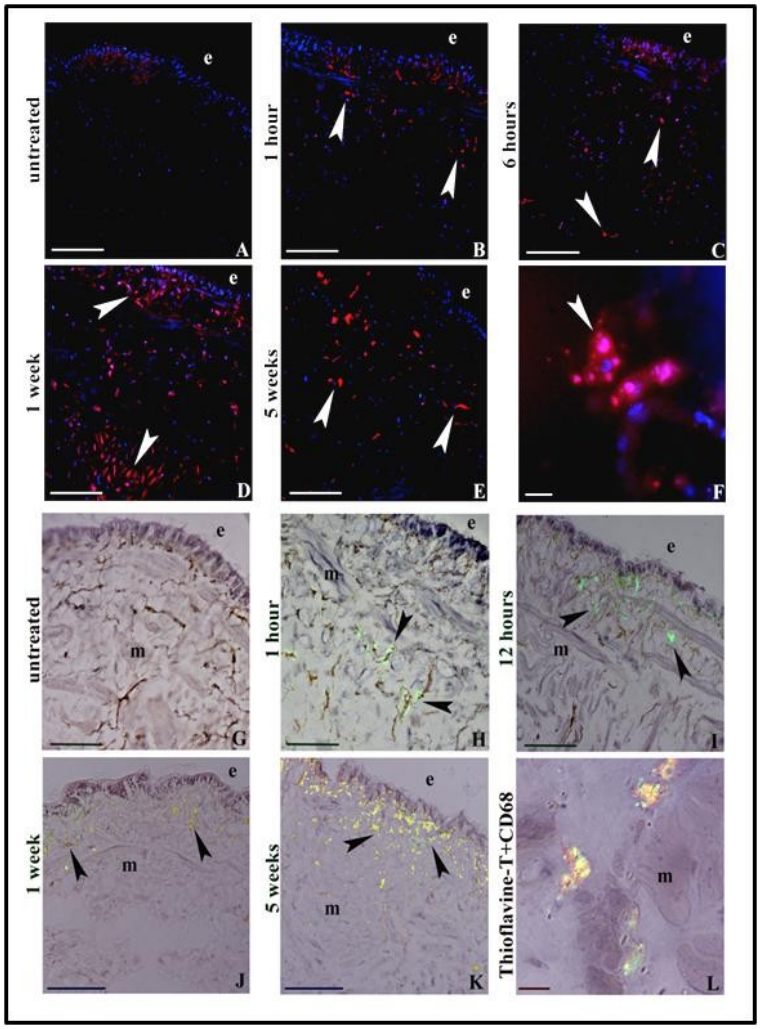


**Fig. 6.**
Anti-IL18 (**A-F**) and Thioflavine-T staining (**G-L**) on cryosections of untreated (**A, G**) and MWCNT-treated leeches (**B-F, H-L**) at different time points.
Double staining of Thioflavin-T (yellow) and macrophage markers CD68 (red) (**L**).
(e: epithelium;
m: muscle;
white arrowheads: immune-responsive cells;
black arrowheads: amyloid material).
Bars in A-E, G-K: 100 µm; bars in F, L: 10 µm. (Girardello et al., 2015b).

We also observed a positivity for Thioflavin-T, confirming the production of amyloid fibrils after MWCNT treatment (**Fig. 6 G-L**). This production was part of the typical response to stress conditions already described both in vertebrates and in invertebrates (Alboni et al., 2011; Grimaldi et al., 2014, 2012a). Moreover, macrophages were confirmed as the main producers of amyloid fibrils by coupling CD68 immunostaining with Thioflavin-T method (**Fig. 6 L**).

*4.1.6 Apoptosis detection assay*

TUNEL test was performed on n.t. and MWCNT exposed leech tissues (6h and 1week). Both in negative control and in n.t. leech tissues, no apoptotic nuclei were detected (**Fig. 7 A, B**). Few TUNEL$^{+}$ nuclei were visible in MWCNT exposed leeches (**Fig. 7 C, D**), indicating the presence of apoptotic cells among muscle fibres (**Fig. 7 E**).

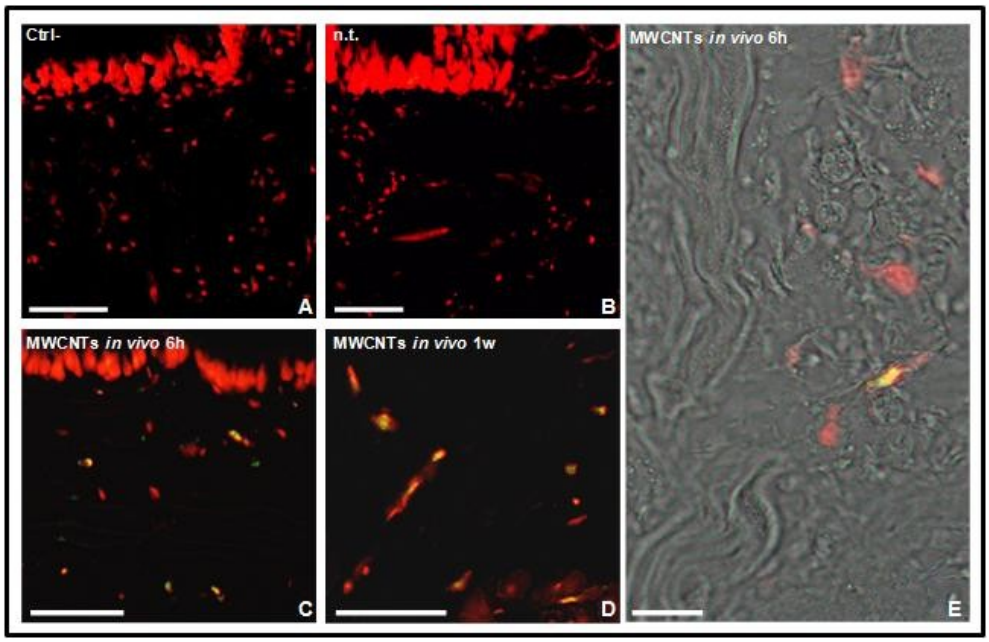


**Fig. 7.** TUNEL assay for apoptosis in leech body wall sections. Negative control (**A**). N.t. (**B**) and MWCNT treated leeches (**C, D**). Combined optical and fluorescence images of leech body wall showing a TUNEL+ cell migrating among muscle fibers (**E**). Nuclei, counterstained propidium iodide, result in red while TUNEL positivity in green. The merge results in yellow. Bars in A-D: 50 µm; Bar in E: 20 µm.

## 4.2 Matrigel injection assay

### *4.2.1 Light and Electron Microscopy*

In control MG samples no migrating cells were visible (**Fig. 8 A**), while MG specimens supplemented with r*Hm*AIF-1 were colonized by a large number of cells (**Fig. 8 B, C**). These cells were positive for May Grunwald Giemsa differential staining (**Fig. 8 E-G**). In MG pellets, supplemented only with MWCNTs, a reduced number of cells with the same characteristics were present (**Fig. 8 D, H**).

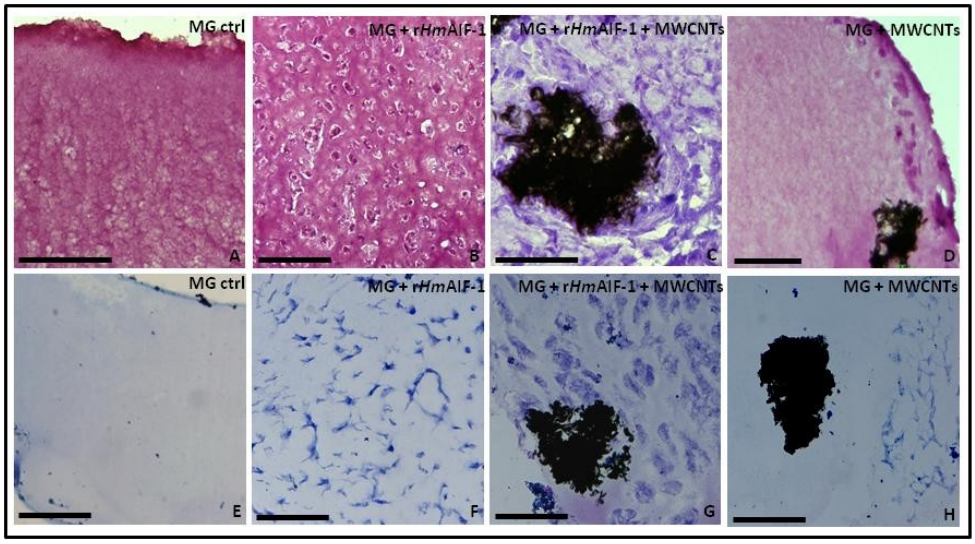


**Fig. 8.** Morphological analysis of MG samples. (**A**) Control MG is practically empty. (**B**, **C**) r*Hm*AIF-1 containing samples presenting several migrating cells. (**D**) MWCNTs supplemented MG: only few cells are visible. (**E-H**) May Grunwald Giemsa staining. Bars in A-H: 50 µm. (Girardello et al., 2015a).

TEM analysis showed that these cells had an elongated shape with a cytoplasm rich in electron-dense granules. They had a pronounced migratory phenotype showing pseudopodia and an active degradation of the surrounding matrix (**Fig. 9 A, B**).

The MWCNTs, added to the MG, were clearly visible both by optical (LM) and TEM analysis. At LM only large aggregates of nanotubes were distinguishable, surrounded by a clot of cells, whereas at TEM the MWCNTs were visible both dispersed throughout the matrix and grouped in aggregates characterized by different sizes (**Fig. 9 C, D**). In r*Hm*AIF-1 and MWCNT supplemented MG pellets, a great number of

migrating cells were present (**Fig. 9 E**) and MWCNTs were visible both in intracellular vesicles (**Fig. 9 F**) as well as dispersed in the cytoplasm (**Fig. 9 G**).

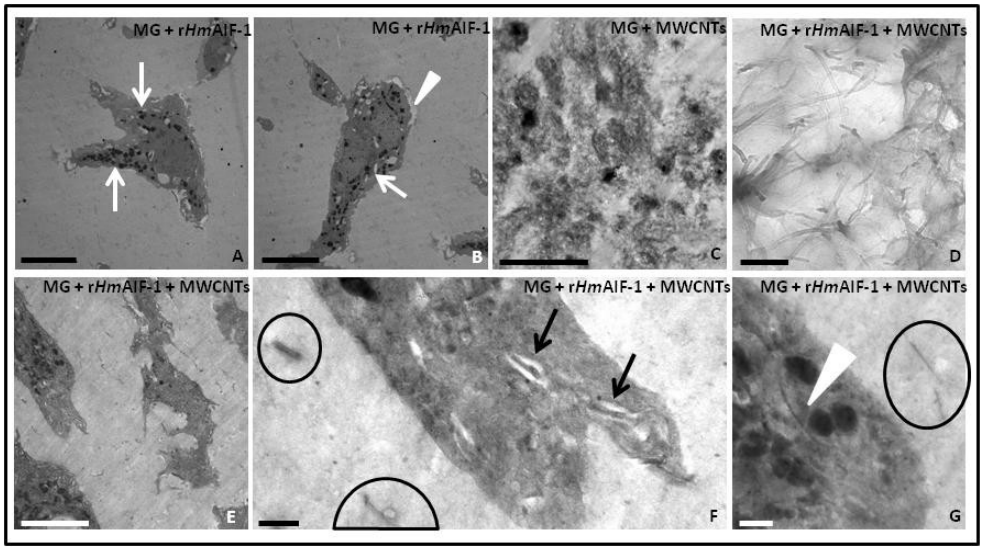


**Fig. 9.** TEM images of MG samples. (**A, B**) r*Hm*AIF-1 supplemented MG contains cells with a pronounced migratory phenotype electron-dense cytoplasmic granules (arrow), and in active degradation of surrounding matrix (arrowhead). (**C**) In samples in which MWCNTs were added, the nanomaterial was clearly visible both dispersed throughout the matrix both grouped in aggregates differently sized (**C**). (**D**) MWCNTs at higher magnification. (**E**) Cells migrating through the matrix in r*Hm*AIF-1 and MWCNTs supplemented MG. (**F, G**) MWCNTs are visible in matrix (circle), in intracellular vesicles (arrow) and freely dispersed in the cytoplasm (arrowhead). Bars in A-C, E: 5 µm; Bars in D: 200 nm; Bars in F, G: 500 nm. (Girardello et al., 2015a).

### *4.2.2 Immunocytochemical characterization*

In all samples, the cells infiltrating the MG and surrounding the MWCNT aggregates were strongly positive for the antibodies anti-CD68 (**Fig. 10 A-C**) and anti-*Hm*AIF-1 (**Fig. 10 D-F**). In negative control experiments no signal was detected (**Fig. 10 G**).

In MWCNTs and r*Hm*AIF-1 supplemented MG, cells were positive for Thioflavin-S, indicating the presence of amyloid fibrils (**Fig. 10 H**). No positivity was detected for this dye in the cells migrated in MWCNT supplemented MG pellet (**Fig. 10 I**).

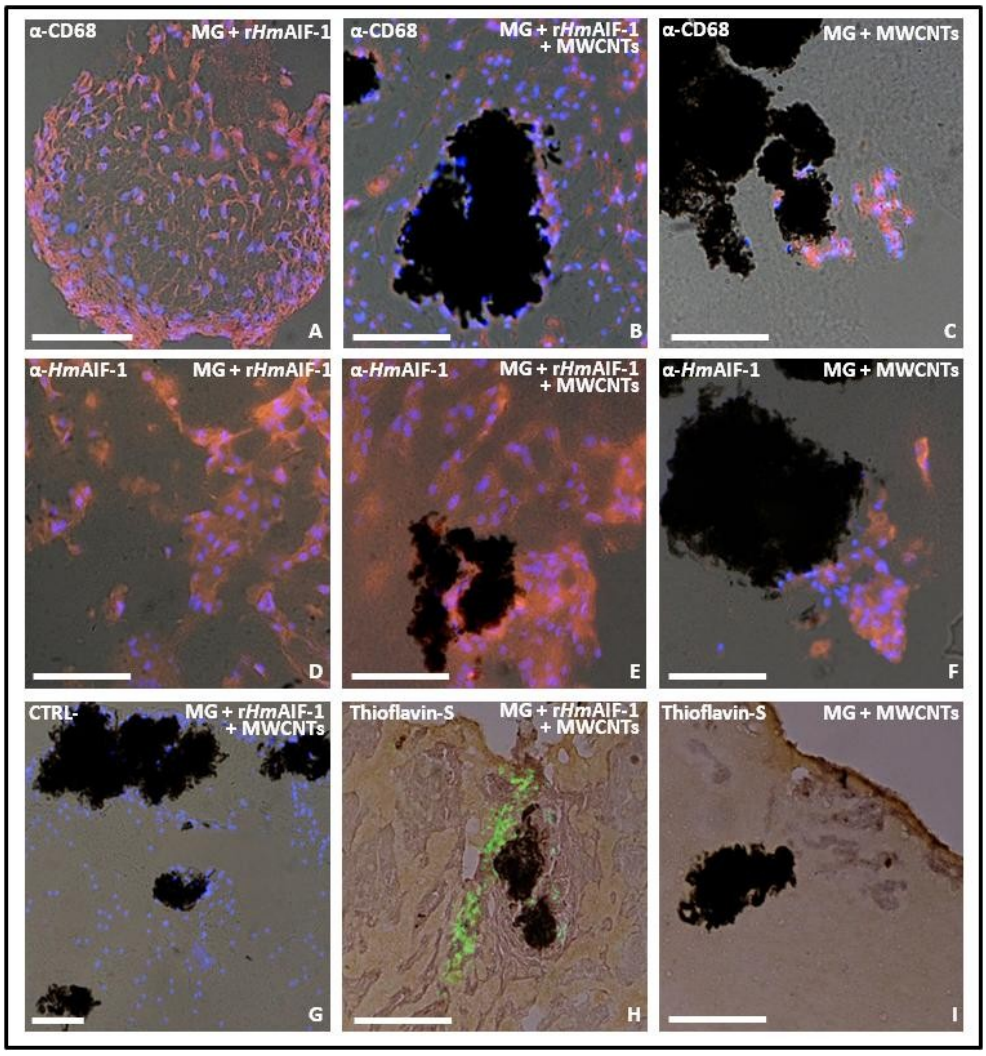


**Fig. 10.** Immunocytochemical characterization of MG infiltrating cells. α-CD68 (**A-C**) and α-HmAIF-1 (**D-F**) are detected by a Cy3-conjugated secondary antibody (red). Nuclei are counterstained with DAPI (blue). (**G**) Negative control. (**H-I**) Thioflavin-S method. In rHmAIF-1 and MWCNTs supplemented MG, macrophages actively produce amyloid material (yellow in H) while in only MWCNTs supplemented MG these cells are negative for this dye (I). Bars in A-I: 50 µm. (Girardello et al., 2015a).

### *4.2.3 Cell proliferation assay*

The BrdU assay was performed to assess the proliferative ability of cells infiltrated in the MG sponge. Leeches macrophages, chemoactracted in MG sponges by means of *Hm*AIF-1, presented $BrdU^{+}$ nuclei (red signal) (**Fig. 11 A**). The negative control experiments, in which the primary antibody was omitted, no BrdU signal was observed (**Fig. 11 B**).

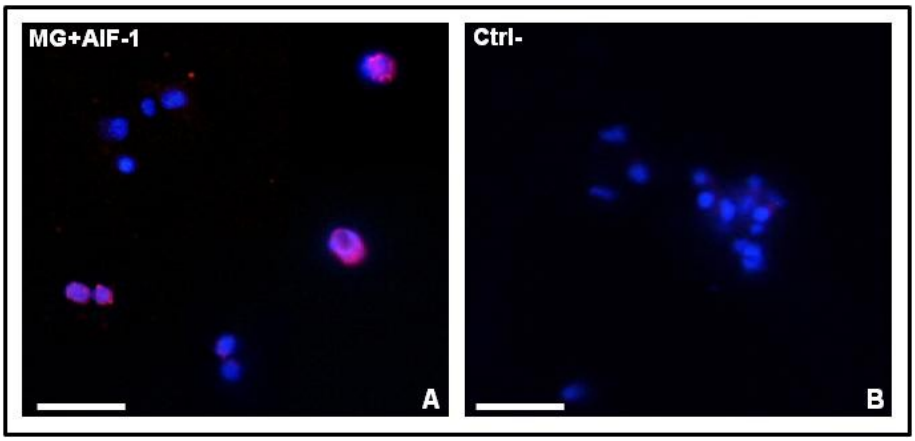


**Fig. 11.** Proliferation assay in MG. Cell migrated in MG sponges with BrdU+ nuclei (in red) (**A**). In negative control (**B**) the primary antibody was omitted. Nuclei were counterstained with DAPI (blue). Bars in A, B: 10 µm.

### *4.2.4 Apoptosis detection assay*

In the MG assay, several TUNEL$^{+}$ (green/yellow) nuclei were visible in the positive control sample (**Fig. 12 A**), while in the negative control no signal was detected (**Fig. 12 B**).

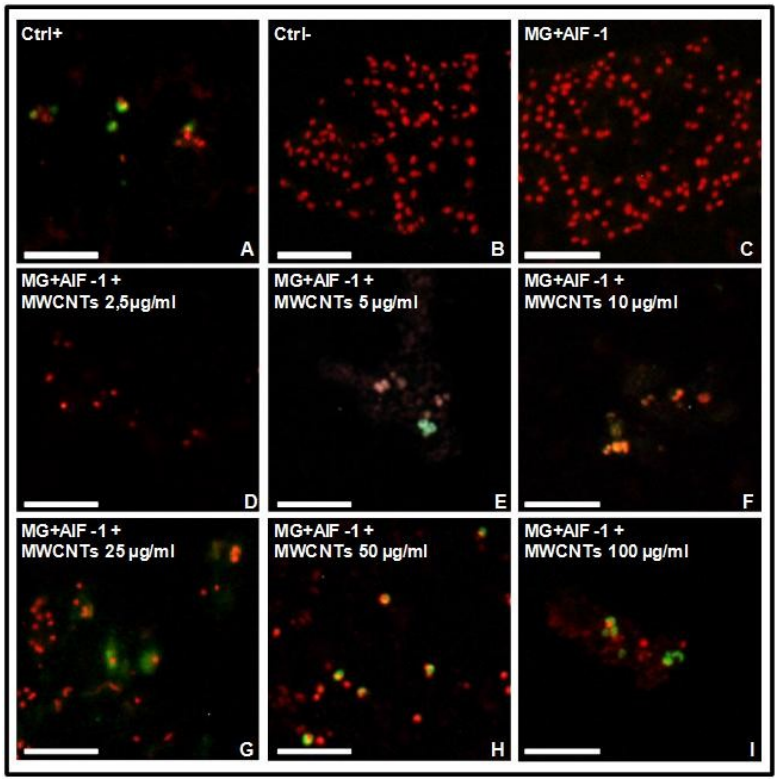


**Fig. 12.** TUNEL assay for apoptosis on MG sections. (A) positive and (B) negative controls. MG supplemented with *Hm*AIF-1 (C) and with *Hm*AIF-1 and increasing concentration of MWCNTs (D-I). Nuclei, counterstained with propidium iodide, result in red while TUNEL positivity in green. The merge results in yellow. Bars in A-I: 50 µm.

In the cells infiltrating the MG supplemented with *Hm*AIF-1 no evidence of apoptosis was detected (**Fig. 12 C**), whereas in MWCNT supplemented MG samples the number of TUNEL$^{+}$ nuclei appeared to increase in a dose-dependent manner (**Fig. 12 D-I**), indicating that are MWCNTs responsible for apoptosis induction in the cells migrated in the matrix.

## 4.3 *In vitro* treatment

### *4.3.1 Leech macrophages primary cell culture*

After 1 week *in vivo*, *Hm*AIF-1 supplemented MG had been removed from the leeches and cells were placed in culture. Starting from 1 day after seeding, cultured cells appeared grouped in clones (**Fig. 13 A, B**), while 1 week after seeding an increased cell number was appreciable (**Fig. 13 C**), as demonstrated by cell counting (**Fig. 13 D**).

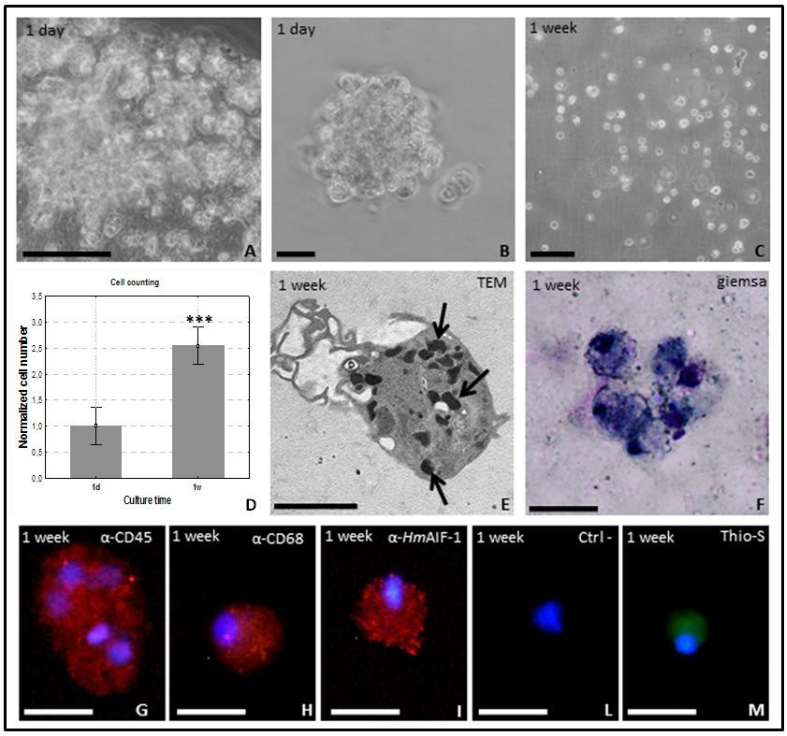


**Fig. 13.** Phase contrast image of cultured cells 1 day (**A, B**) and 1 week after seeding (**C**). Quantitative evaluation of cell numbers (**D**). Column 1: cells cultured for 1 day Column 2: cells cultured for 1 week. ***p<0.01. These cells are ultrastructurally similar to macrophages with a cytoplasm filled with electron-dense granules (arrows in **E**), are Giemsa positive cells (**F**) and immuno-stained with CD45 (**G**), CD68 (**H**) and *Hm*AIF-1 (**I**) antibodies, markers of macrophages cells. (**L**) Negative control in which the primary antibody was omitted. These cells show also a weak positivity to Thioflavin-S staining (yellow in **M**). Nuclei are counterstained with DAPI (blue in G-M). Bars in A, C: 50 µm; bars in B, D, F-M: 10 µm; bar in E: 2 µm. (Girardello et al., 2015a).

TEM analysis (**Fig. 13 E**) showed that these cells exhibited the same morphological characteristics described in the MG injection assay.
Cultured cells, after 1 week, resulted positive for May Grunwald Giemsa differential staining (**Fig. 13 F**) and expressed monocyte-macrophage specific markers, such as CD45 (**Fig. 13 G**), CD68 (**Fig. 13 H**) and *Hm*AIF-1 (**Fig. 13 I**). In negative control sample, in which primary antibodies were omitted, no signal was detectable (**Fig. 13 L**). Moreover these cells showed a weak positivity for Thioflavin-S staining method, indicating scarce amyloid fibril production (**Fig. 13 M**).

*4.3.2 MWCNT in vitro treatment*

Cultured macrophages were then incubated for 24h with increasing concentrations of MWCNTs dispersed in culture medium (2.5, 5, 10, 25, 50 and 100 µg/mL). Treated cells maintain their positivity for CD45 (**Fig. 14 A-F**) and *Hm*AIF-1 (**Fig. 14 G-L**).

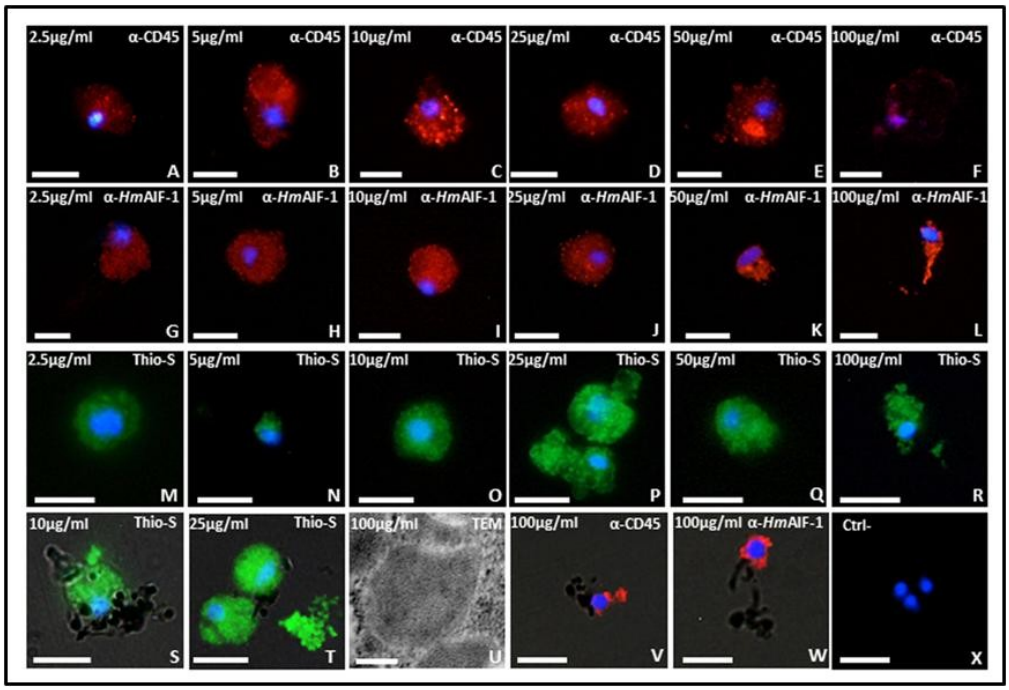


**Fig. 14.** Cells extracted from MG after 1 week from injection and treated for 24h with increasing concentration of MWCNTs (2.5, 5, 10, 25, 50 and 100 µg/mL) are $CD45^{+}$ (red in **A-F**), *Hm*$AIF\text{-}1^{+}$ (red in **G-L**) and show an increasing positivity for Thioflavin-S staining (yellow in **M-R**). Combined fluorescence/transmission (**S, T**) and TEM images clearly show the amyloid fibril deposition (yellow in **S, T**) and organized fibrillar material (arrowhead in **U**) by $CD45^{+}$/*Hm*$AIF\text{-}1^{+}$ macrophages (**V-W**) strictly associated with MWCNT aggregates. Nuclei in blue are stained with DAPI. No signal is detected in negative control experiments (**X**). Bars in A-T, V-X: 10 µm; bar in U: 500 nm. (Girardello et al., 2015a).

Moreover, after MWCNTs treatment, macrophages resulted highly positive for Thioflavin-S staining (**Fig. 14 M-R**). Ultrastructural analysis at TEM highlighted that spatially organized amyloid fibrils were accumulated in dilated reticulum cisternae (**Fig. 14 U**) and then released in the extracellular environment (**Fig. 14 T**). Combined fluorescence/transmission images clearly showed the strictly association between *Hm*AIF-1$^+$ and CD45$^+$ macrophages with MWCNTs aggregates (**Figure 14 V, W**). Furthermore, the number of amyloid fibrils increased with the MWCNT concentration augment, as demonstrated by fluorescence intensity quantification (**Fig. 15**).

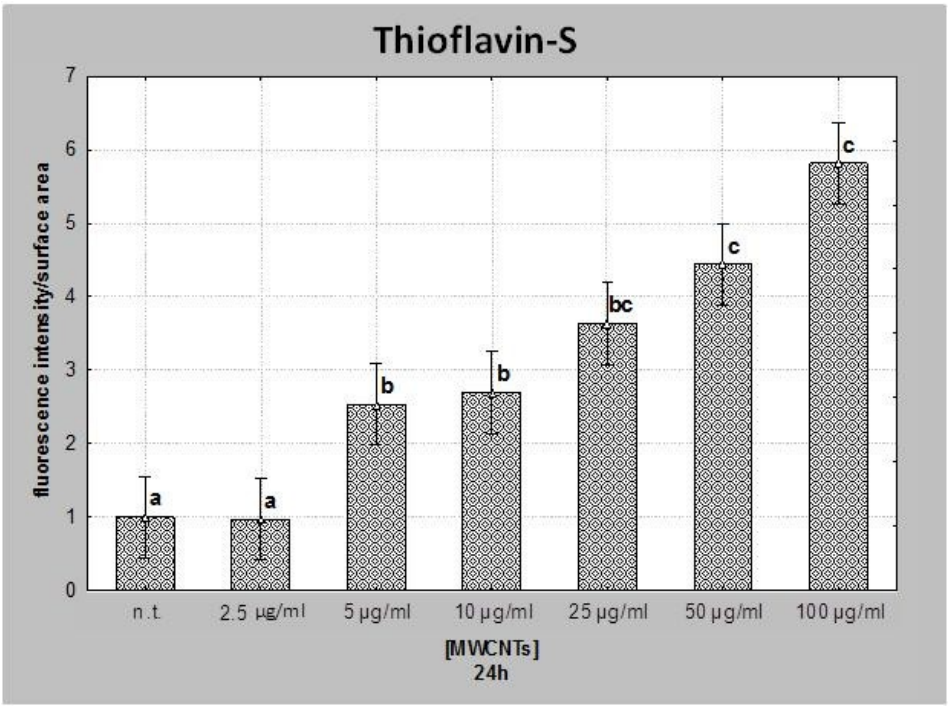


**Fig. 15.** Histogram showing fluorescence intensity for surface unit after Thioflavin-S assay. Values are normalized on the n.t. sample. Statistical differences were calculated by One-Way ANOVA followed by Tukey's post-hoc test, vertical bars denote 0.95 confidence intervals, different letters indicate statistically significant differences ($p<0.05$).

### *4.3.3 Cell proliferation assay*

After 24 and 48 hours from seeding, a large number of BrdU$^+$ cells was observed (green signal) (**Fig. 16 B, C**). 24 and 48h of MWCNT treatment highly reduced the number of proliferating cells (**Fig. 16 D-I, Fig. 16 J-O**). An high dose of MWCNTs (100µg/mL) totally inhibited cell proliferation and no BrdU$^+$ cells were detectable after 24 and 48h from treatment

(**Fig. 16 I, O**). The control samples, in which the primary antibody was omitted, were negative (**Fig. 16 A**).

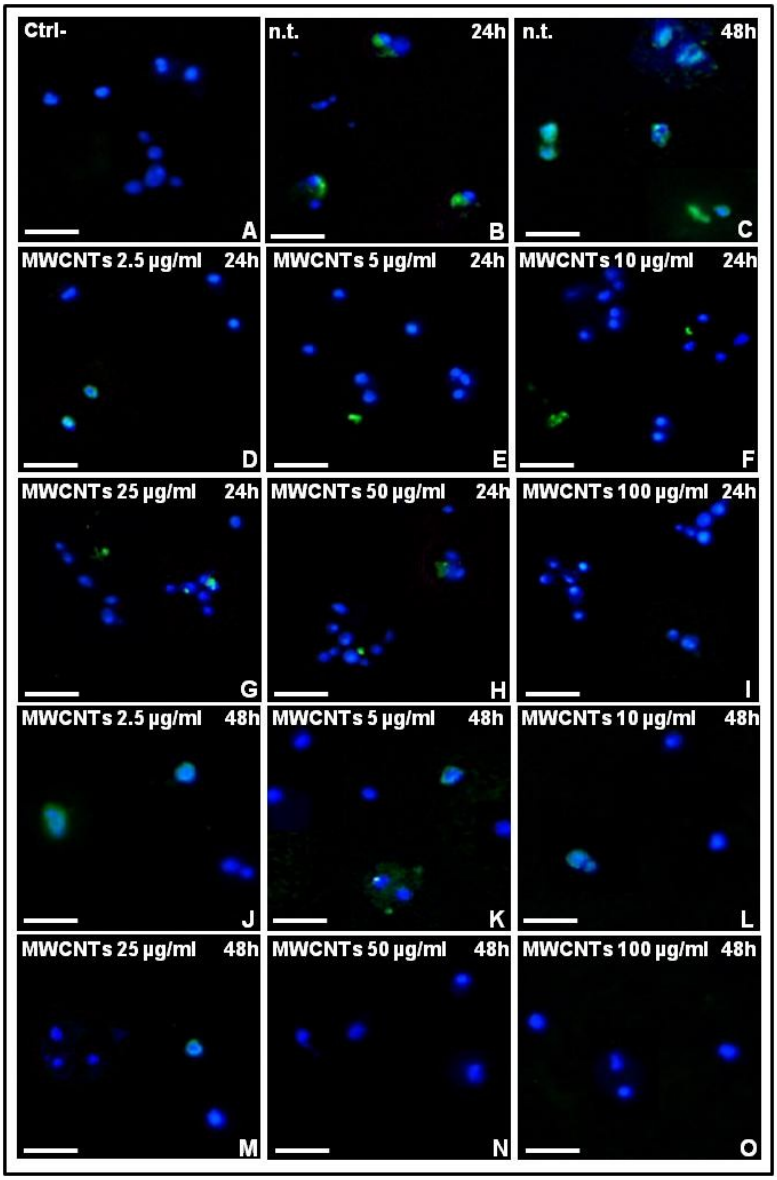


**Fig. 16.** Proliferation assay after MWCNT *in vitro* treatment (**A-O**). Compared to the negative control (**A**), in which the primary antibody was omitted, the major part of cells in n.t. samples are $BrdU^{+}$ (green) both at 24h (**B**) and 48h (**C**). In MWCNT treated samples the number of positive cells seems to decrease in a dose and time dependent manner (**D-O**). Nuclei were counterstained with DAPI (blue). Bars in A-P: 10 µm.

Cell counting showed a remarkable decrease in $BrdU^+$ cells even at low doses (2.5, 5 and 10 µg/mL) of MWCNTs both at 24 and 48h. The effect is even more evident after 48 hours from administration of higher doses (25, 50 and µg/mL) of MWCNTs (**Fi. 17 A, B**).

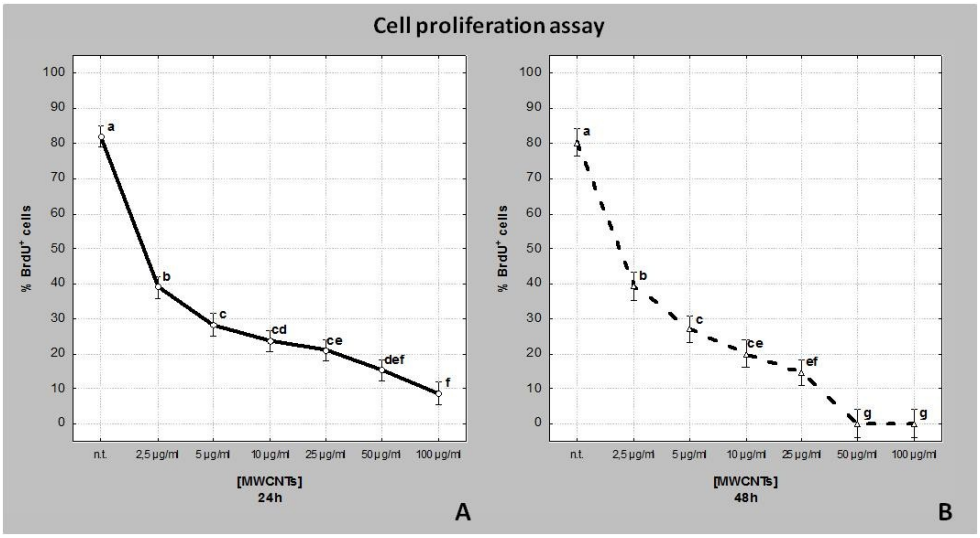


**Fig. 17.** The graphs show the percentage of $BrdU^+$ cells after 24h (**A**) and 48h (**B**) MWCNTs treatment. Statistical differences were calculated by Factorial ANOVA followed by Tukey's post-hoc test; vertical bars denote 0.95 confidence intervals, different letters indicate statistically significant differences ($p<0.05$).

### *4.3.4 Apoptosis detection assay*

The apoptosis evaluation assay was also performed after MWCNT *in vitro* treatment. Apoptotic nuclei were stained in yellow, as confirmed by the positive control (**Fig. 18 A**) while all nuclei were counterstained in red by propidium iodide, as shown in the negative control (**Fig. 18 B**).

In both n.t. samples (**Fig. 18 C, D**) and in cells incubated for 24 hours with low concentrations of MWCNTs (2.5 and 5 µg/mL) (**Fig. 18 E, F**) no apoptotic nuclei were visible. The number of $TUNEL^+$ cells remarkably increased after administration of higher doses of MWCNTs (**Fig. 18 G-J**). After 48h from treatment apoptosis is induced in large number of cells (**Fig. 18 K-P**) at any MWCNT concentrations.

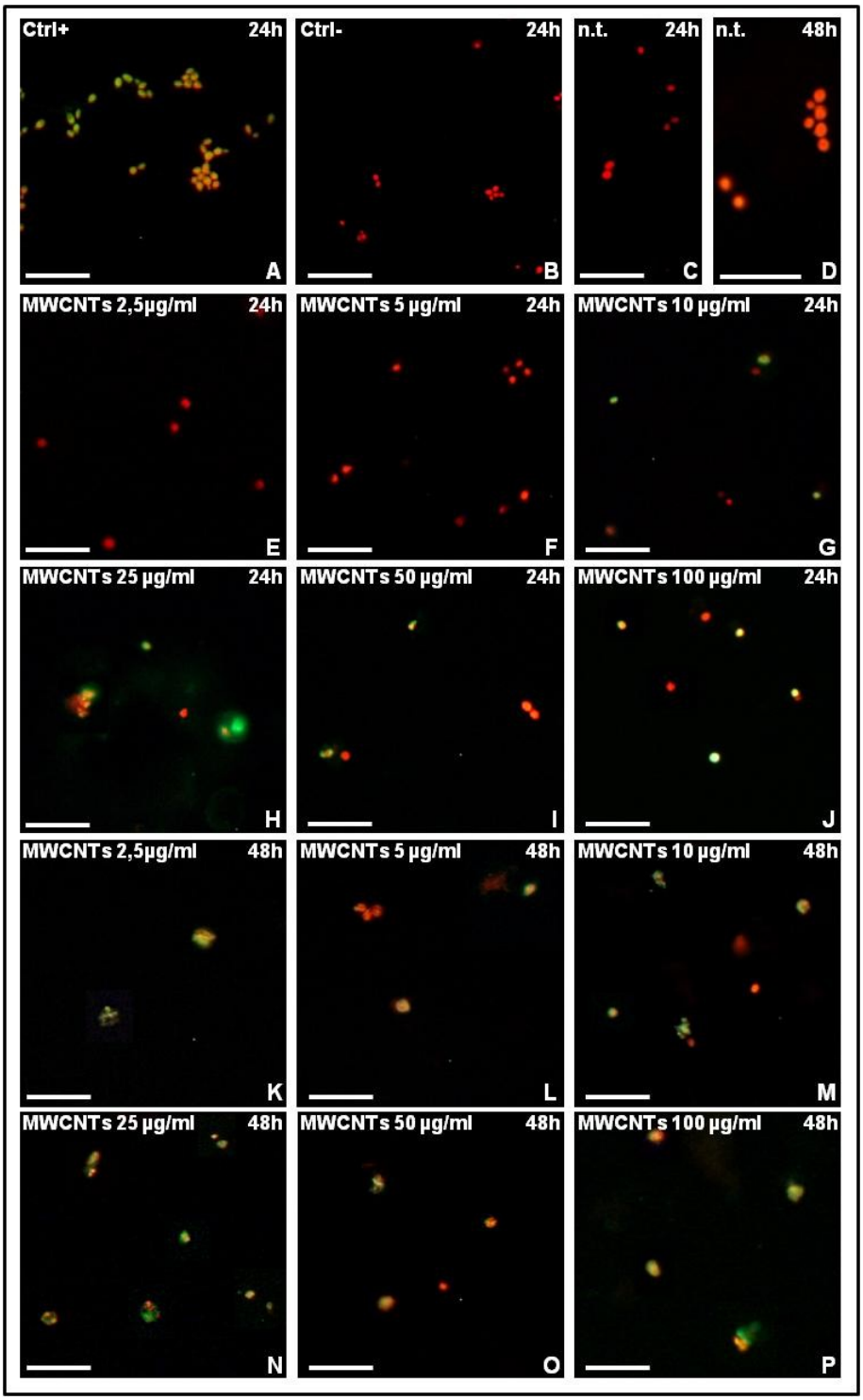


**Fig. 18.** TUNEL assay for apoptosis after 24h (**A-C, E-J**) and 48h (**K-P**) MWCNT *in vitro* treatment. Nuclei were counterstained with propidium iodide (red). TUNEL positivity is visible in green/yellow. Bars in A-P: 20 µm.

Cell counting showed that apoptotic cell number was very low in n.t and low-dose treated samples (2.5 and 5 µg/mL) for 24h. At the dose of 10 µg/mL, it underwent a sudden increase to then reach about 60% of total cells at higher MWCNT doses (**Fig. 19 A**). The 48h MWCNT treatment seemed to have a more rapid effect. TUNEL$^+$ cells were about the 80% at the lowest dose (2.5 µg/mL) and reached the 100% with the 100 µg/mL treatment (**Fig. 19 B**).

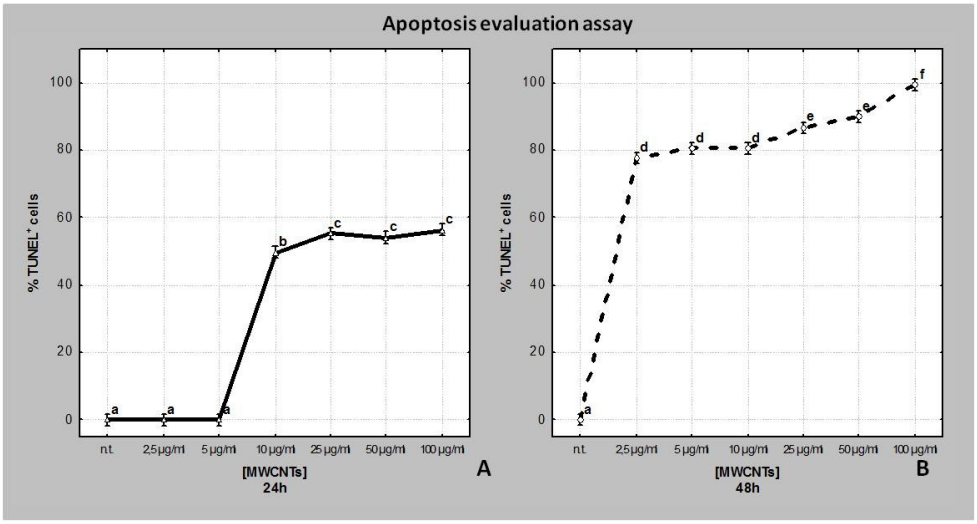


**Fig. 19.** Apoptosis evaluation assay. The graph illustrate the percentage of TUNEL$^+$ cells after 24 (**A**) and 48h (**B**) MWCNTs *in vitro* treatment. Statistical differences were calculated by Factorial ANOVA followed by Tukey's post-hoc test; vertical bars denote 0.95 confidence intervals, different letters indicate statistically significant differences ($p<0.05$).

### *4.3.5 ROS production*

ROS production was evaluated by means of $H_2$DCFDA assay. In n.t. samples, both after 24h (**Fig. 20 A**) and 48h (**Fig. 20 B**), no signal was detected. After 24h MWCNT in vitro treatment, ROS production was observed from concentrations of 2.5 µg/mL up to 100 µg/mL (**Fig. 20 C-H**). In particular, ROS signal was localized in cells in close contact with MWCNTs bundles (**Fig. 20 I**). A high $H_2$DCFDA positivity was observed also after 48h MWCNTs treatment (**Fig. 20 J-O**).

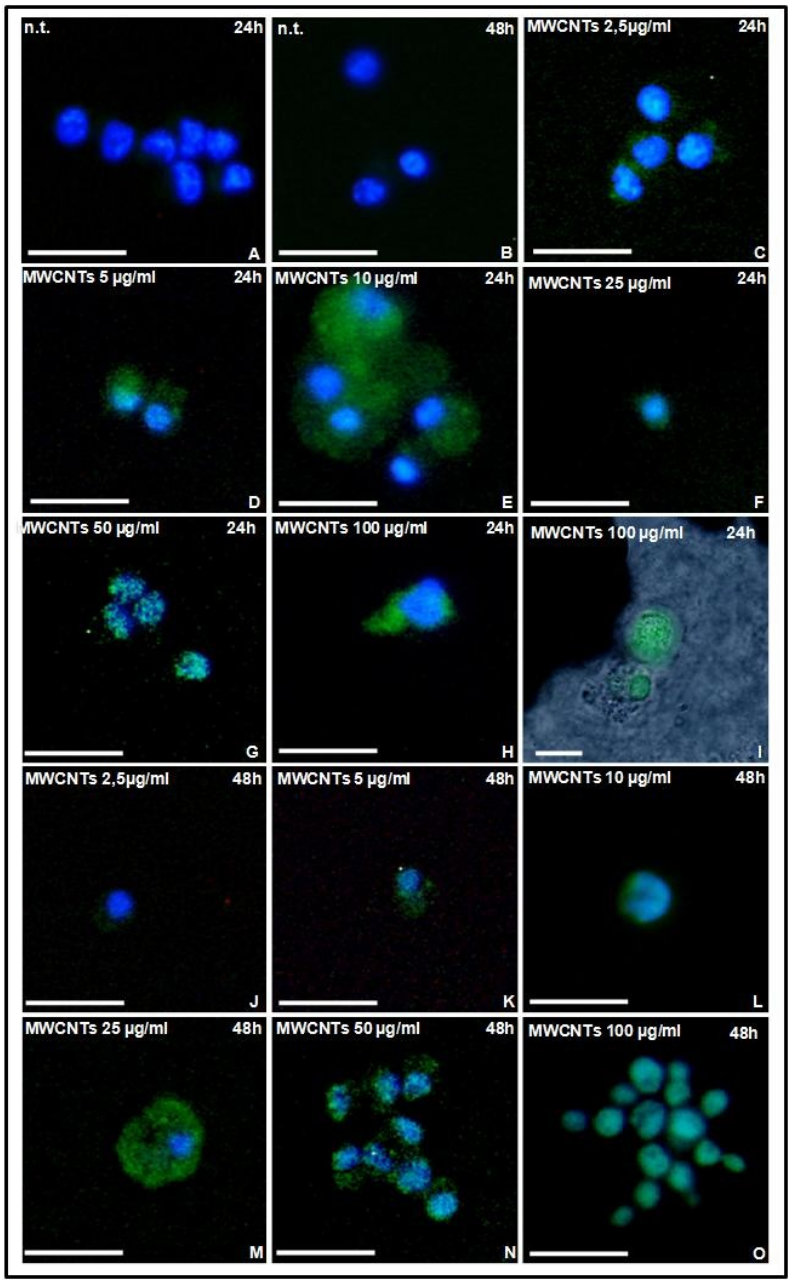


**Fig. 20.** ROS production (**A-O**). $H_2$DCFH-DA positivity (green) is not visible in n.t. macrophages both at 24h (**A**) and 48h (**B**). After 24h *in vitro* treatment with increasing concentration of MWCNTs a strong positivity is detectable (**C-H**). Combined optical and fluorescence detail showing $H2DCFDA^+$ cells close to a MWCNTs bundle (**I**). The same dose-dependent ROS production is appreciable after 48h treatment (**J-O**). Bars in A-O: 10 µm.

Fluorescence intensity measurement, showed a significant increase in ROS production after treatment with high doses of MWCNTs (25, 50 and

100 µg/mL) for 24h (**Fig. 21 A**), while after 48h, the increase of ROS resulted evident starting from the 10 µg/mL dose up to the highest dose (**Fig. 21 B**).

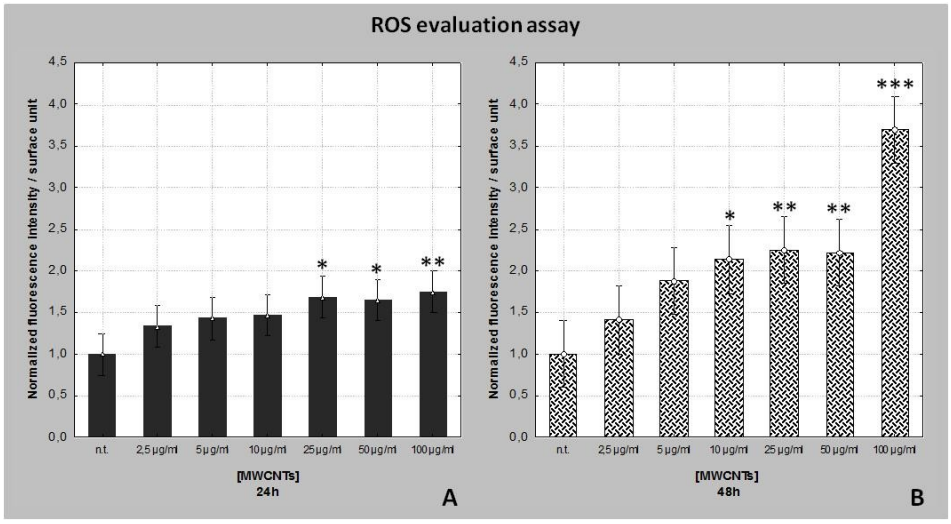


**Fig. 21.** Histogram showing fluorescence intensity for surface unit after $H_2$DCFH-DA assay on 24 (**A**) and 48h (**B**) MWCNT-treated cells. Statistical differences were calculated by Factorial ANOVA followed by Tukey's post-hoc test, vertical bars denote 0.95 confidence intervals, *p < 0.05, **p < 0.01, ***p < 0.001 (between n.t. and treatments).

## 4.4 Inflammatory markers in leeches

### *4.4.1 MIF cloning and immunolocalization*

A cDNA sequence coding a gene homologous to mammal MIF was identified in the EST library from the leech CNS in the *Hirudo* transcriptome database (Macagno et al., 2010).

Based on the available sequence, specific primers were designed and used for RT-PCR amplification. cDNA was then cloned and sequenced (**Fig. 22 A**). The gene, named *H*MIF, has a coding sequence of 336 bp. The open reading frame (ORF) encodes a 111 amino acid protein with a calculated molecular mass of 12.5 kDa. The *H*MIF genomic sequence revealed the presence of three exons separated by small introns. The *H*MIF amino acid sequence presents a 35% identity with the human protein and an identity range between 32 and 52% with the MIF proteins of other Vertebrates and invertebrates (**Fig. 22 B**). Phylogenetic analysis shows that *H*MIF has a closer relationship with a vertebrate than with the other invertebrate species (**Fig. 22 C**).

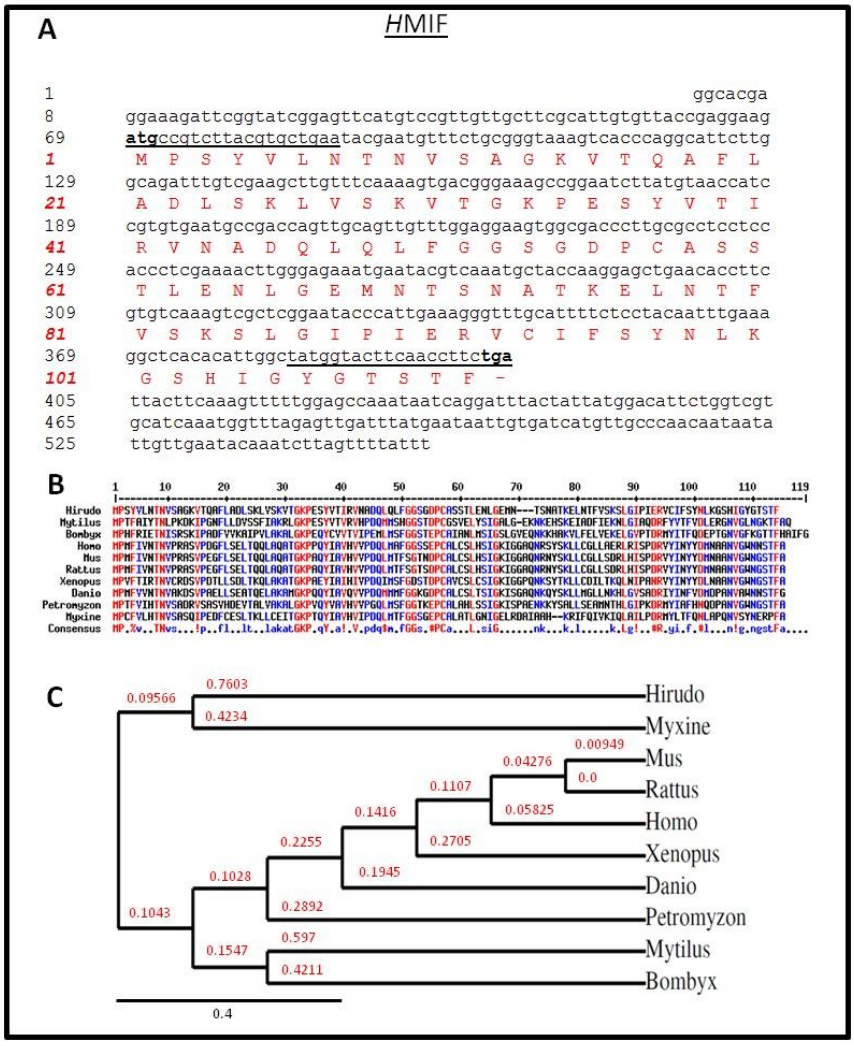


**Fig. 22.** Complete cDNA and primary sequence of leech *H*MIF (**A**). Forward and reverse primer sequences used for amplification are underlined. Start and stop codons are in bold. (**B**) Multiple alignment of MIF indicating identity between sequences from different selected species. Red residues correspond to 100% identity rate. Lower rate values are indicated with blue (60%) and black (<50%) letters. (**C**) Phylogenetic tree based on the primary structure of MIF by comparing our sequence with the following species: *Bombyx mori* (NP_001040199), *Danio rerio* (NP_001036786), *Homo sapiens* (CAA80598), *Mus musculus* (NP_034928), *Mytilus galloprovincialis* (AEN25591), *Myxine glutinosa* (AAP33795), *Petromyzon marinus* (AAP33793), *Rattus norvegicus* (NP_112313), *Xenopus laevis* (NP_001083650). Node values indicate percent bootstrap confidence derived from 1000 replicates. The bar shows the genetic distance. Phylogenetic analysis were performed with TreeDyn (v198.3).

Whole mount immunolocalizations were performed on samples of leech CNS consistent of 4 ganglia and the connectives connecting them. The middle connective was injured immediately after dissection to stimulate the innate immune system. No positivity was detected in the ganglia

(**Fig. 23 A**). Few positive cells were found along the connective, in correspondence of the injury in both n.t. (**Fig. 23 B-C**) and 6h LPS-treated samples (**Fig. 23 D-E**). In negative control experiments no signal was detected (**Fig. 23 F**).

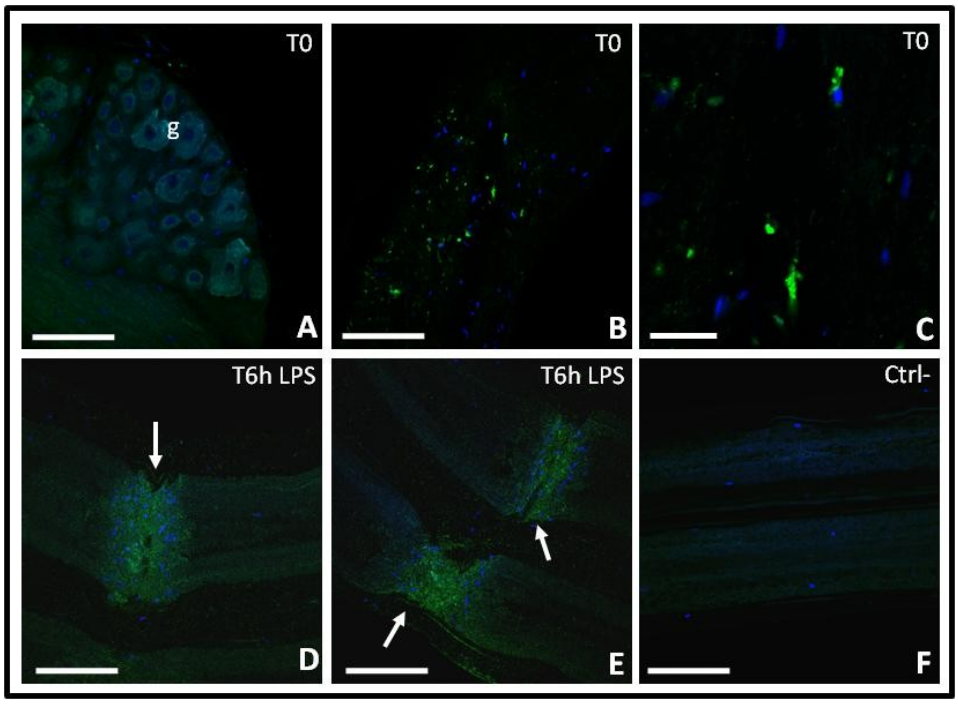


**Fig. 23.** Anti-MIF whole mount immunolocalization on leech CNS (**A-F**). Few positive microglial cells are visible at ganglia level (g) in dissected and immediately fixed (T0) CNS (**A-C**). A diffuse positivity is visible al crush level (arrows) in LPS treated CNS (**D-E**). α-MIF is detected by a FITC-conjugated secondary antibody (green). In negative control (**F**) only secondary antobody was used. Nuclei are cunterstained with hoechst. Bars in A-F: 20 µm.

Immunolocalization on cryosections of leech body wall showed that MIF was constitutively expressed in unlesioned animals (**Fig. 24 A**). This factor was mainly expressed in cells located in the connective tissue underlying the body wall epithelium and surrounding the fields of muscle fibers. A similar pattern was observed in samples analysed 6 h after PBS injection, indicating that the mechanical stress induced by the injection or the conveyed solution alone did not exert a significant effect on MIF expression in the body wall of challenged animals (**Fig. 24 B-C**). Interestingly, 6 h after LPS injection, numerous cells were clearly recognizable in the challenged area. These cells were $MIF^{+}$ and mainly

localized under the epithelium and among the muscle fibers (**Fig. 24 D-E**).

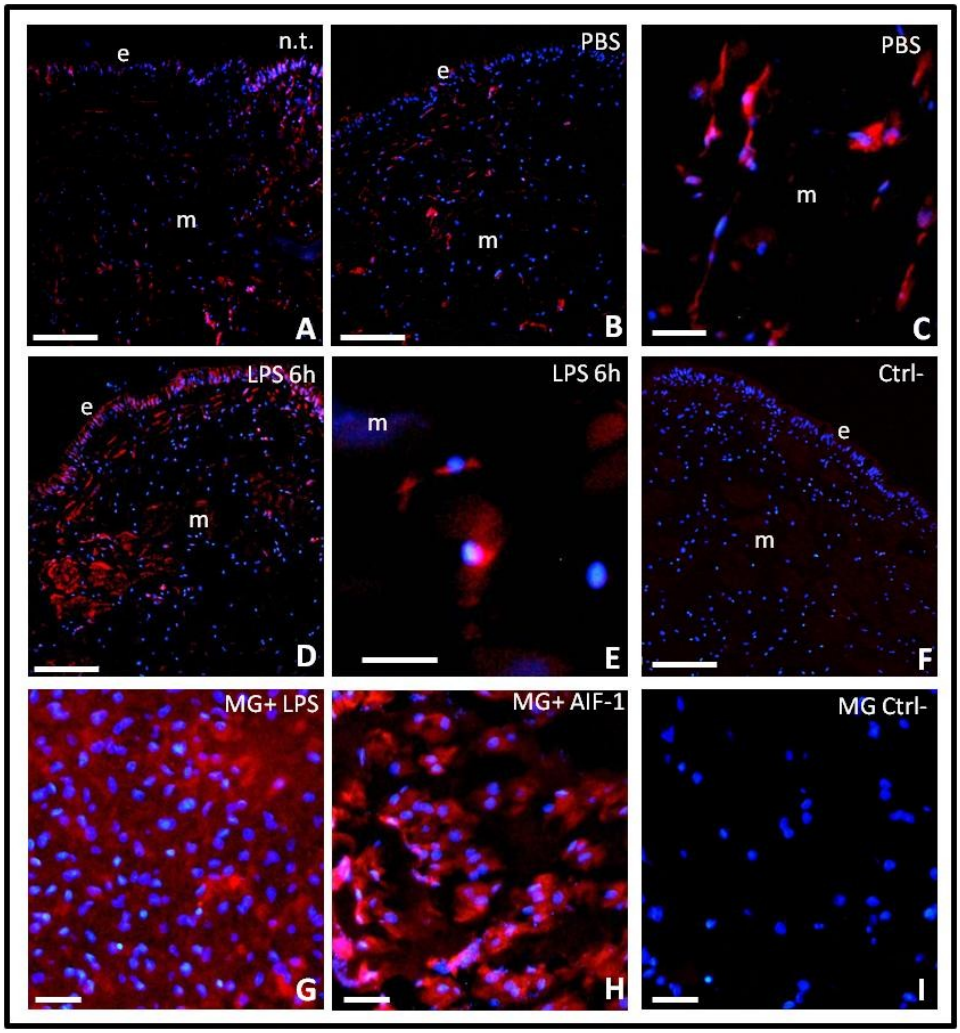


**Fig. 24.** Anti-MIF immunolocalization on cryosections of leech body wall (**A-F**) and MG pellet (**G-I**). Note the population of resident macrophages in untreated (n.t.) animal (**A**). The same pattern of expression is visible 6h after PBS injection (**B-C**). 6h after LPS injection, numerous positive cells are visible underneath the epithelium (e) and among the muscle fibers (m) (**D-E**). Macrophages migrated in MG added with LPS or r*Hm*AIF-1 show high positivity for this marker (**G-H**). α-MIF is detected by a Cy3-conjugated secondary antibody (red). Nuclei are counterstained with DAPI (blue). Negative controls (**F, I**) were performed by incubating only secondary antobody. Bars in A-B, D-F: 100 µm; Bars in C, G-I: 20 µm; Bar in E: 10 µm.

To better characterize the migrating cell expressing MIF, 300 µL of biomatrix MG supplemented with r*Hm*AIF-1 or LPS were injected into the body wall of leeches, since we previously reported that the r*Hm*AIF-1 or LPS injection (Girardello et al., 2015a; Schorn et al., 2015b) in the

leech promoted the recruitment of macrophages cells. In cryosections of MG pellet added with LPS or r*Hm*AIF-1 a great number of MIF$^{+}$ cells were observed (**Fig. 24 G-H**). No signal was detected in negative controls experiments (**Fig. 24 F, I**) in which the primary polyclonal anti-MIF antibody was omitted and sections were incubated only with the secondary antibody.

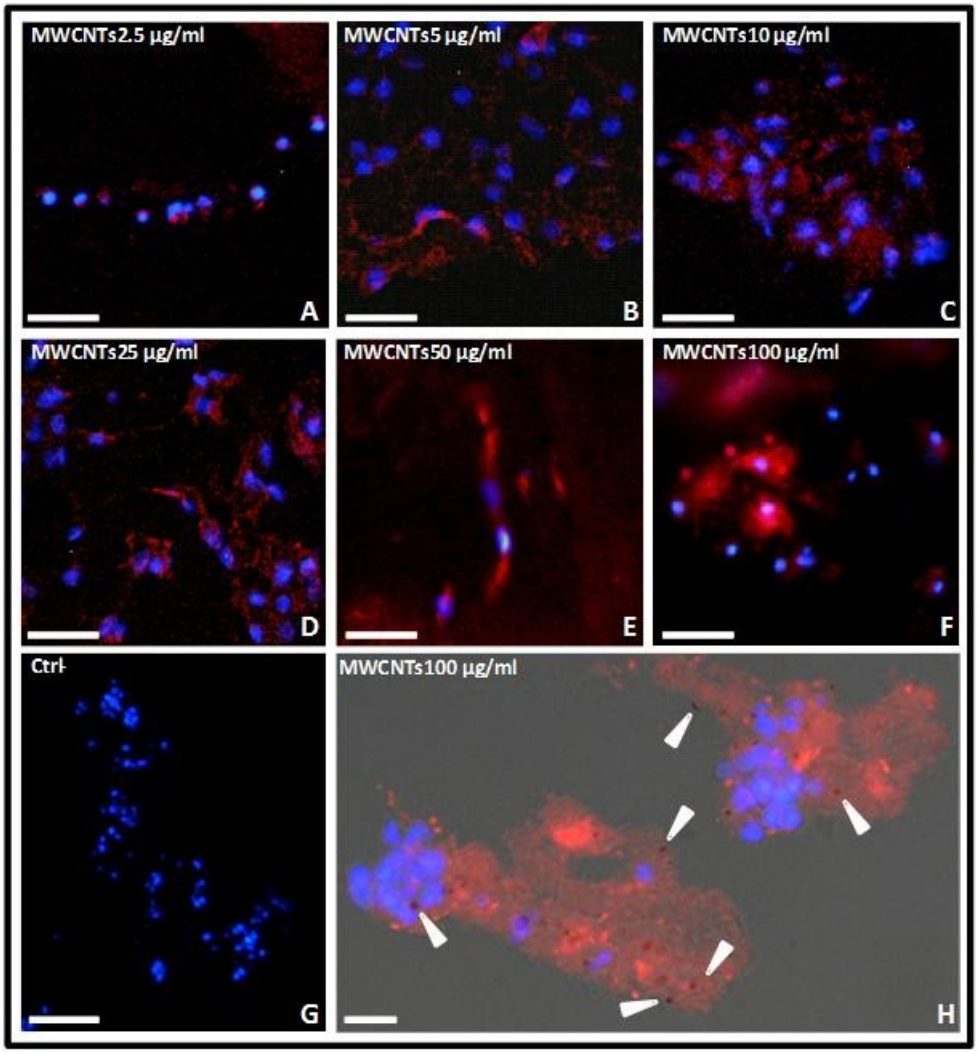


**Fig. 25.** Anti-MIF immunolocalization on cryosections of MG supplemented with r*Hm*AIF-1 and an increasing concentration of MWCNTs. Macrophages infiltrating the MG sponges result high positive for this marker (**A-F**). Negative control (**G**) was performed by omitting the primary antibody. Combined fluorescence/transmission image (**H**) showing MIF$^{+}$ macrophages strictly associated to MWCNTs aggregates (arrowheads). α-MIF is detected by a Cy3-conjugated secondary antibody (red) while nuclei are counterstained with DAPI (blue). Bars in A-F: 20 µm; bar in G: 50 µm; bar in H: 10 µm.

Moreover, anti-MIF immunolocalizations on MG supplemented with r*Hm*AIF-1 and an increasing concentration of MWCNTs (from 2.5 up to 100 µg/mL) were performed (**Fig. 25 A-H**). Macrophages migrated into all MG sponges resulted positive for this marker, while only in samples supplemented with 50 and 100 µg/mL of MWCNTs a diffuse positivity in the matrix surrounding the cells was detected (**Fig. 25 E-F**). In negative control sample, the primary antibody was omitted (**Fig. 25 G**). Combined transmission/fluorescence image (**Fig. 25 H**) showed MWCNT aggregates surrounded by $MIF^{+}$ macrophages.

### *4.4.2 GMF cloning and immunolocalization*

An homolog of human GMF was identified in the leech nervous system. cDNA was cloned and sequenced using specific primers designed on the predicted sequences available in the databases. The gene has a coding sequence of 429bp, encoding a 142 amino acid protein (**Fig. 26 A**).

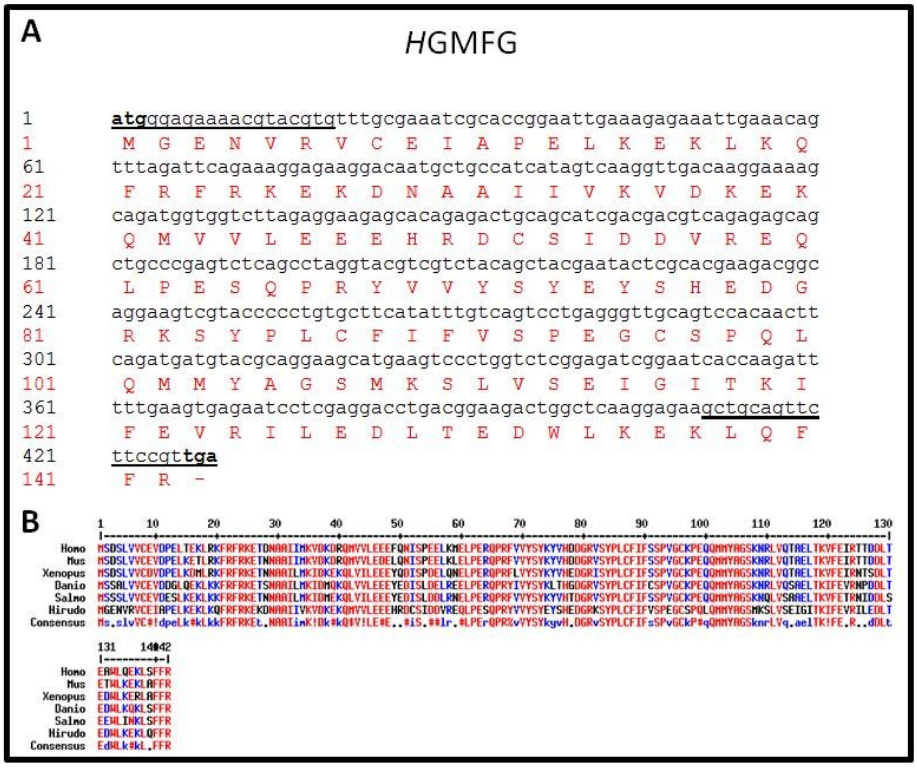


**Fig. 26.** Complete cDNA and primary sequence of leech *H*GMFG (**A**). Forward and reverse primer sequences used for amplification are underlined. Start and stop codons are in bold. Multiple alignment of GMFG primary sequences (**B**), indicating identity between sequences from different selected species. Red residues correspond to 100% identity rate. Lower rate values are indicated with blue (60%) and black (<50%) letters.

Sequence analysis revealed that the sequence belongs to ADF-gelsolin superfamily.

The protein was named *H*GMFG, presenting 63% identity with human GMFG and 60% identity with human GMFB. Multiple alignment of show high identity between sequences from different selected species (**Fig. 26 B**).

Whole mount immunolocalization using a polyclonal antibody raised against human GMFG was performed on leech injured CNS at different time-points. From T0 to T3d, a widespread punctiform signal was detected in the cytoplasm of macroglial cells, at ganglia level (**Fig. 27 A-C**).

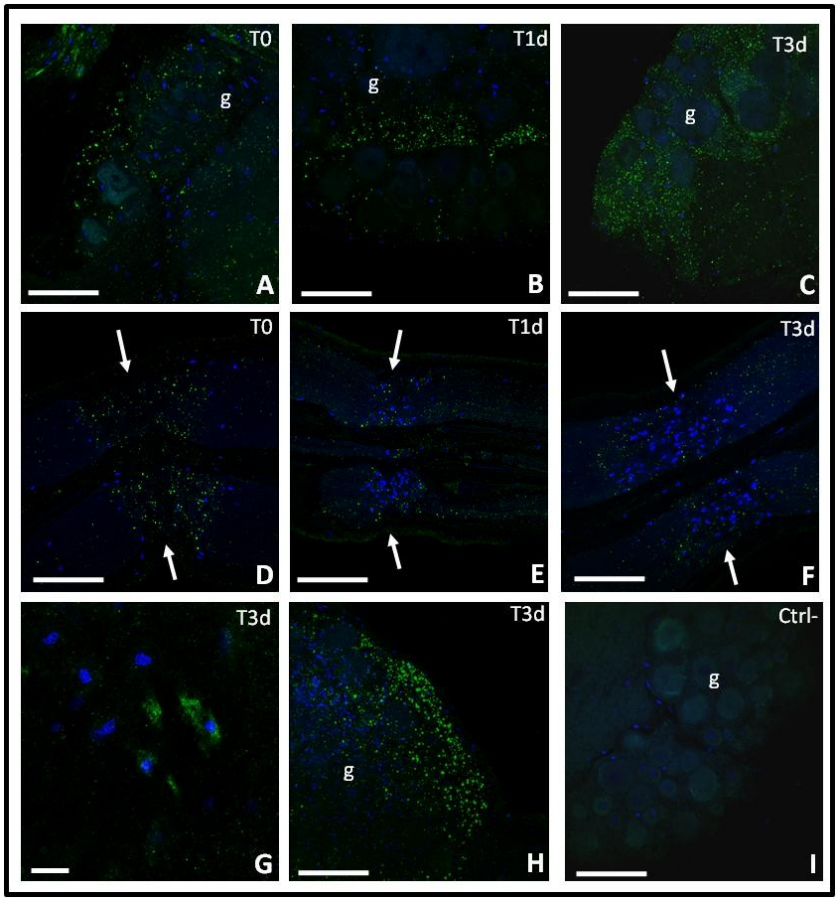


**Fig. 27.** Anti-GMF whole mount immunolocalization on leech CNS. Samples were injured and incubated at different time points (T0 hour, 1 and 3 days). Confocal laser scanner images at ganglia (g) (**A-C**) and injured connectives level (arrows) (**D-F**). Few positive microglial cells are visible among neurons (**G**). In **H** is shown a 20 section planes projection. Negative control (**I**) was performed by incubating only secondary antibody. Nuclei are counterstained with hoechst. Bars in A-F, H-I: 20 µm; Bar in G: 10 µm.

The same pattern of expression was detectable in the injured connective, surrounding microglial cells accumulated at lesion site (**Fig. 27 D-F**). Only few microglial cells in a ganglion resulted clearly positive for this marker (**Fig. 27 G**). The control sample, in which the primary antibody was omitted, was negative (**Fig. 27 I**).

In leech body wall injected with r*Hm*AIF-1, numerous GMFG$^{+}$ migrating cells were detectable underneath the epithelium and among the muscle fibers (**Fig. 28 A-B**). The numerous cells infiltrating the LPS or r*Hm*AIF-1 supplemented MG resulted high positive for the antibody anti GMFG. It is interesting to note that the strong positivity for this marker was mainly localized at the level of pseudopodia, involved in cell migration (**Fig. 28 D-E**). Control sections, performed by omitting the primary antibody, were negative (**Fig. 28 C, F**).

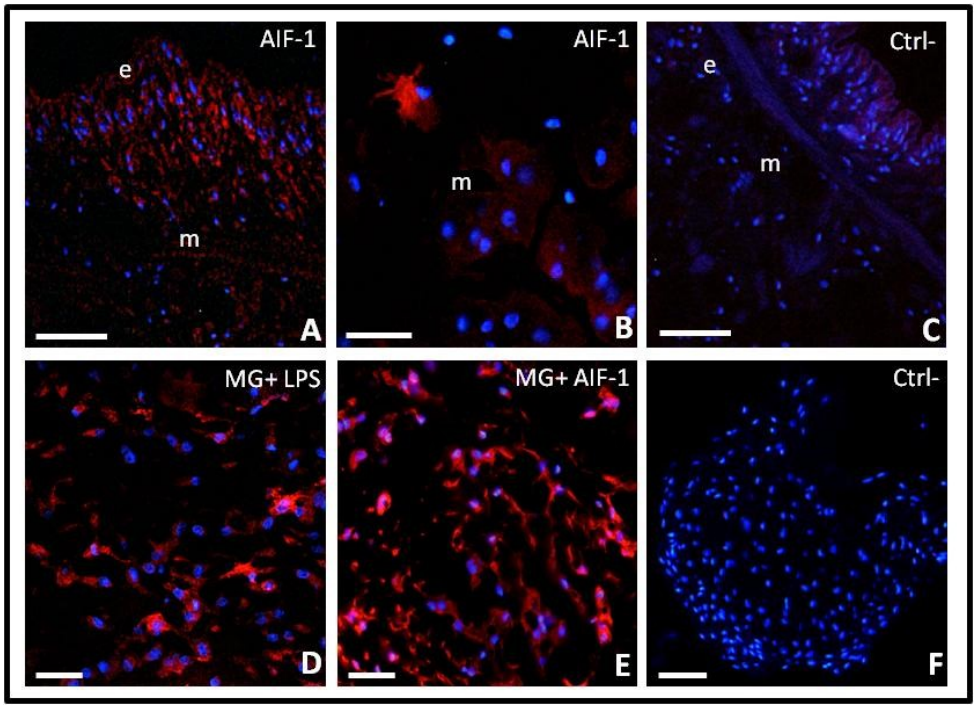


**Fig. 28.** Anti-GMFG immunolocalization on cryosections of leech body wall after 6h from r*Hm*AIF-1 injection (**A-C**) and MG pellets loaded with LPS or r*Hm*AIF-1 (**D-F**). α-GMFG is detected by a Cy3-conjugated secondary antibody (red). Numerous positive cells are visible underneath the epithelium (e) and among the muscle fibers (m). (**A-B**). Macrophages infiltrating the MG sponges result high positive for this marker (**D-E**). Negative controls (**C, F**) were performed by omitting the primary antibody. Nuclei in blue are counterstained with DAPI. Bars in A, C, F: 50 µm; Bars in B, D, E: 20 µm.

Numerous GMFG$^{+}$ migrating cells were detectable also in MWCNT supplemented MG samples (**Fig. 29 A-F**). The control slide, in which the primary antibody was omitted, resulted negative (**Fig. 29 G**). Combined transmission/fluorescence images showed the association between GMFG$^{+}$ macrophages and MWCNT aggregates (**Fig. 29 H, I**).

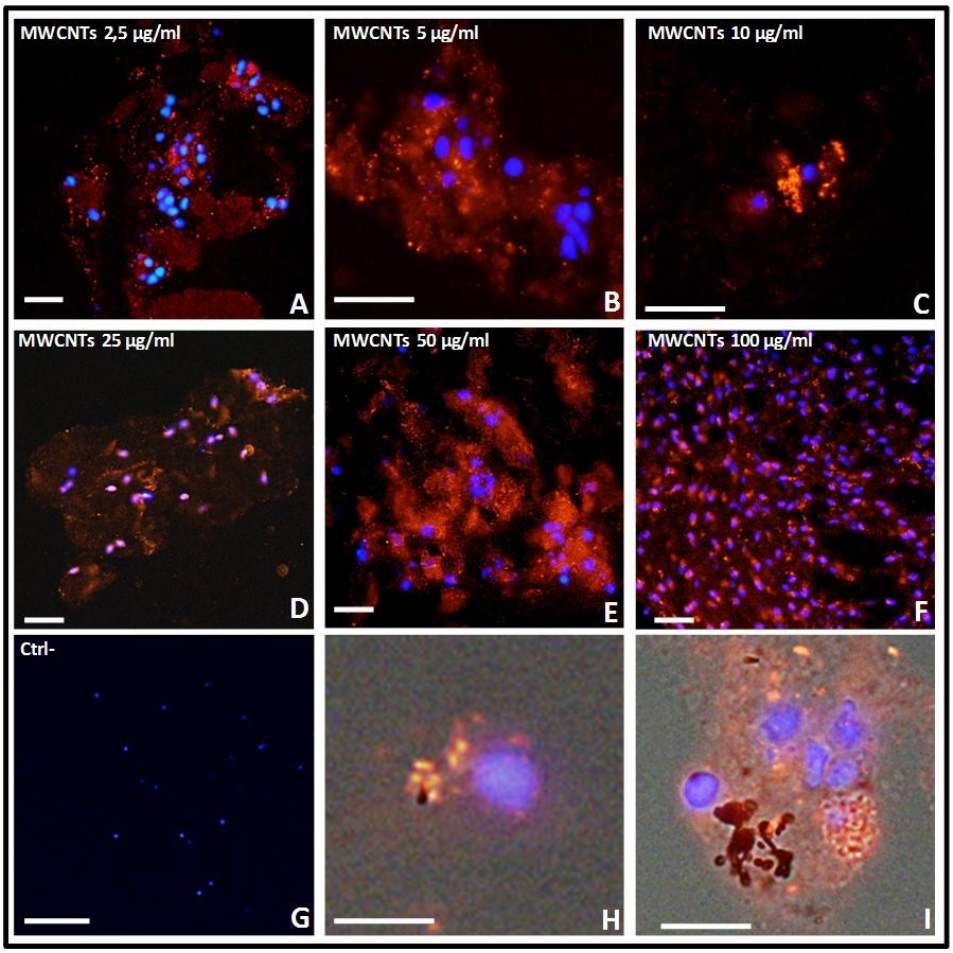


**Fig. 29.** Anti-GMFG immunolocalization on cryosections of MG supplemented with r*Hm*AIF-1 and an increasing concentration of MWCNTs. α-GMFG is detected by a Cy3-conjugated secondary antibody (red). The most part of macrophages infiltrating MWCNT supplemented MG resulted positive for this marker (**A-F**). In negative control (**G**) the primary antibody was omitted. Nuclei (blue) were counterstained with DAPI. Bars in A-F: 20 µm; bar G: 100 µm; bar in H: 5 µm; bar in I: 10 µm.

# 5. Discussion

Different contaminants, such as organic compounds (Fleeger et al., 2007; Grimaldi et al., 2012b; Ma-Hock et al., 2009) or metals (Banni et al., 2009; Bouraoui et al., 2009; Dondero et al., 2011; Maria and Bebianno, 2011), can increase the risk of cell and tissue damages. Referring to NMs, although numerous studies has been conducted since last decades, much remains unknown about their interactions with living cells (Chang et al., 2009; Du et al., 2013). With regard to the wide use of engineered NMs and their possible environmental discharge, is becoming increasingly important to study their behaviour in the environment.
In particular, since MWCNTs are already worldwide used and their production is increasing and increasing, their fate and behaviour in the environment and their interaction with cells and organisms might be taken into account (Du et al., 2013; Farré et al., 2011). In this study, we take advantage of an invertebrate model, the medicinal leech, to evaluate a set of aspects of the innate immune response to MWCNTs both *in vivo* and *in vitro* after different types of treatment.

## 5.1 Environmental exposure assay

This assay aims to mimic a possible environmental dispersion of MWCNTs, allowing us to understand the effects of this nanomaterial at the organism level. Our study shows that internalization of MWCNTs in leech tissues, validated by KOH digestion, may occur, indicating that MWCNTs mainly enter through the skin or by oral uptake during food intake.
Morphological analyses reveal the presence of MWCNT aggregates in the musculocutaneous sac and in macrophage cytoplasm. Moreover, a massive remodelling of extracellular matrix plays a role in sustain inflammation by the formation of a scaffold that support angiogenesis and immunocompetent cells migration (Oberdörster et al., 2005; Tettamanti et al., 2004).
AAS and EDS analysis confirm that no metals, such as aluminum, cobalt and iron, are detectable neither in leech exposure water nor in leech tissues, supporting that the immune responses observed are evoked by

MWCNTs and not by metal oxide impurities. Moreover, our results are consistent with literature, in which MWCNTs are seen to induce inflammation and fibrosis in different tissues in rodents (Albini et al., 2015; Lam et al., 2006).

The MWCNT-induced inflammation observed in leeches suggests the ability of this NM to overcome superficial barriers and then to promote angiogenesis, fibroplasia, immune cells migration, pro-inflammatory cytokine production and amyloid fibrils formation.

In leeches the innate immune system myeloid lineage cells, such as macrophages, perform different types of responses in relation to the antigen. Small dimensions antigens, i.e. bacteria are phagocytized while larger ones induce both cytotoxic response and encapsulation. The massive migration of macrophages towards stimulated region observed after MWCNT exposure is the same response occurring after injury or bacterial injection (Schorn et al., 2015b).

These cells derive from undifferentiated precursors, expressing the common leukocyte marker CD45, which are conveyed to the body wall by newly formed vessels. Once in the peripheral vessels, the precursors leave the bloodstream and differentiate into mature macrophages with migratory and phagocytic capacity, as demonstrated by their positivity to CD68 immunostaining and acid phosphatase reaction (Grimaldi et al., 2006).

CD45 expression trend, observed after MWCNT treatment, suggest that cyclic recruitment of monocytes aimed at maintaining an elevated number of macrophages at the inflammation site.

In addition to cytokines, already known as actors of the innate immune system (Schorn et al., 2015b), a new player in innate immune responses has been recently identified as amyloid fibril production (Albini et al., 2015). Amyloidogenesis is proposed as a detoxifying event (Alboni et al., 2011) evolutionarily conserved both in Vertebrates (Albini et al., 2015), and invertebrates (Falabella et al., 2012; Grimaldi et al., 2012a, 2012b). This event occurs also in leeches after MWCNT exposure, as demonstrated by Thioflavin-T staining. Moreover, amyloid fibril and IL-18 production increases progressively with MWCNT exposure time, in a time-dependent way, suggesting a correlation between these two events

during macrophage activation. These data are supported by recent studies showing a relation between IL-18 and amyloidogenesis process (Alboni et al., 2011, 2010).

## 5.2 Matrigel injection assay

Despite extensive investigation focused on the inflammatory response induced by carbon nanotubes, the mechanisms of interaction and entrance of these nanomaterials in the cells are still unclear.

In order to better understand this point, we focused our attention on leech macrophages observing the *in vivo* behaviour of these cells toward the nanomaterial. For this purpose we use a consolidated experimental approach based on a novel developed assay that allows the isolation of a specific cell population using the biomatrice Matrigel injected in the leech body wall (Girardello et al., 2015a; Grimaldi et al., 2011, 2009, 2008). First, we have investigated the effects of MWCNTs alone on the macrophage recruitment. Nanotubes alone induce the migration of a reduced number of macrophages into the MG sponges. The number of recruited cells in MG, allowing us to better analyze the internalization process of this nanomaterial, increase in the MG loaded with both MWCNTs and the cytokine r*Hm*AIF-1, which has been recently demonstrated to be a powerful chemoattractant for leech macrophages (Schorn et al., 2015b). One week from injection, r*Hm*AIF-1 invokes a larger number of cells within the Matrigel and MG pellets are rich in cells which are positive for both CD68 and *Hm*AIF-1, specific monocyte-macrophage markers (Grimaldi et al., 2006; Schorn et al., 2015b; Tian et al., 2006; Yang et al., 2005). Ultrastructural analysis at TEM revealed that in leech macrophages MWCNTs are both internalized in vesicles and freely dispersed in the cytoplasm.

These preliminary data suggest that short and curled MWCNTs may be internalized by phagocytosis or during the process of matrix degradation, while straight and rigid MWNCTs seem to be able to pierce cell membranes during cells migration and are then found free in the cytosol. Our findings are in accordance with the observations of other authors on vertebrate macrophages (Di Giorgio et al., 2011; Nagai and Toyokuni, 2012; Pulskamp et al., 2007). Moreover, since recent experimental

studies show that carbon nanotubes influence the aggregation process of proteins associated with neurodegenerative diseases like amyloid fibrils production, we demonstrated, by using the colorimetric methods of Thioflavin-S (Grimaldi et al., 2012a), that MWCNTs are able to induce amyloid deposits in correspondence of MWCNTs/macrophages associations. The presence of these fibrils in MWCNTs and r*Hm*AIF-1 supplemented MG confirms the strong reaction of macrophages to the nanomaterial, whereas the poor amyloid production by macrophages in samples containing only MWCNTs could be due to the small amount of cells within the matrix. The difference in number of cells recruited in the MG added only with MWCNTs in respect with MG supplemented with *Hm*AIF-1 is probably due to the fact that the chemoattractant induces a more rapid migratory response than MWCNTs alone. Starting from these preliminary results, the next goal of our work is to obtain *in vitro* expansion of macrophages primary leech cells that can be used as a sensitive method to evaluate the presence of the nanomaterial in contaminated water.

## 5.3 *In vitro* treatment

Our data on MWCNT injection show the ability of MWCNTs to induce macrophage migration and activation within the MG matrix *in vivo*. Starting from these results, *in vitro* studies have been necessary to clarify the interactions between MWCNTs and macrophages and the effects of this NM on immune cells.

We have isolated these cells *in vivo*, by means of the biopolymer MG supplemented with r*Hm*-AIF-1, in order to obtain primary culture of leech macrophages. After 1 week culture, the same specific macrophage markers (CD45, CD68, *Hm*AIF-1) observed *in vivo* are expressed by these cells.

The ability of MWCNTs to induce amyloid fibrils production, already observed in the *in vivo* assay, has been confirmed and the amounts of amyloid fibrils have been assessed by measuring Thioflavin-S fluorescence. This dye is strictly specific for amyloid fibril structure and it can be used as a detector of their production. A significant increase in Thioflavin-S staining has been observed in exposed macrophages with

respect to untreated cells. This concentration-dependent amyloid fibril production is necessary for the formation of a scaffold around MWCNTs aggregates, creating a barrier to contain the exogenous material.

## 5.4 Proliferation, apoptosis and ROS production

Our recent data show that environmental dispersion of MWCNTs induces a strong immune response in the medicinal leech, causing, among other effects, a massive migration of macrophages (positive for CD45 and CD68 markers) (Girardello et al., 2015b). Moreover, ultrastructural analysis demonstrated that MWCNTs are be able to pierce cell membranes, leading to possible ROS increase and consequently to the onset of cell death mechanisms (Girardello et al., 2015a). In this study, we focused on these aspects, investigating the effects of MWCNTs on leeches both *in vivo*, by environmental exposure and subcutaneous injection, and *in vitro*.

The proliferation assay on MG sponges demonstrates that our consolidated experimental approach for macrophage isolation (Girardello et al., 2015a; Grimaldi et al., 2011, 2009) does not cause damages to cells, which retain their proliferative ability. On the other hand, after MWCNT *in vitro* treatment this ability significantly decreases.

As revealed by TUNEL assay, both MWCNT environmental dispersion and injection are able to induce apoptosis. Moreover, our *in vitro* approach lead us to affirm that there is a correlation between apoptosis and MWCNT treatment, and that the observed effect is dose and time dependent. These data are consistent with other studies indicating the induction of apoptosis as an indicator of NMs toxicity (Torres and Fadeel, 2013). In addition, we provide evidences of an increase in ROS production after MWCNT exposure. Since ROS increase is generally considered a major contributor to NM toxicity (Saria et al., 2014; Shvedova et al., 2012), we assume that it can also concur in apoptosis induction. Moreover, since MWCNTs were observed in the cytoplasm of cells showing nor morphological alterations nor membrane ruptures, we are confident that ROS and apoptosis are induced by MWCNT entrance and not by membrane damages.

In conclusion, our study provides evidence to support that MWCNTs are able to induce, both *in vivo* and *in vitro*, a plethora of inflammatory responses leading cells to a strong production of ROS, a reduced proliferation rate and the onset of programmed cell death pathways. In particular, *in vitro* treatment demonstrated that the observed responses are correlated to both MWCNTs doses and exposure time.
Taken together, our results represent another relevant piece in the puzzle of NM toxicity. Moreover, since autophagic cell death pathway activation is emerging as a possible consequence of MWCNT treatment (Tsukahara et al., 2015), in the future we will attempt to clarify this aspect in order to completely understand MWCNT-induces toxicity.

## 5.5 Inflammatory markers in leeches

In the present study, we have demonstrated that, in the medicinal leech, the factors MIF and GMFG are highly expressed by macrophage-like cell exhibiting a similar function to MIF and GMFG of vertebrates. Moreover, we show that, in leeches, as in Vertebrates, these molecules are constitutively expressed in untreated animals but they are dramatically enhanced after any stimulation, such as LPS or cytokine injection and MWCNT treatment.
Despite *H*MIF sequence has been identify in the EST library from the leech CNS and then sequenced, the presence of the protein in the CNS is not confirmed yet. Whole mount immunolocalization shows a feeble positivity in the nerve cord, indicating that this protein in not abundant in this department. In fact, at confocal microscopy, only few positive cells are visible at lesion site. On the other hand, MIF is highly expressed by migrating cells in the body wall after LPS injection but also by resident macrophages in untreated leeches suggesting a constitutive expression of this cytokine. Using the biopolymer MG as *Hm*AIF-1 or LPS-rich microenvironment we have been able to isolate and better characterize these cells from an immunocytochemical point of view. In r*Hm*AIF-1 supplemented MG sponge cryosections a remarkable positivity for MIF antibody is detectable in macrophage cytoplasm, while in LPS supplemented samples a spread positivity throughout the matrix is clearly visible, suggesting that MIF is released by LPS activated

macrophages. Moreover, the same spread positivity is observed in high dose MWCNT supplemented samples, indicating the ability of this NM to activate macrophages. Overall, these data indicate that, in leech as well as in mammals (Bacher et al., 1998; Roger et al., 2003), MIF is constitutively expressed by macrophages and released after inflammatory stimuli.

With regard to GMF, as already described for MIF, we found a basal expression of GMFG in leech CNS. In this tissues GMFG is detectable as a spotted signal localized in macroglial cell cytoplasm and in the area around the injured connectives where microglial cells in active migration are accumulated. These results are consistent with literature data on mammals, where GMFG is found only at low levels in the CNS (Ikeda et al., 2006). By contrast, GMFG is highly expressed in the body wall and in particular in many cells located among the muscle fibers and migrating towards the *Hm*AIF-1 injected area. These migrating cells are macrophages, as confirmed by the immunohistochemical analysis of MG sponge supplemented with LPS or r*Hm*AIF-1, which are known to be specific leech macrophages chemoattractant (Girardello et al., 2015a; Schorn et al., 2015b). Indeed a high level of expression of this marker is mainly detected in the cytoplasmic expansions of the MWCNT supplemented MG infiltrated cells. These data lead us to speculate that this molecule could be involved, like in Vertebrates, in actin cytoskeleton remodelling during the migrating process (Gandhi et al., 2010).

# 6. Conclusions

Environmental pollution is an issue that needs to be addressed. Human or animal exposure to different compounds has been shown to lead to tissue, cells and DNA damages rousing to several disorders and pathologies (Lam et al., 2006; Simate et al., 2012). As far as concern NMs, although this topic has been studied since decades, much remains unclear about their behaviour in association with the biotic compartment (Du et al., 2013; Oberdörster et al., 2005). Between NMs, MWCNTs are currently worldwide produced and used in different applications. This large-scale production drastically increases the risk of their dispersion in the environment, becoming a potential hazard to animal and human health. For these reasons, the effects of MWCNTs, as well as other NMs, need to be studied from all point of view.

In this context, Annelids have been studied since long time because of their immune reactions, in response to very different stimuli, which is very functionally similar to those of vertebrates involving the same molecules (de Eguileor et al., 2003, 2000a; Grimaldi et al., 2006; Hayashi and Engelmann, 2013). Here we use the medicinal leech to evaluate a set of aspects of the innate immune response to MWCNTs both *in vivo* and *in vitro*. Our recent studies show that MWCNTs environmental exposure causes in the leech an extremely rapid inflammatory response, inducing a strong cytokine production (in particular IL-18) and involving mainly $CD45^+/CD68^+$ macrophage-like cells (Girardello et al., 2015b), suggesting the ability of this NM to overcome superficial barriers.

Moreover, a novel developed assay based on the use of a biomatrix (MATRIGEL) (Grimaldi et al., 2011, 2009, 2008) was used to study macrophages behaviours after MWCNT *in vivo* injection, showing the ability of this NM to enter the cells not only by active phagocytosis but also by piercing cell membranes (Girardello et al., 2015a).

Leeches macrophages primary cultures have also been studied before and after MWCNTs treatment. Our results demonstrate that MWCNTs are able to induce, both *in vivo* and *in vitro*, a plethora of inflammatory responses leading cells to a strong production of ROS, a reduced proliferation rate and the onset of programmed cell death pathways. In

particular, *in vitro* treatment demonstrated that the observed responses are correlated to both MWCNT dose and exposure time. Taken together, our results represent another relevant piece in the puzzle of nanomaterial toxicity. Moreover, since autophagic cell death pathway activation is emerging as a possible consequence of MWCNT treatment (Tsukahara et al., 2015), in the future we will attempt to clarify this aspect in order to completely understand MWCNTs-induces toxicity.

Finally, it is important to emphasize that nowadays the scientific community has the urgent need to reduce *in vivo* study in accordance with international guidelines concerning animal testing (Boyles et al., 2015).

In the light of the facts, our data, not only represent a cornerstone in the determination of the toxicity of pristine MWCNTs, but they also attest the relevance of our alternative model to study, both *in vivo* and *in vitro*, the possible harmful effects of any NM.

Further research is necessary to deeply investigate the fate of MWCNTs once in the cell. In this perspective, it would be interesting to understand how much biopersistant are MWCNTs and whether macrophages are able to completely reject them. Another issue that should be addressed is the detection of an exposure limit to avoid an ecological disaster and to protect environmental, animal and human health. Finally, our experimental model and our pool of techniques may be developed to become a sensitive tool to study the presence and the effects of any NM in the aquatic compartment.

# 7. Bibliography

2011/696/EU. 2011. Commission Reccomendation on the definition of nanomaterial. *Official Journal of the European Union*, 54: 38–40

Aerbajinai W, Lee K, Chin K, Rodgers GP. 2013. Glia maturation factor-γ negatively modulates TLR4 signaling by facilitating TLR4 endocytic trafficking in macrophages. *Journal of immunology (Baltimore, Md. : 1950)*, 190: 6093–103

Aerbajinai W, Liu L, Chin K, Zhu J, Parent C a, Rodgers GP. 2011. Glia maturation factor-{gamma} mediates neutrophil chemotaxis. *Journal of leukocyte biology*, 90: 529–538

Albini A, Pagani A, Pulze L, Bruno A, Principi E, Congiu T, Gini E, Grimaldi A, Bassani B, De Flora S, de Eguileor M, Noonan DM. 2015. Environmental impact of multi-wall carbon nanotubes in a novel model of exposure: systemic distribution, macrophage accumulation, and amyloid deposition. *International journal of nanomedicine*, 10: 6133–45

Alboni S, Cervia D, Sugama S, Conti B. 2010. Interleukin 18 in the CNS. *Journal of neuroinflammation*, 7: 9

Alboni S, Montanari C, Benatti C, Blom JMC, Simone ML, Brunello N, Caggia F, Guidotti G, Marcondes MCG, Sanchez-Alavez M, Conti B, Tascedda F. 2011. Constitutive and LPS-regulated expression of interleukin-18 receptor beta variants in the mouse brain. *Brain, Behavior, and Immunity*, 25: 483–493

Ali D, Ahmed M, Alarifia S, Ali H. 2014. Ecotoxicity of single-wall carbon nanotubes to freshwater snail Lymnaea luteola L.: Impacts on oxidative stress and genotoxicity. *Environmental Toxicology*, 30: 674–682

Alloy MM, Roberts AP. 2011. Effects of suspended multi-walled carbon nanotubes on daphnid growth and reproduction. *Ecotoxicology and Environmental Safety*, 74: 1839–1843

Asai K, Fujita K, Yamamoto M, Hotta T, Morikawa M, Kokubo M, Moriyama A, Kato T. 1998. Isolation of novel human cDNA (hGMF-gamma) homologous to Glia Maturation Factor-beta gene. *Biochimica et biophysica acta*, 1396: 242–4

Bach J-P, Deuster O, Balzer-Geldsetzer M, Meyer B, Dodel R, Bacher M. 2009. The role of macrophage inhibitory factor in tumorigenesis and central nervous system tumors. *Cancer*, 115: 2031–2040

Bacher M, Meinhardt a, Lan HY, Dhabhar FS, Mu W, Metz CN, Chesney J a, Gemsa D, Donnelly T, Atkins RC, Bucala R. 1998. MIF expression in the rat brain: implications for neuronal function. *Molecular medicine (Cambridge, Mass.)*, 4: 217–230

Banni M, Bouraoui Z, Clerandeau C, Narbonne JF, Boussetta H. 2009. Mixture toxicity assessment of cadmium and benzo[a]pyrene in the sea worm Hediste diversicolor. *Chemosphere*, 77: 902–906

Blanco GA, Escalada AM, Alvarez E, Hajos S. 1997. LPS-induced stimulation of phagocytosis in the sipunculan worm Themiste petricola: possible involvement of

human CD14, CD11B and CD11C cross-reactive molecules. *Developmental and comparative immunology*, 21: 349–62

Bouraoui Z, Banni M, Ghedira J, Clerandeau C, Narbonne JF, Boussetta H. 2009. Evaluation of enzymatic biomarkers and lipoperoxidation level in Hediste diversicolor exposed to copper and benzo[a]pyrene. *Ecotoxicology and Environmental Safety*, 72: 1893–1898

Boyles MSP, Young L, Brown DM, MacCalman L, Cowie H, Moisala A, Smail F, Smith PJW, Proudfoot L, Windle AH, Stone V. 2015. Multi-walled carbon nanotube induced frustrated phagocytosis, cytotoxicity and pro-inflammatory conditions in macrophages are length dependent and greater than that of asbestos. *Toxicology in Vitro*, 29: 1513–1528

Calandra T. 2003. Macrophage migration inhibitory factor and host innate immune responses to microbes. *Scandinavian journal of infectious diseases*, 35: 573–576

Chang X, Ji G, Sui Q, Huang J, Yu G. 2009. Rapid photocatalytic degradation of PCP-Na over NaBiO3 driven by visible light irradiation. *Journal of Hazardous Materials*, 166: 728–733

Cooper EL, Roch P. 2003. Earthworm immunity: a model of immune competence. *Pedobiologia*, 47: 676–688

Cossarizza A, Cooper EL, Suzuki MM, Salvioli S, Capri M, Gri G, Quaglino D, Franceschi C. 1996. Earthworm Leukocytes That Are Not Phagocytic and Cross-React with Several Human Epitopes Can Kill Human Tumor Cell Lines. *Experimental Cell Research*, 224: 174–182

Coutris C, Hertel-Aas T, Lapied E, Joner EJ, Oughton DH. 2012. Bioavailability of cobalt and silver nanoparticles to the earthworm Eisenia fetida. *Nanotoxicology*, 6: 186–95

Cox GM, Kithcart a. P, Pitt D, Guan Z, Alexander J, Williams JL, Shawler T, Dagia NM, Popovich PG, Satoskar a. R, Whitacre CC. 2013. Macrophage Migration Inhibitory Factor Potentiates Autoimmune-Mediated Neuroinflammation. *The Journal of Immunology*, 191: 1043–1054

Dai H. 2002. Carbon nanotubes: Synthesis, integration, and properties. *Accounts of Chemical Research*, 35: 1035–1044

de Eguileor M, Grimaldi a, Tettamanti G, Valvassori R, Cooper EL, Lanzavecchia G. 2000a. Different types of response to foreign antigens by leech leukocytes. *Tissue & cell*, 32: 40–48

de Eguileor M, Grimaldi a, Tettamanti G, Valvassori R, Cooper EL, Lanzavecchia G. 2000b. Lipopolysaccharide-dependent induction of leech leukocytes that cross-react with vertebrate cellular differentiation markers. *Tissue & cell*, 32: 437–445

de Eguileor M, Grimaldi A, Tettamanti G, Congiu T, Protasoni M, Reguzzoni M, Valvassori R, Lanzavecchia G. 2001a. Ultrastructure and functional versatility of hirudinean botryoidal tissue. *Tissue & cell*, 33: 332–341

de Eguileor M, Grimaldi A, Tettamanti G, Ferrarese R, Congiu T, Protasoni M, Perletti G, Valvassori R, Lanzavecchia G. 2001b. Hirudo medicinalis: A new model for testing activators and inhibitors of angiogenesis. *Angiogenesis*, 4: 299–312

de Eguileor M, Tettamanti G, Grimaldi a, Boselli a, Scarì G, Valvassori R, Cooper EL, Lanzavecchia G. 1999. Histopathological changes after induced injury in leeches. *Journal of invertebrate pathology*, 74: 14–28

de Eguileor M, Tettamanti G, Grimaldi A, Congiu T, Ferrarese R, Perletti G, Valvassori R, Cooper EL, Lanzavecchia G. 2003. Leeches: immune response, angiogenesis and biomedical applications. *Current pharmaceutical design*, 9: 133–147

Demir E, Vales G, Kaya B, Creus A, Marcos R. 2011. Genotoxic analysis of silver nanoparticles in Drosophila. *Nanotoxicology*, 5: 417–424

Di Giorgio ML, Bucchianico S Di, Ragnelli AM, Aimola P, Santucci S, Poma A. 2011. Effects of single and multi walled carbon nanotubes on macrophages: Cyto and genotoxicity and electron microscopy. *Mutation Research - Genetic Toxicology and Environmental Mutagenesis*, 722: 20–31

Donaldson K, Murphy F a, Duffin R, Poland C a. 2010. Asbestos, carbon nanotubes and the pleural mesothelium: a review of the hypothesis regarding the role of long fibre retention in the parietal pleura, inflammation and mesothelioma. *Particle and fibre toxicology*, 7: 5

Donaldson K, Stone V, Tran CL, Kreyling W, Borm PJA. 2004. Nanotoxicology. *Occupational and environmental medicine*, 61: 727–8

Dondero F, Banni M, Negri A, Boatti L, Dagnino A, Viarengo A. 2011. Interactions of a pesticide/heavy metal mixture in marine bivalves: a transcriptomic assessment. *BMC genomics*, 12: 195

Drago F, Sautière PE, Le Marrec-Croq F, Accorsi A, Van Camp C, Salzet M, Lefebvre C, Vizioli J. 2014. Microglia of medicinal leech (Hirudo medicinalis) express a specific activation marker homologous to vertebrate ionized calcium-binding adapter molecule 1 (Iba1/alias aif-1). *Developmental Neurobiology*, 74: 987–1001

Du J, Wang S, You H, Zhao X. 2013. Understanding the toxicity of carbon nanotubes in the environment is crucial to the control of nanomaterials in producing and processing and the assessment of health risk for human: A review. *Environmental Toxicology and Pharmacology*, 36: 451–462

Edgington AJ, Roberts AP, Taylor LM, Alloy MM, Reppert J, Rao AM, Mao J, Klaine SJ. 2010. The influence of natural organic matter on the toxicity of multiwalled carbon nanotubes. *Environmental Toxicology and Chemistry*, 29: 2511–2518

Engelmann P, Cooper EL, Németh P. 2005. Anticipating innate immunity without a Toll. *Molecular Immunology*, 42: 931–942

Falabella P, Riviello L, Pascale M, Di Lelio I, Tettamanti G, Grimaldi A, Iannone C, Monti M, Pucci P, Tamburro AM, deEguileor M, Gigliotti S, Pennacchio F. 2012. Functional amyloids in insect immune response. *Insect Biochemistry and Molecular Biology*, 42: 203–211

Farré M, Sanchís J, Barceló D. 2011. Analysis and assessment of the occurrence, the fate and the behavior of nanomaterials in the environment. *TrAC - Trends in Analytical Chemistry*, 30: 517–527

Fleeger JW, Gust KA, Marlborough SJ, Tita G. 2007. Mixtures of metals and polynuclear aromatic hydrocarbons elicit complex, nonadditive toxicological interactions in

meiobenthic copepods. *Environmental toxicology and chemistry / SETAC*, 26: 1677–1685

Fowler DM, Koulov A V., Alory-Jost C, Marks MS, Balch WE, Kelly JW. 2006. Functional amyloid formation within mammalian tissue. *PLoS Biology*, 4: 0100–0107

Gandhi M, Smith BA, Bovellan M, Paavilainen V, Daugherty-Clarke K, Gelles J, Lappalainen P, Goode BL. 2010. GMF is a cofilin homolog that binds Arp2/3 complex to stimulate filament debranching and inhibit actin nucleation. *Current biology : CB*, 20: 861–7

Girardello R, Drago F, de Eguileor M, Valvassori R, Vizioli J, Tettamanti G, Grimaldi A. 2015a. Cytokine impregnated biomatrix: a new tool to study multi-wall carbon nanotubes effects on invertebrate immune cells. *journal of nanomedicine and nanotechnology*, 6: 323

Girardello R, Tasselli S, Baranzini N, Valvassori R, de Eguileor M, Grimaldi A. 2015b. Effects of Carbon Nanotube Environmental Dispersion on an Aquatic Invertebrate, Hirudo medicinalis. *Plos One*, 10: e0144361

Gottschalk F, Sun T, Nowack B. 2013. Environmental concentrations of engineered nanomaterials: Review of modeling and analytical studies. *Environmental Pollution*, 181: 287–300

Grieb G, Merk M, Bernhagen J, Bucala R. 2010. Macrophage migration inhibitory factor (MIF): a promising biomarker. *Drug news & perspectives*, 23: 257–64

Grimaldi A. 2016. Origin and fate of hematopoietic stem precursor cells in the leech Hirudo medicinalis A Grimaldi Abstract The hematopoietic process by which blood cells are formed has been intensely studied for over a century using several model systems . An increasing a. *Invertebrate Survival Journal*, 13: 257–268

Grimaldi a, Tettamanti G, Rinaldi L, Perletti G, Valvassori R, Eguileor M De. 2004. Role of cathepsin B in leech wound healing. *ISJ*, 38–46

Grimaldi A, Banfi S, Gerosa L, Tettamanti G, Noonan DM, Valvassori R, de Eguileor M. 2009. Identification, isolation and expansion of myoendothelial cells involved in leech muscle regeneration. *PLoS ONE*, 4: e7652

Grimaldi A, Banfi S, Vizioli J, Tettamanti G, Noonan DM, de Eguileor M. 2011. Cytokine Loaded Biopolymers as a Novel Strategy to Study Stem Cells during Wound-Healing Processes. *Macromolecular Bioscience*, 11: 1008–1019

Grimaldi A, Bianchi C, Greco G, Tettamanti G, Noonan DM, Valvassori R, de Eguileor M. 2008. In vivo isolation and characterization of stem cells with diverse phenotypes using growth factor impregnated biomatrices. *PLoS ONE*, 3: e1910.

Grimaldi A, Ferrarese R, Tettamanti G, Valvassori R, de Eguileor M. 2013. Ras activation in Hirudo medicinalis angiogenic process. *Invertebrate Survival Journal*, 10: 7–14

Grimaldi A, Girardello R, Malagoli D, Falabella P, Tettamanti G, Valvassori R, Ottaviani E, de Eguileor M. 2012a. Amyloid / Melanin distinctive mark in invertebrate immunity. *Invertebrate Survival Journal*, 9: 153–162

Grimaldi A, Tettamanti G, Congiu T, Girardello R, Malagoli D, Falabella P, Valvassori R, Ottaviani E, de Eguileor M. 2012b. The main actors involved in parasitization of

Heliothis virescens larva. *Cell and Tissue Research*, 350: 491–502

Grimaldi A, Tettamanti G, Girardello R, Pulze L, Valvassori R, Malagoli D, Ottaviani E, de Eguileor M. 2014. Functional amyloid formation in LPS activated cells from invertebrates to vertebrates. *Invertebrate Survival Journal*, 11: 286–297

Grimaldi A, Tettamanti G, Perletti G, Valvassori R, de Eguileor M. 2006. Hematopoietic cell formation in leech wound healing. *Current pharmaceutical design*, 12: 3033–3041

Handy RD, von der Kammer F, Lead JR, Hassellöv M, Owen R, Crane M. 2008. The ecotoxicology and chemistry of manufactured nanoparticles. *Ecotoxicology (London, England)*, 17: 287–314

Hayashi Y, Engelmann P. 2013. Earthworm's immunity in the nanomaterial world : new room , future challenges. *Invertebrate Survival Journal*, 10: 69–76

Hayashi Y, Engelmann P, Foldbjerg R, Szabó M, Somogyi I, Pollák E, Molnár L, Autrup H, Sutherland DS, Scott-Fordsmand J, Heckmann LH. 2012. Earthworms and humans in vitro: Characterizing evolutionarily conserved stress and immune responses to silver nanoparticles. *Environmental Science and Technology*, 46: 4166–4173

Huguet G, Molinas M. 1996. Myofibroblast-like cells and wound contraction in leech wound healing. *The Journal of Experimental Zoology*, 275: 308–316

Huguet G, Molinas M. 1994. The pseudoblastema in the wound healing process of the leechHirudo medicinalis L. (Hirudinea): Changes in cell junctions. *Journal of Experimental Zoology*, 269: 23–36

Hussain S, Sangtian S, Anderson SM, Snyder RJ, Marshburn JD, Rice AB, Bonner JC, Garantziotis S. 2014. Inflammasome activation in airway epithelial cells after multi-walled carbon nanotube exposure mediates a profibrotic response in lung fibroblasts. *Particle and Fibre Toxicology*, 11: 28–44

Iijima S. 1991. Helical microtubules of graphitic carbon. *Nature*, 354: 56–58

Ikeda K, Kundu RK, Ikeda S, Kobara M, Matsubara H, Quertermous T. 2006. Glia maturation factor-gamma is preferentially expressed in microvascular endothelial and inflammatory cells and modulates actin cytoskeleton reorganization. *Circulation Research*, 99: 424–433

Kagan VE, Bayir H, Shvedova AA. 2005. Nanomedicine and nanotoxicology: two sides of the same coin. *Nanomedicine: Nanotechnology, Biology and Medicine*, 1: 313–316

Kaplan R, Zaheer A, Jaye M, Lim R. 1991. Molecular Cloning and Expression of Biologically Active Human Glia Maturation Factor-? *Journal of Neurochemistry*, 57: 483–490

Kawata K, Osawa M, Okabe S. 2009. In vitro toxicity of silver nanoparticles at noncytotoxic doses to HepG2 human hepatoma cells. *Environmental Science and Technology*, 43: 6046–6051

Kennedy AJ, Gunter JC, Chappell MA, Goss JD, Hull MS, Kirgan RA, Steevens JA. 2009. Influence of nanotube preparation in aquatic bioassays. *Environmental toxicology and chemistry / SETAC*, 28: 1930–1938

Lam C-W, James JT, McCluskey R, Arepalli S, Hunter RL. 2006. A review of carbon nanotube toxicity and assessment of potential occupational and environmental health risks. *Critical reviews in toxicology*, 36: 189–217

Le Marrec-Croq F, Drago F, Vizioli J, Sautière PE, Lefebvre C. 2013. The leech nervous system: A valuable model to study the microglia involvement in regenerative processes. *Clinical and Developmental Immunology*, 2013: 274019

Liu Z, Tabakman S, Welsher K, Dai H. 2009. Carbon Nanotubes in Biology and Medicine: In vitro and in vivo Detection, Imaging and Drug Delivery. *Nano research*, 2: 85–120

Macagno ER, Gaasterland T, Edsall L, Bafna V, Soares MB, Scheetz T, Casavant T, Da Silva C, Wincker P, Tasiemski A, Salzet M. 2010. Construction of a medicinal leech transcriptome database and its application to the identification of leech homologs of neural and innate immune genes. *BMC genomics*, 11: 407

Ma-Hock L, Treumann S, Strauss V, Brill S, Luizi F, Mertler M, Wiench K, Gamer AO, van Ravenzwaay B, Landsiedel R. 2009. Inhalation toxicity of multiwall carbon nanotubes in rats exposed for 3 months. *Toxicological sciences : an official journal of the Society of Toxicology*, 112: 468–81

Mann KH. 1962. Leeches (Hirudinea) their structure, physiology, ecology and embryology

Maria VL, Bebianno MJ. 2011. Antioxidant and lipid peroxidation responses in Mytilus galloprovincialis exposed to mixtures of benzo(a)pyrene and copper. *Comparative Biochemistry and Physiology - C Toxicology and Pharmacology*, 154: 56–63

Milutinović B, Kurtz J. 2016. Immune memory in invertebrates. *Seminars in Immunology*, 28: 328–342

Mitchell GB, Khandaker MH, Rahimpour R, Xu L, Lazarovits AI, Pickering JG, Suria H, Madrenas J, Pomerantz DK, Feldman RD, Kelvin DJ. 1999. CD45 modulation of CXCR1 and CXCR2 in human polymorphonuclear leukocytes. *European journal of immunology*, 29: 1467–76

Moore RD, Mumaw V, Schoenberg MD. 1960. Optical microscopy of ultrathin tissue sections. *Journal of ultrastructure research*, 4: 113–116

Nagai H, Toyokuni S. 2012. Differences and similarities between carbon nanotubes and asbestos fibers during mesothelial carcinogenesis: Shedding light on fiber entry mechanism. *Cancer Science*, 103: 1378–1390

Nicholls JG, Baylor D a. 1968. Specific modalities and receptive fields of sensory neurons in CNS of the leech. *Journal of Neurophysiology*, 31: 740–756

Nowack B, Bucheli TD. 2007. Occurrence, behavior and effects of nanoparticles in the environment. *Environmental Pollution*, 150: 5–22

Oberdörster G, Oberdörster E, Oberdörster J. 2005. Nanotoxicology: An emerging discipline evolving from studies of ultrafine particles. *Environmental Health Perspectives*, 113: 823–839

Park MVDZ, Neigh AM, Vermeulen JP, de la Fonteyne LJJ, Verharen HW, Briedé JJ, van Loveren H, de Jong WH. 2011. The effect of particle size on the cytotoxicity,

inflammation, developmental toxicity and genotoxicity of silver nanoparticles. *Biomaterials*, 32: 9810–9817

Paterson G, Macken A, Thomas K V. 2011. The need for standardized methods and environmental monitoring programs for anthropogenic nanoparticles. *Analytical Methods*, 3: 1461

Poland C a, Duffin R, Kinloch I, Maynard A, Wallace W a H, Seaton A, Stone V, Brown S, Macnee W, Donaldson K. 2008. Carbon nanotubes introduced into the abdominal cavity of mice show asbestos-like pathogenicity in a pilot study. *Nature nanotechnology*, 3: 423–428

Poulsen SS, Saber AT, Williams A, Andersen O, Købler C, Atluri R, Pozzebon ME, Mucelli SP, Simion M, Rickerby D, Mortensen A, Jackson P, Kyjovska ZO, Mølhave K, Jacobsen NR, Jensen KA, Yauk CL, Wallin H, Halappanavar S, Vogel U. 2015. MWCNTs of different physicochemical properties cause similar inflammatory responses, but differences in transcriptional and histological markers of fibrosis in mouse lungs. *Toxicology and Applied Pharmacology*, 284: 16–32

Pulskamp K, Diabaté S, Krug HF. 2007. Carbon nanotubes show no sign of acute toxicity but induce intracellular reactive oxygen species in dependence on contaminants. *Toxicology Letters*, 168: 58–74

Ravichandran P, Baluchamy S. 2010. Multiwalled carbon nanotubes activate NF- j B and AP-1 signaling pathways to induce apoptosis in rat lung epithelial cells. *Apoptosis*, 15: 1507–1516

Rawat N, Sandhya, Subaharan K, Eswaramoorthy M, Kaul G. 2016. Comparative in vivo toxicity assessment places multiwalled carbon nanotubes at a higher level than mesoporous silica nanoparticles. *Toxicology and industrial health*, 748233715622307

Rittinghausen S, Hackbarth A, Creutzenberg O, Ernst H, Heinrich U, Leonhardt A, Schaudien D, Miller B, Searl A, Donaldson K, Hoenerhoff M, et al. 2014. The carcinogenic effect of various multi-walled carbon nanotubes (MWCNTs) after intraperitoneal injection in rats. *Particle and Fibre Toxicology*, 11: 59

Roach T, Slater S, Koval M, White L, McFarland EC, Okumura M, Thomas M, Brown E. 1997. CD45 regulates Src family member kinase activity associated with macrophage integrin-mediated adhesion. *Current Biology*, 7: 408–417

Roberts AP, Mount AS, Seda B, Souther J, Qiao R, Lin S, Pu CK, Rao AM, Klaine SJ. 2007. In vivo biomodification of lipid-coated carbon nanotubes by Daphnia magna. *Environmental Science and Technology*, 41: 3028–3029

Roger T, Froidevaux C, Martin C, Calandra T. 2003. Macrophage migration inhibitory factor (MIF) regulates host responses to endotoxin through modulation of Toll-like receptor 4 (TLR4). *Journal of endotoxin research*, 9: 119–123

Saria R, Mouchet F, Perrault A, Flahaut E, Laplanche C, Boutonnet J-C, Pinelli E, Gauthier L. 2014. Short term exposure to multi-walled carbon nanotubes induce oxidative stress and DNA damage in Xenopus laevis tadpoles. *Ecotoxicology and Environmental Safety*, 107: 22–29

Sawyer RT. 1986. Leech biology and behaviour 1: anatomy, physiology and behaviour.

Oxford University press

Schikorski D, Cuvillier-Hot V, Leippe M, Boidin-Wichlacz C, Slomianny C, Macagno E, Salzet M, Tasiemski A. 2008. Microbial challenge promotes the regenerative process of the injured central nervous system of the medicinal leech by inducing the synthesis of antimicrobial peptides in neurons and microglia. *Journal of immunology (Baltimore, Md. : 1950)*, 181: 1083–1095

Schnorr JM, Swager TM. 2011. Emerging applications of carbon nanotubes. *Chemistry of Materials*, 23: 646–657

Schorn T, Drago F, Eguileor M De, Valvassori R, Vizioli J, Tettamanti G, Grimaldi A. 2015a. The Allograft Inflammatory Factor-1 ( AIF-1 ) homologous in Hirudo medicinalis ( medicinal leech ) is involved in immune response during wound healing and graft rejection processes Abstract Allograft inflammatory factor-1 ( AIF-1 ) is a 17 kDa cytokine-in. *ISJ*, 1: 129–141

Schorn T, Drago F, Tettamanti G, Valvassori R, de Eguileor M, Vizioli J, Grimaldi A. 2015b. Homolog of allograft inflammatory factor-1 induces macrophage migration during innate immune response in leech. *Cell and Tissue Research*, 359: 853–864

Shoults-Wilson WA, Reinsch BC, Tsyusko O V, Bertsch PM, Lowry G V, Unrine JM. 2011a. Effect of silver nanoparticle surface coating on bioaccumulation and reproductive toxicity in earthworms (Eisenia fetida). *Nanotoxicology*, 5: 432–444

Shoults-Wilson WA, Zhurbich OI, McNear DH, Tsyusko O V., Bertsch PM, Unrine JM. 2011b. Evidence for avoidance of Ag nanoparticles by earthworms (Eisenia fetida). *Ecotoxicology*, 20: 385–396

Shvedova AA, Pietroiusti A, Fadeel B, Kagan VE. 2012. Mechanisms of carbon nanotube-induced toxicity : Focus on oxidative stress. *Toxicology and Applied Pharmacology*, 261: 121–133

Simate GS, Iyuke SE, Ndlovu S, Heydenrych M, Walubita LF. 2012. Human health effects of residual carbon nanotubes and traditional water treatment chemicals in drinking water. *Environment International*, 39: 38–49

St-Pierre J, Ostergaard HL, Thomas M, D'Oro U, Ashwell J, Hermiston M, Xu Z, Weiss A, Saunders A, Johnson P, Avraham S, et al. 2013. A Role for the Protein Tyrosine Phosphatase CD45 in Macrophage Adhesion through the Regulation of Paxillin Degradation. *PLoS ONE*, 8: e71531

Tettamanti G, Grimaldi A, Congiu T, Perletti G, Raspanti M, Valvassori R, de Eguileor M. 2005. Collagen reorganization in leech wound healing. *Biology of the cell / under the auspices of the European Cell Biology Organization*, 97: 557–568

Tettamanti G, Grimaldi A, Ferrarese R, Palazzi M, Perletti G, Valvassori R, Cooper EL, Lanzavecchia G, de Eguileor M. 2003a. Leech responses to tissue transplantation. *Tissue & cell*, 35: 199–2012

Tettamanti G, Grimaldi A, Rinaldi L, Arnaboldi F, Congiu T, Valvassori R, de Eguileor M. 2004. The multifunctional role of fibroblasts during wound healing in Hirudo medicinalis (Annelida, Hirudinea). *Biology of the Cell*, 96: 443–455

Tettamanti G, Grimaldi A, Valvassori R, Rinaldi L, de Eguileor M. 2003b. Vascular

endothelial growth factor is involved in neoangiogenesis in Hirudo medicinalis (Annelida, Hirudinea). *Cytokine*, 22: 168–179

Tettamanti G, Malagoli D, Benelli R, Albini A, Grimaldi A, Perletti G, Noonan DM, de Eguileor M, Ottaviani E. 2006. Growth factors and chemokines: a comparative functional approach between invertebrates and vertebrates. *Current medicinal chemistry*, 13: 2737–2750

Tian Y, Kelemen SE, Autieri M V. 2006. Inhibition of AIF-1 expression by constitutive siRNA expression reduces macrophage migration, proliferation, and signal transduction initiated by atherogenic stimuli. *American journal of physiology. Cell physiology*, 290: C1083–C1091

Torres F, Fadeel B. 2013. Programmed Cell Death: Molecular Mechanisms and Implications for Safety Assessment of Nanomaterials. *Accounts of Chemical Research*, 46: 733–742

Trowbridge IS, Thomas ML. 1994. CD45: an emerging role as a protein tyrosine phosphatase required for lymphocyte activation and development. *Annu Rev Immunol*, 12: 85–116

Tsuiki H, Asai K, Yamamoto M, Fujita K, Inoue Y, Kawai Y, Tada T, Moriyama a, Wada Y, Kato T. 2000. Cloning of a rat glia maturation factor-gamma (rGMFG) cDNA and expression of its mRNA and protein in rat organs. *Journal of biochemistry*, 127: 517–523

Tsukahara T, Matsuda Y, Haniu H. 2015. The Role of Autophagy as a Mechanism of Toxicity Induced by Multi-Walled Carbon Nanotubes in Human Lung Cells. *International Journal of Molecular Sciences*, 16: 40–48

Utans U, Arceci RJ, Yamashita Y, Russell ME. 1995. Cloning and characterization of allograft inflammatory factor-1: A novel macrophage factor identified in rat cardiac allografts with chronic rejection. *Journal of Clinical Investigation*, 95: 2954–2962

van der Meer JWM, Joosten LAB, Riksen N, Netea MG. 2015. Trained immunity: A smart way to enhance innate immune defence. *Molecular Immunology*, 68: 40–44

Wang X, Guo J, Chen T, Nie H, Wang H, Zang J, Cui X. 2012. Toxicology in Vitro Multi-walled carbon nanotubes induce apoptosis via mitochondrial pathway and scavenger receptor. *Toxicology in Vitro*, 26: 799–806

Yang ZF, Ho DW, Lau CK, Lam CT, Lum CT, Poon RTP, Fan ST. 2005. Allograft inflammatory factor-1 (AIF-1) is crucial for the survival and pro-inflammatory activity of macrophages. *International Immunology*, 17: 1391–1397

Zaheer A, Zaheer S, Sahu SK, Knight S, Khosravi H, Mathur SN, Lim R. 2007. A novel role of glia maturation factor: induction of granulocyte-macrophage colony-stimulating factor and pro-inflammatory cytokines. *Journal of neurochemistry*, 101: 364–76

Zaheer A, Zaheer S, Thangavel R, Wu Y, Sahu SK, Yang B. 2008. Glia maturation factor modulates Beta-amyloid-induced glial activation, inflammatory cytokine/chemokine production and neuronal damage. *Brain Research*, 1208: 192–203

Zaheer S, Wu Y, Sahu SK, Zaheer A. 2011. Suppression of neuro inflammation in experimental autoimmune encephalomyelitis by glia maturation factor antibody. *Brain Research*, 1373: 230–239

Zhang L, Hu C, Wang W, Ji F, Cui Y, Li M. 2014. Acute toxicity of multi-walled carbon nanotubes, sodium pentachlorophenate, and their complex on earthworm Eisenia fetida. *Ecotoxicology and Environmental Safety*, 103: 29–35

Zhang Q, Huang JQ, Qian WZ, Zhang YY, Wei F. 2013. The road for nanomaterials industry: A review of carbon nanotube production, post-treatment, and bulk applications for composites and energy storage. *Small*, 9: 1237–1265

Zhu JW, Doan K, Park J, Chau AH, Zhang H, Lowell CA, Weiss A. 2011. Receptor-like Tyrosine Phosphatases CD45 and CD148 Have Distinct Functions in Chemoattractant-Mediated Neutrophil Migration and Response to S. aureus. *Immunity*, 35: 757–769

# Research Articles

PLOS ONE

RESEARCH ARTICLE

# Effects of Carbon Nanotube Environmental Dispersion on an Aquatic Invertebrate, *Hirudo medicinalis*

**Rossana Girardello, Stefano Tasselli, Nicolò Baranzini, Roberto Valvassori, Magda de Eguileor, Annalisa Grimaldi***

Department of Biotechnology and Life Sciences, University of Insubria, Varese, Italy

* annalisa.grimaldi@uninsubria.it



OPEN ACCESS

**Citation:** Girardello R, Tasselli S, Baranzini N, Valvassori R, de Eguileor M, Grimaldi A (2015) Effects of Carbon Nanotube Environmental Dispersion on an Aquatic Invertebrate, *Hirudo medicinalis*. PLoS ONE 10(12): e0144361. doi:10.1371/journal.pone.0144361

**Editor:** Mei LI, Jinling Institute of Technology, CHINA

**Received:** July 2, 2015

**Accepted:** November 17, 2015

**Published:** December 4, 2015



**Data Availability Statement:** All relevant data are within the paper.

**Funding:** This work was supported by the MIUR (Ministero dell'Universita' e della Ricerca) PRIN (program of scientific research of major national interest) 2010-2011 to MdeE and by CARIPLO foundation 2012 (Grant number CUPJ31J11004830003, URL http://www.fondazionecariplo.it) to VR. The funders had no role in study design, data collection and analysis, decision to publish, or preparation of the manuscript.

## Abstract

The recent widespread applications of nanomaterials, because of their properties, opens new scenarios that affect their dispersal in the environment. In particular multiwall carbon nanotubes (MWCNTs), despite their qualities, seem to be harmful for animals and humans. To evaluate possible toxic effects caused by carbon nanotube environmental dispersion, with regard to aquatic compartment, we proposed as experimental model a freshwater invertebrate: *Hirudo medicinalis*. In the present study we analyse acute and chronic immune responses over a short (1, 3, 6 and 12 hours) and long time (from 1 to 5 weeks) exposure to MWCNTs by optical, electron and immunohistochemical approaches. In the exposed leeches angiogenesis and fibroplasia accompanied by massive cellular migration occur. Immunocytochemical characterization using specific markers shows that in these inflammatory processes the monocyte-macrophages ($CD45^+$, $CD68^+$) are the most involved cells. These immunocompetent cells are characterized by sequence of events starting from the expression of pro-inflammatory cytokines (in particular IL-18), and amyloidogenensis. Our combined experimental approaches, basing on high sensitive inflammatory response can highlight adverse effects of nanomaterials on aquatic organisms and could be useful to assess the MWCNTs impact on aquatic, terrestrial animal and human health.

## Introduction

The use and manufacturing of nanomaterials are paralleled with a rapid expanding of their environmental discharge that are expected to be important in determining toxicity. These nanoscale pollutants are non-biodegradable and for this reason, it is difficult to clean up once the environment is contaminated. Nanoparticles (NPs) can be found mixed in the air, in the soil and more often being washed from the soil into the water (rivers and lakes) being harmful to the health of many animals, including humans [1,2].

Although some researches have shown a lack of toxic effects [3], several studies have reported potential impacts of carbon nanotubes (CNTs) on both aquatic and soil organisms which can uptake nanomaterials via skin contact or oral uptake through the gastrointestinal

**Competing Interests:** The authors have declared that no competing interests exist.

tract [4,5]. CNTs dissolved in water and accumulate in soils through accidental spills, application of sewage sludge, deposition of airborne manufactured nanoparticles, use of manufactured nanoparticles in agrochemicals or soil remediation. [6], can induce toxic effects in different organisms [7–10] or can be accumulated in several animals such as earthworms [11–13], gastropod molluscs [4], zooplankton [14–17]. However, for these nanomaterials the mechanisms determining the toxicity are still unclear. CNTs toxicity deriving from mammalian tests show that they are cytotoxic and genotoxic for different types of cells such as macrophages where the exposure induces the release of reactive oxygen species (ROS) [18], necrosis, chromosomal aberrations, apoptosis [19] and inflammatory cytokine expression, such as IL-8 [20]. Therefore studying the NPs evoked inflammatory processes could be crucial to understand the potential effects of nanomaterial as stressor on organisms.

In this work, we evaluate the inflammatory response induced in the leech *Hirudo medicinalis* after in vivo exposure to MWCNTs. The interest in using this animal model is due to its anatomical and physiological features that allows to observe and study events linked to the cellular immune response. In particular, it can be easily and unambiguously evaluated in leech's body wall, which is a predominantly avascular muscular district containing a few immunocompetent cells of myeloid origin, i.e. macrophages, granulocytes and NK [21]. In addition our previous papers [22–27] and a recent report [28] indicated the existence in leech of several CDs (cluster of differentiation) proteins, similar to mammalian CDs, which can be used as markers to easily identify cells involved in the immune response. Once the leech innate immune systems recognizes foreign antigens, the responses against non-self material, lesion or bacterial challenge in the body wall are rapidly induced (24 hours) and can be studied by morphological and histochemical analyses [21,26].

Our data indicate that in leech MWCNTs, induce macrophage recruitment and amyloid deposition, highlighting the potential risks for public health link to carbon nanotubes aquatic environmental diffusion.

## Materials and Methods

All experiments were performed in triplicate.

### MWCNTs preparation

Commercially available and industrially employed Nanocyl Thin Multi-wall Carbon Nanotubes NANOCYL™ NC7000 were obtained from NANOCYL (Belgium, Sambreville). The MWCNTs have an average 9.5 nm external diameter by 1.5 μm mean length with surface area of 250–300 $m^2$/g. They were manufactured by a CCVD (catalytic carbon vapor deposition) process with a purity of 90% C and 10% metal oxide, of which 9.6% was aluminum oxide with traces of iron and cobalt [29]. In these experiments, the pristine MWCNTs were used directly without any chemical processing before use. MWCNTs powder was weighed, dissolved in water and sonicated in an ultrasonic bath 15 min for two cycles to avoid aggregation of particles. The concentration MWCNTs was determined basing on previous data in literature [30] reporting specific biochemical parameters alteration (i.e. mitochondrial enzymatic activity) after in vivo MWCNTS exposure.

### In vivo study design

Leeches (*H. medicinalis*, Annelida, Hirudinea, from Ricarimpex, Eysines, France), measuring 10 cm, kept in water at 20°C in aerated tanks and fed weekly with calf blood. *H. medicinalis* were exposed to [400mg/L] MWCNTs powder dissolved in water. Animals extensively agitate the water as part of their normal activities, generating a continuous re-suspension of

nanotubes, preventing their aggregation in water, and thereby continuously exposing their body wall. The model reflects that associated to aquatic animals that can be subjected to an uncontrolled direct and indirect exposition to CNTs. Animals were randomly divided into separate experimental groups (five individuals for each time points) and exposed to MWCNTs for 1, 3, 6 e 12 hours, to evaluate the acute response to treatment, and for 1, 2, 3, 4 and 5 weeks to value chronic response. Controls consisted of animals that were kept similarly without MWCNTs in the water. Before sacrifice, control and MWCNTs exposed at specific time points leeches were anesthetized with an 10% ethanol solution and then dissected to remove body wall tissues at the level of $20^{th}$ metamere.

## Assessment of internalization of MWCNTs and metal oxide in leech tissues

Internalization of MWCNTs in leeches was assessed by the following procedure: portions of tissue samples obtained after MWCNTs environmental exposure were excised and digested in 5 N potassium hydroxide (KOH) over night at room temperature, then washed repeatedly in distilled water ($dH_20$) to remove potassium salt, resuspended in 100 μl of $dH_2O$ and dried on a copper grids, (Formvar Carbon Film) for transmission electron (TEM) analysis (Jeol JEM 1010, Tokyo, Japan). Images were acquired with Morada, Olympus (Tokyo, Japan) digital camera. To show that the KOH treatment does not affect MWCNTs structure, crude powder was treated in the same way of tissue sample. As control, pristine MWCNTs were re-suspended in $dH_2O$ and observed.

## Optical and Trasmission Electron Microscopy (TEM)

Tissues from leech body wall, were fixed for 2 h in 0.1 M cacodylate buffer at pH 7.4, containing 2% glutaraldehyde. Specimens were then washed in the same buffer and post-fixed for 1 h with 1% osmium tetroxide in cacodylate buffer, pH 7.4. After standard ethanol dehydration, specimens were embedded in an Epon-Araldite 812 mixture. Sections were obtained with a Reichert Ultracut S ultratome (Leica, Wien, Austria). Semi-thin sections (0.75 μm in thickness) were stained by conventional methods (crystal violet and basic fuchsin, according to Moore et al. [31]) and subsequently observed under the light microscope Nikon Eclipse Ni (Nikon, Tokyo, Japan). Data were recorded with a DS-5M-L1 digital camera system Nikon. Ultrathin sections (80 nm in thickness), stained by uranyl acetate and lead citrate, were observed with a Jeol 1010 EX electron microscope. Data were recorded with a MORADA digital camera system (Olympus).

## Scanning electron microscopy (SEM) and X-ray spectroscopy (EDS)

To obtain three-dimensional imaging by SEM, tissues from leeches untreated or exposed to MWCNTs were fixed in 4% paraformaldehyde for 1 h at room temperature. The specimens, washed in PBS (pH 7.2), were dehydrated in an increasing series of ethanol, cleared in in xylene for 30 minutes and then penetrated with paraffin (melting point, 58–60°C, Bioptica, Milan, Italy), at 60°C over night. Paraffin sections (7 μm) were deparaffinized with xylene and dehydrated in an increasing series of ethanol. Slides were mounted on stubs, sputter coated with a thin layer of gold and then observed with a SEM-FEG XL-30 microscope (Philips, Eindhoven, The Netherlands).

To confirm the presence of aluminum, iron and cobalt associated to the crude MWCNTs powder and evaluate their entrance in leech tissues, samples were observed in backscattered electron mode with a scanning electron microscope coupled with an energy dispersive X-ray analyzer (EDAX Genesis 2000). Samples were stuck onto slide holders and sputter coated with

a thin layer of gold. Photographic maps of element distribution obtained on the image frames were processed by Image Analysis (1994) (Soft-Image Software GmbH). These maps were then superimposed to each source image with Adobe Photoshop (Adobe Systems).

## Atomic Absorption Spectroscopy (AAS)

Chemicals used for the preparation of all standard and sample solutions were metal trace analysis grade: MilliQ water (Millipore) and HCl (Baker 9530, 36.5–38%). The calibration standard solutions were prepared from a 1000 mg/L standard solutions (J.T. Baker Instra-Analyzed), and the blanks were prepared with 0.1M HCl.

All measurements were performed on a Solaar M6 atomic absorption spectrometer (Thermo Fisher): Al, Fe and Co were determined with a graphite furnace (GFAA) coupled with Zeeman background correction. Wavelength, bandpass and all others instrumental parameters were set according manufacturers recommendations.

The conventional instrumental detection limits (IDL, based on three standard deviations of the Blank signal) were calculated for each analytical run, typically ranging 1–3 ng/L.

The reported results are the mean of three measurements.

## Immunohistrochemistry, enzimatic hystochemistry and Thioflavin-T staining

Leech tissues were embedded in polyfreeze tissue freezing medium (OCT, Tebu-Bio, Italy) and immediately frozen in liquid nitrogen. Cryosections (7 μm in thickness) were obtained with a Leica CM 1850 cryotome and slides were immediately used or stored at -20°C.

For indirect immunofluorescence, cryosections were rehydrated with phosphate buffer saline (PBS) for 5 min at room temperature and then incubated for 30 min in a blocking solution with 2% BSA (Bovine Serum Albumin) and 0.1% Tween20 in PBS. Subsequently, sections were incubated for 1h at room temperature with the following polyclonal primary antibodies diluted 1:200 in blocking solution: rabbit anti-human CD45 (Twin Helix, Milano, Italy), which reacts, as previously demonstrated, with leech hematopoietic precursors cells and myeloid leukocytes cells [24]; rabbit anti-human CD68 (Santa Cruz Biotechnology, CA, USA) which reacts, as previously demonstrated, with leech macrophage-like cells [26,32] and rabbit anti-human IL-18 (Abnova, Germany). After washing, sections were incubated for 1h at room temperature with the secondary antibody donkey anti-rabbit Cy3-conjugated (excitation 562 nm, emission 576 nm), diluted 1:200 (Jackson ImmunoResearch Laboratories, Inc., West Grove, USA). After further washing with PBS, cryosections were incubated for 15 min with the nuclear marker DAPI (4',6-diamidino-2-phenylindole). Then, slides were mounted with Cytifluor (Cytifluor, USA). In control experiments, primary antibodies were omitted and sections were treated with BSA-containing PBS and incubated only with the secondary antibodies.

For acid phosphatase (ACP) detection, cryosections were rehydrated with PBS for 5 min, incubated with 0.1 M sodium acetate-acetic acid buffer for 5 min and then treated for 1 hour and 30 min at 37°C with the reaction mixture (0.1 M sodium acetate-acetic acid buffer, 0.01% naphtol AS-BI phosphate, 2% NN-dimethylformamide, 0.06% Fast Red Violet LB and 0.5nM MnCl2). After washings in PBS, the slides were mounted with PBS/glycerol 2:1.

According to Grimaldi et al. [33], amyloid fibrils were specifically highlighted using fluorescent dye Thioflavine T (excitation wavelength of 465 nm emission) [34]. For double staining Thioflavin-T/CD-68, the Thioflavin-T method was first applied, followed by the immunedetection of anti-CD68 antibody.

Samples were examined by light/fluorescence microscope Nikon Eclipse Ni (Nikon, Japan) and pictures were collected with the digital camera Nikon D5-5M (Nikon). Images were combined with Adobe Photoshop (Adobe Systems, Inc.).

### Statistical Analysis

The number of migrating $ACP^+$ cells were counted in each section of three independent experiments for each time lapse using the Image J software package (http://rsbweb.nih.gov/ij/download.html). The number of counted cells is standardized on the untreated leeches. Statistical significance was assessed by an unpaired Student's t test using Origin 5.0 software (Microcal).

### Protein extracts preparation, SDS-PAGE and Western Blot

*H. medicinalis* tissues from the body wall were frozen in liquid nitrogen and then homogenized with a mortar. For SDS-PAGE, leech homogenates were suspended in extraction buffer (2X Laemmli's Buffer in the presence of a protease inhibitor cocktail (Sigma, Milan, Italy). The particulate material was removed by centrifugation at 13000 rpm for 10 min at 4°C in a refrigerated Eppendorf Minispin microcentrifuge. Supernatants were denatured at 100°C for 10 min.

Equal amounts of protein extracts were separated in analytical SDS-PAGE using 10% acrylamide minigels. Molecular weights were determined by concurrently running broad range standards from Bio-Rad (Bio-Rad, Richmond, MA, USA). Proteins separated by SDS-PAGE were transferred onto Bio-Rad nitrocellulose filters. Membranes were then saturated with 5% non fat dried milk in Tris buffered saline (TBS, 20 mM Tris-HCl buffer, 500 mM NaCl, pH 7.5) at room temperature for 2 hr, and incubated for 90 min with rabbit polyclonal anti-CD45 antibody (1:500 dilution in 5% TBS-milk). After washing the membrane three times with TBS-Tween 0,1%, the antigens were revealed with the secondary anti-rabbit IgG antibody HRP-conjugated (Jackson ImmunoResearch Laboratories), diluted 1:5000. After washing, the immunocomplexes were revealed with luminol LiteAblot® PLUS Enhanced Chemiluminescent Substrate (EuroClone S.p.A., Pero, Italy). In control experiments, anti-CD45 antibody was omitted. Bands were normalized, using the ImageJ software package (http://rsbweb.nih.gov/ij/download.html), with the housekeeping protein GAPDH, which was detected with a rabbit polyclonal anti-human GAPDH IgG (Proteintech™, Chicago, USA) diluted 1:2000. The expression level of CD45 in exposed leeches was reported relatively to control untreated animals. Experiments were performed in triplicate and data represent the mean values ± SEM. Statistical significance was assessed by an unpaired Student's t test.

## Results

### Determination of MWCNT presence in tissues

The internalization of MWCNTs has been first validated by means of KOH digestion tissues derived from exposed animal (for detail see experimental procedure in the material and method section). TEM analysis showed that nanotubes from digested exposed-animals tissues (Fig 1A) had the same characteristics of MWCNT crude powder, used as control Fig 1B). Furthermore, sonication and KOH treatment do not affected MWCNTs morphology (Fig 1C and 1D).

### Morphological analysis of untreated and MWCNT exposed leech tissues

*H. medicinalis* body wall is made of an epithelium enwrapping thick layers of muscle fibers packed in groups (Fig 2A). Under the muscular sac, virtually avascular, there is the botryoidal

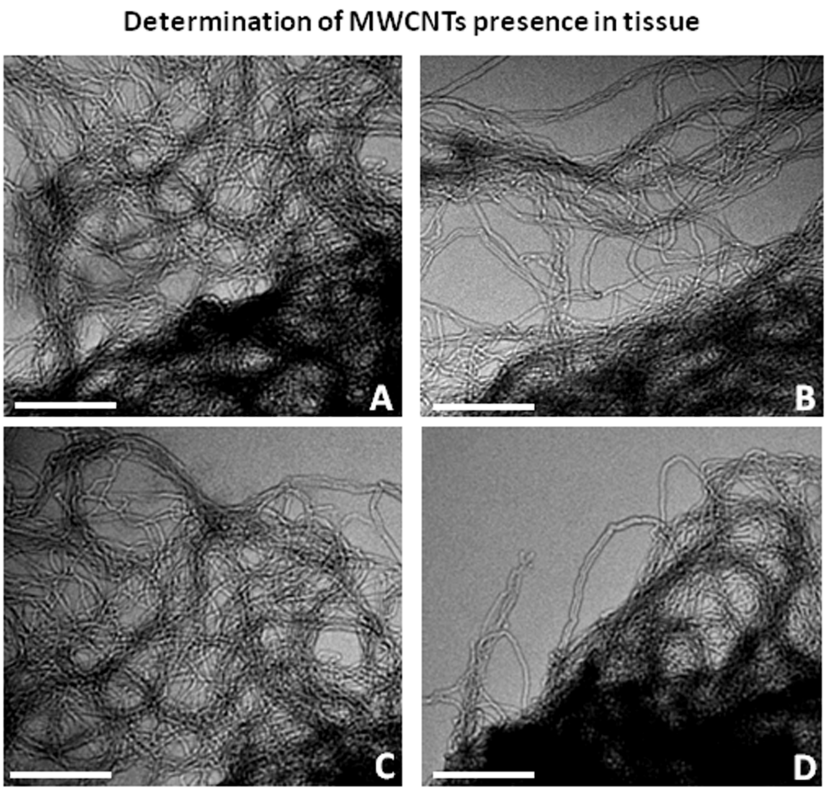


**Fig 1. Determination of MWCNTs presence in tissues (A-D).** (A) MWCNTs extracted by means of KOH digestion from exposed-animals tissues. (B-D) MWCNTs crude powder (used as control) raw (B), after sonication (C) and after KOH treatment (D). Bars in A-D: 500nm.

doi:10.1371/journal.pone.0144361.g001

tissue embedded in the parenchyma localized between the gut and the body wall (Fig 2A). Starting from 1h up to 12 h after MWNTs treatment, a network of blood vessels were evident in the thickness of muscle-cutaneous sac (Fig 2C). The angiogenic process, typical of inflammatory phase, is considered part of innate immune responses. The formation of new vessels is due to a remodeling of the botryoidal tissue in which, by a dehiscence process, a lumen and immunocompetent circulating cells became visible (Fig 2D). Parallel a massive fibroplasia affecting the entire body wall was observed. Leech fibroblasts, responsible for synthesis and remodeling of the extracellular matrix, were spindle-shaped, with numerous lipid droplets in the cytoplasm and laminar projections forming a microenvironment where fibrillogenesis occurred (Fig 2E and 2F).

Analyses at optical microscope showed that the inflammatory state, already observed in short-time-treated animals, also persisted after a prolonged period of MWCNTs exposure. Starting from 1 up to 5 weeks of MWCNTs treatment, the muscle-cutaneous sac were highly vascularized (Fig 2G–2I) and infiltrated by a large number of cells (Fig 2G, 2H and 2I) derived from circulating cells as previously demonstrated [24]. Ultrastructural analysis at TEM showed

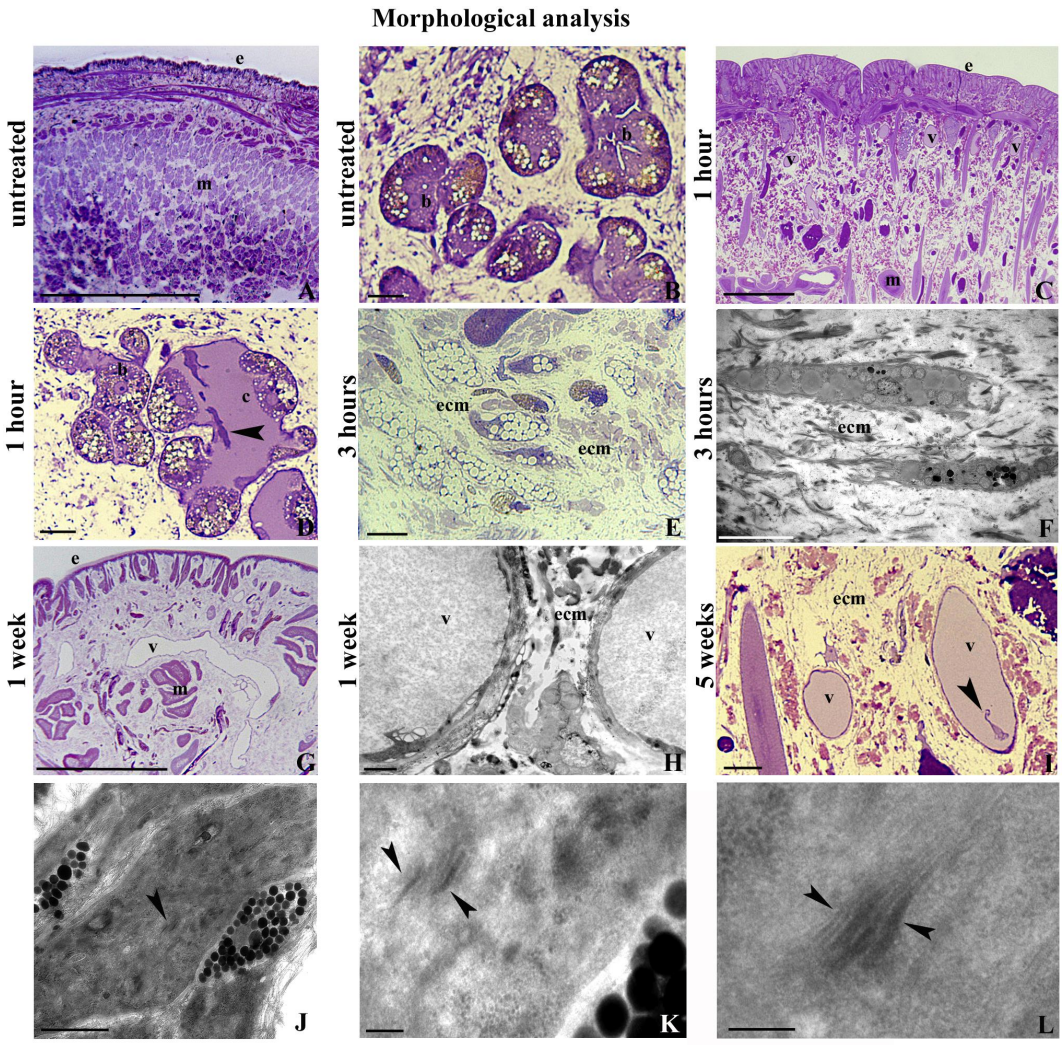


**Fig 2. Morphological analysis (A-L).** Morphological at optical (A-E, C, I) and transmission electron microscopes (F, H, J-L) analyses of sections from *H. medicinalis* body wall. The body wall of untreated leeches results practically avascular (A) and the botryoidal tissue (b) appears as a solid chord of clustered cells (B). After 1 hour from MWCNTs treatment, numerous neo-vessels (v) are found among muscles (m) and under the epithelium (e) (C). Within the new cavities (c) lined by the botryoidal tissue (b), immunocompetent circulating precursors cells (arrowhead) are clearly distinguishable (D). After 3 hours from treatment, numerous fibroblasts are visible immersed in an abundant extracellular matrix ECM (E, F). After 1 (G, H) up to 5 weeks (I) from MWCNTs treatment, numerous vessels (v) and fibroblasts (arrowheads) are still visible in the body wall. (J-L) Detail of MWCNTs (arrowheads) freely dispersed in the cytoplasm of macrophage-like cells. Bars in A, C, G: 100μm; Bars in B, D-E, I: 10μm; Bar in F: 5μm; Bar in H: 2μm; Bar in J: 500nm; Bars in K-L: 200nm.

doi:10.1371/journal.pone.0144361.g002

that particulate acquisition was evident as engulfment of particles settled in the cytoplasm of infiltrating cells showing typical macrophage features (Fig 2J–2L), as we recently demonstrated [35]. These data suggest that macrophages constitute the cells primarily involved in the recognition of this exogenous (non self) material.

## Characterization of cells involved in the inflammatory response caused by MWCNTs exposure

In order to characterize the cell types recruited in the muscle body wall after MWCNTs exposure and to confirm the hypothesis that MWCNTs can induce an immune response activation, immuno-staining experiments, enzymatic histochemistry and colorimetric analyses were performed on cryosections of tissues collected starting from 1 hour up to 5 week after treatment. Immunofluorescence experiments confirmed that the circulating cells, within the neo formed lumen (Fig 3A) and in the peripheral vessels (Fig 3B), were positive for the antibody anti-CD45, the marker commonly used to identify vertebrates leukocytes and leech precursors of circulating cells [24]. The expression of CD45 in control and in MWCNTs treated animals was confirmed by Western blot assay (Fig 3C). Immunoblot analysis of leech body wall extracts validated the presence of two immunoreactive products of about 145 kDa and 180 kDa. These molecular weights were consistent with those found in vertebrates, in which different isoforms of CD45 has been identified with a molecular weight ranging from 140 kDa to 240 kDa [36]. The expression profile of the two isoforms varied in relation to the timing of nanotube administration (Fig 3D). 1 hour after MWCNT treatment, the 180 kDa isoform expression increased significantly in respect to the basal expression level of untreated leeches while the expression of the 145 kDa isoform dramatically decreased starting from 3 week after MWCNTs exposure. Summarizing, the total amount of CD45 expression showed a cyclical pattern, with a peak of expression after 3 hours and after 1 week from treatment. GAPDH was used as internal reference and bands intensity appeared homogeneously distributed in the loaded samples. No specific signals were observed on the negative control experiments performed omitting the primary antibody.

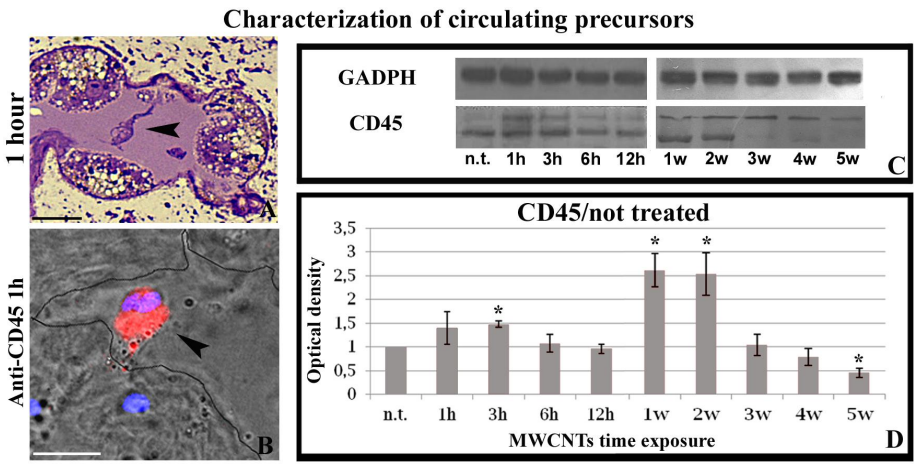


**Fig 3. Characterization of circulating precursors cells (A-D).** Morphological (A) and immunohistochemical (B) analysis of cryosections from *H. medicinalis* body wall. The circulating precursors (arrowhead) visible in lumen of neo-vessels are highly positive for anti-CD45 antibody. Nuclei were counterstained with 4,6-diamidino-2-phenylindole (DAPI; blue). (C-D) Western blot analysis. A protein extracts from the body wall of untreated (n.t) and MWCNTs treated leeches from 1 to 12 hours and from 1 to 5 weeks were probed with the anti-CD45 antibody. The housekeeping protein D-glyceraldehyde-3-phosphate dehydrogenase (GAPDH) was used as a loading control. In all samples, the anti-CD45 detected specific immunoreactive band 24 of about 145 kDa (C), according to the molecular weight ladder (kDa). CD45 protein was quantified by densitometry from three experiments. *P<0.05 compared with untreated leeches (D). Bars in A-B: 10μm.

doi:10.1371/journal.pone.0144361.g003

To characterize the large amount of cells infiltrating the extracellular matrix among the muscle fibers and the new vessels, histo- and immuno-cytochemical enzymatic approaches were used. Unlike control leeches, in animals exposed to MWCNTs, starting from 1 hour up to 5 weeks, an increased amount of migrating cells were observed in the muscle body wall. Numerous migrating cells were positive for the acid phosphatase reaction (Fig 4A–4E), selectively staining lysosomal enzyme of cells with phagocytic activity, such as macrophages. Results showed that the number of migrating cells increased after 1h from MWCNTs exposure, the highest value was reached after 3h and persisted even after 5 weeks from treatment, as demonstrated by cell counting performed on 3 representative images of each time lapse, and was statistically significant (Fig 4F). The same cells, visible underneath the epithelium and migrating towards the MWCNTs aggregates located in the muscular layer, expressed the typical macrophage marker CD68 (Fig 4G–4L) and the evolutionarily highly conserved pro-inflammatory cytokine IL-18 [37,38] (Fig 5A–5F). We have previously demonstrated, both in vertebrates and invertebrates, the link among stress condition, immune responses and amyloid fibril production [33,39]. Here we verified whether MWCNTs were able to induce the production of amyloid fibrils as well. By using the specific Thioflavin-T colorimetric method (Fig 5G–5L) and performing double localization CD68/Thioflavin-T experiments, we confirmed macrophages as main producers of amyloid fibrils (Fig 5L).

## EDS and AAS analyses

EDS analysis was performed in order to confirm the possible presence, in the leech exposure solution, of metal oxide impurities associated to MWCNTs and to describe their possible entrance in leech tissues. Even if microanalytical EDS analysis confirmed the presence of aluminum associated to MWCNTs aggregates (Fig 6A–6C), no signal was detected for this metal in leech tissues after MWCNTs exposure (Fig 6D–6F). No picks were instead detected for iron and cobalt (Fig 6C, 6E and 6F).

The concentration of aluminum oxide in leech exposure water, assessed by AAS was, of 0,25 μg/L, while the concentration of iron and cobalt were below the IDL (instrumental detection limits).

# Discussion

Every exposure to different contaminants, such as organic compounds [30,40,41] or metals [42–45], increases the risk of damage to tissues, cells, DNA and other vital molecules. For the mentioned stressors each exposure potentially can cause programmed cell death, genetic mutations, cancers, immune and endocrine system disorders [46]. With respect to nanomaterials, after decades of research, much remains unknown about how MWCNTs interact with cell behaviors [47,48]. Our data suggest that more attention should be required controlling not only the use and manufacturing of engineered nanomaterials but also their environmental discharge. Indeed, utilizing an animal model with a relative simple anatomy, in this work we demonstrated that MWCNTs exposure can stimulate a response of the innate immune system of organisms. The evidenced strong inflammatory responses induced in leeches by nanotube exposure, suggests that this nanomaterial is able to penetrate superficial barriers, and to promote angiogenesis, fibroplasia, massive migration of immune cells, and pro-inflammatory cytokines such as IL-18 in turn linked to amyloid fibril formation.

Internalization of MWCNTs is validated by KOH digestion of tissues and the gross accumulation of MWCNTs in the leech tissues indicates that they mainly enter through the skin. Moreover, optical and ultrastructural analysis at TEM confirm the presence of MWCNTs aggregates in the muscular layer and dispersed in the cytoplasm of macrophage-like cells. After

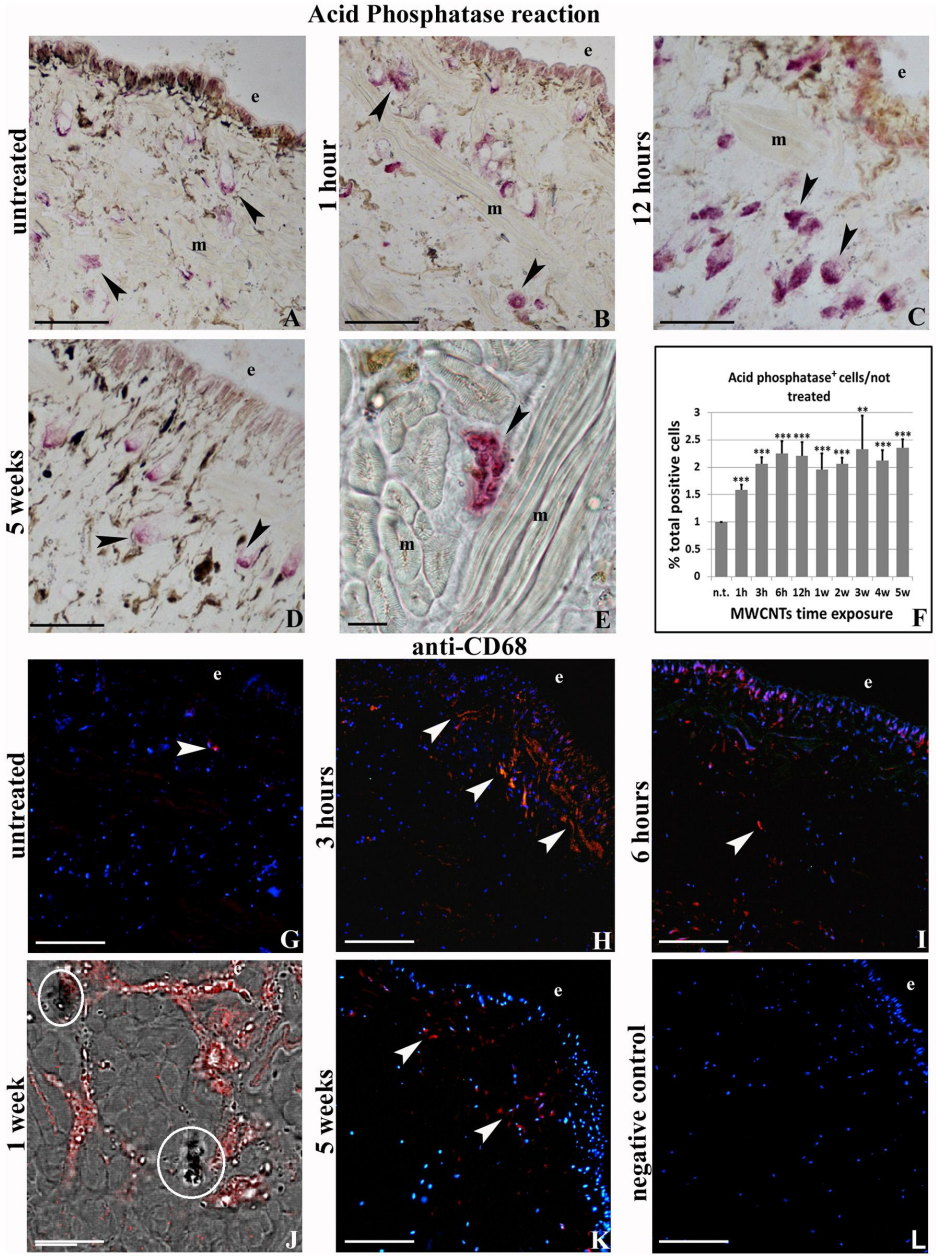


**Fig 4. Acid phosphatase reaction (A-F) and anti CD68 immunofluorescence staining (G-L).** Resident in untreated (A, G) and migrating macrophages-like cells in treated leeches (B-E) and (H-L), located under the epithelium (e) and among the muscle fibers (m), are positive for acid phosphatase reaction (arrowheads in A-F) and for anti-CD68 (G-L). (F) Quantitative evaluation of cell numbers. Column 1: number of cells in untreated sample, columns 2–10: number of cells in MWCNTs treated sample from 1h up to 5 weeks. *p<0.01. (J) Combined transmission and fluorescence images showing $CD68^+$ cells (in red) in spatial association with MWCNTs aggregates (circled). Bars in A-E, G-I, K-L: 100μm; Bar in F, J: 10μm.

doi:10.1371/journal.pone.0144361.g004

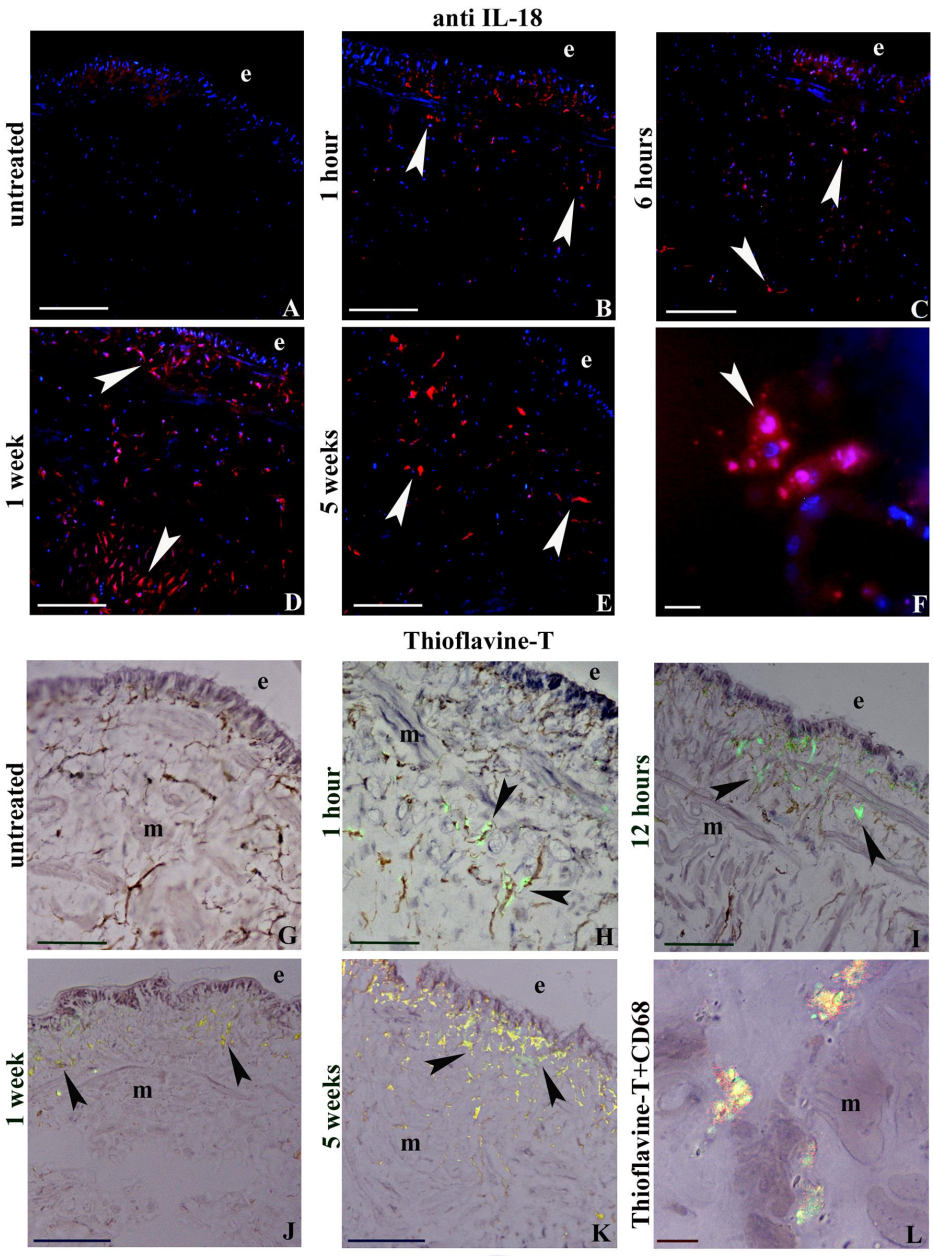


**Fig 5. Anti-IL18 (A-F) and Thioflavine-T staining (G-L).** (A-F) Localization of IL-18. Note the population of resident in untreated (A) and migrating (B- F) immune-responsive cells (arrowheads) located under the epithelium (e) and among the muscle (m). Nuclei are counterstained with DAPI (blue). (G-K) Thioflavin-T method. Amyloid material is stained in yellow (arrowheads). (L) Double-staining of Thioflavin-T (yellow) and macrophage markers CD68 (red) in a cryosection of 3 hours MWCNTs treated leech body wall. Bars in A-E, G-K: 100μm; EDS analysis.

doi:10.1371/journal.pone.0144361.g005

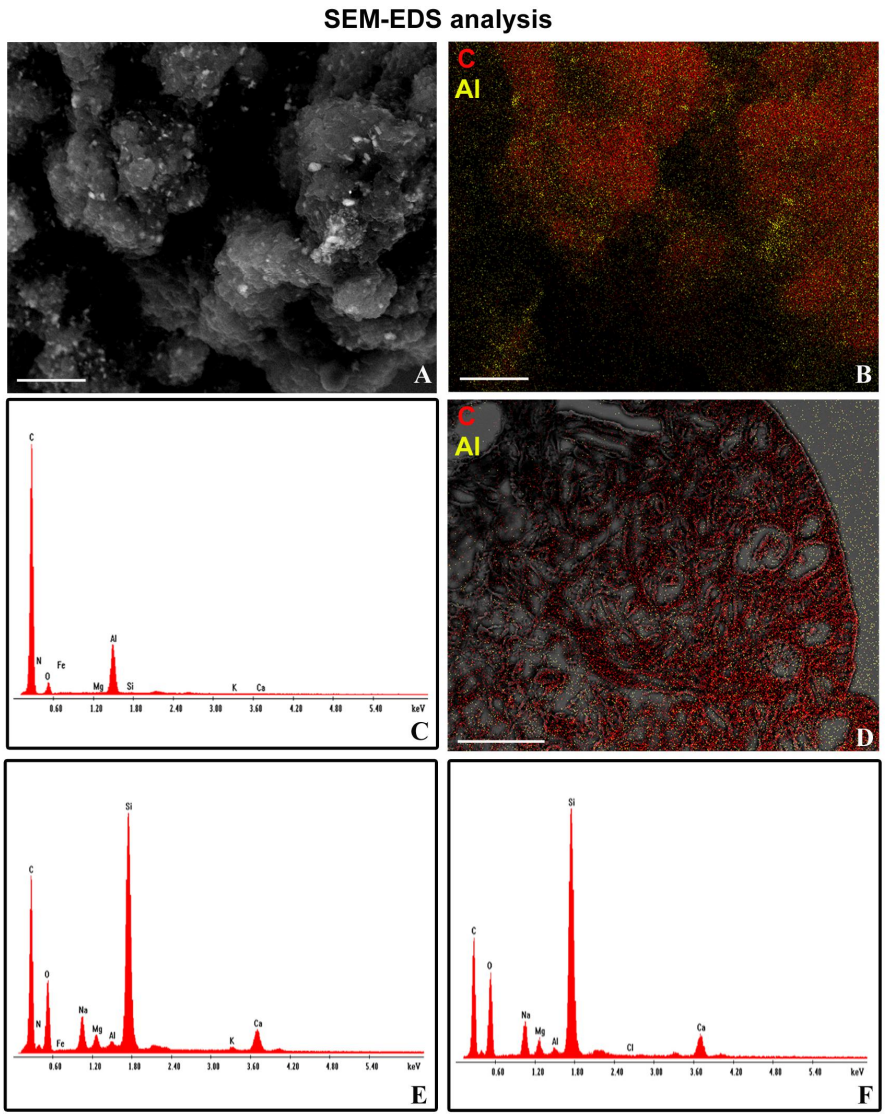


**Fig 6. SEM-EDAX analysis (A-F).** SEM (A) and Elemental mapping images (B) of MWCNTs crude powder (red: Carbonio; yellow: Aluminum). EDAX spectrum for MWCNTs crude powder (C). Combined SEM-EDAX elemental mapping image of a section of *H. medicinalis* body wall 5 weeks after treatment (D). EDAX spectra for treated (E) and untreated (F) tissue samples. Bars in A, B: 10μm; bar in D: 100μm.

doi:10.1371/journal.pone.0144361.g006

MWCNTs exposure, we observed a massive remodeling of extracellular matrix that plays a key role in terms of immune response since the collagen is reorganized to form a scaffold that drives and supports new vessels branching and immunocompetent cells migration [25,49].

AAS analysis confirmed that the concentration of aluminum oxide in the leech exposure solution is even lower than that accepted for human health in drinking water (as reported in

the guide line of World Health Organization 2011 [50]) and no metals, such as aluminum, cobalt and iron, were detectable in leech tissues by EDS analysis. These data confirm that the tested responses in leeches are caused by MWCNTs and not by metal oxide impurities in the exposure solution. Our data are also supported by previous finding in rodents, showing that MWCNTs were capable of producing inflammation and fibrosis in different tissues regardless of the process by which they were synthesized and the types and amounts of metals they contained [1,51].

*H. medicinalis*, like other invertebrates, has an innate immune system which provides for a nonspecific response characterized by proliferation and migration of immune cells towards stimulated area. In leeches the innate immune system utilizes the cells of myeloid lineage such as macrophages, granulocytes and NK performing different types of responses in relation to the antigen. Small dimensions antigens, i.e. bacteria penetrating into the body wall, are phagocytized while larger ones induce both cytotoxic response and encapsulation. In particular, after injury or bacterial injection a massive migration of macrophages towards stimulated region occurs [26,52]. The same responses are observed in leeches after MWCNTs exposure. The undifferentiated precursors, expressing the common leukocyte marker CD45, are conveyed by vessels to the body wall where they can leave the bloodstream. Here they differentiate into mature CD68 positive cells with migratory and phagocytic capacity, as demonstrated by their positivity to the acid phosphatase reaction [24]. The different expression of CD45, at various time of exposure, leads to hypothesize that a cyclic call of monocytes on the inflammation site to maintain high and constant the macrophage number occurs. As we previously demonstrated [26,53], the cytokines released by macrophages, endothelial cells and fibroblasts, are potent angiogenic factors which stimulate chemo-attraction, proliferation, secretion and cell migration. Recently a new player in innate immune responses has been identified and amyloidogenesis is proposed as a fundamental detoxifying event [39] that during evolution also acquired physiological additional functions packaging melanin and driving the pigment towards a non-self-invader both in vertebrates [54] and in invertebrates [33,55].

Here we find that, after MWCNTs exposure, leech CD68 positive macrophages produce amyloid material, as demonstrated by Thioflavin-T staining. Recently, a correlation between amyloidogenesis and the production of IL-18 (a cytokine highly conserved and responsible for activation and regulation of innate immune system) has been demonstrated [37,38]. We observed that in leeches the expression of IL-18 in concomitance with Thioflavin-T signals increases in a time-dependent way and progressively with MWCNTs exposure time. Here we suggest that in leeches IL-18 and amyloid material production are associated processes within macrophage cell activation.

## Conclusions

Our combined experimental approaches, basing on high sensitive inflammatory response can highlight adverse effects of nanomaterials on aquatic organisms. These simple experimental approaches and the use of an anatomically simple model such as leeches, where the effects of stressful events are unequivocally interpretable, are an important tool that can be finalized to monitor the diffusion of MWCNTs in the water environment and the effects of this nanomaterial as stressor on organisms.

## Acknowledgments

Dr. Rossana Girardello is a student of the Ph.D. program in Biotechnology, Biosciences and Surgical Technologies, School in Biological and Medical Sciences, University of Insubria. The authors wish to thank Terenzio Congiu (Department of surgical and morphological sciences,

University of Insubria), for his technical assistance in EDS analysis, Enrico Caruso and Marco Lanfranchi (Department of theoretical and applied sciences, University of Insubria) for their technical assistance in AAS analysis.

## Author Contributions

Conceived and designed the experiments: AG RG. Performed the experiments: RG ST NB. Analyzed the data: AG RG. Contributed reagents/materials/analysis tools: RV MdE. Wrote the paper: AG RG. Critical review of the manuscript: MdE.

## References

1. Lam C-W, James JT, McCluskey R, Arepalli S, Hunter RL. A review of carbon nanotube toxicity and assessment of potential occupational and environmental health risks. Crit Rev Toxicol. 2006; 36: 189–217. doi: 10.1080/10408440600570233 PMID: 16686422
2. Simate GS, Iyuke SE, Ndlovu S, Heydenrych M, Walubita LF. Human health effects of residual carbon nanotubes and traditional water treatment chemicals in drinking water. Environ Int. Elsevier Ltd; 2012; 39: 38–49. doi: 10.1016/j.envint.2011.09.006
3. Petersen EJ, Zhang L, Mattison NT, O'Carroll DM, Whelton AJ, Uddin N, et al. Potential release pathways, environmental fate, and ecological risks of carbon nanotubes. Environ Sci Technol. 2011; 45: 9837–9856. doi: 10.1021/es201579y PMID: 21988187
4. Ali D, Yadav PG, Kumar S, Ali H, Alarifi S, Harrath AH. Sensitivity of freshwater pulmonate snail Lymnaea luteola L., to silver nanoparticles. Chemosphere. Elsevier Ltd; 2014; 104: 134–140. doi: 10.1016/j.chemosphere.2013.10.081
5. Baun A, Hartmann NB, Grieger K, Kusk KO. Ecotoxicity of engineered nanoparticles to aquatic invertebrates: a brief review and recommendations for future toxicity testing. Ecotoxicology. 2008; 17: 387–395. doi: 10.1007/s10646-008-0208-y PMID: 18425578
6. Cornelis G, Kirby JK, Beak D, Chittleborough D, McLaughlin MJ. A method for determination of retention of silver and cerium oxide manufactured nanoparticles in soils. Environ Chem. 2010; 7: 298–308. doi: 10.1071/EN10013
7. Demir E, Vales G, Kaya B, Creus A, Marcos R. Genotoxic analysis of silver nanoparticles in Drosophila. Nanotoxicology. 2011; 5: 417–424. doi: 10.3109/17435390.2010.529176 PMID: 21039182
8. Hayashi Y, Engelmann P, Foldbjerg R, Szabó M, Somogyi I, Pollák E, et al. Earthworms and humans in vitro: Characterizing evolutionarily conserved stress and immune responses to silver nanoparticles. Environ Sci Technol. 2012; 46: 4166–4173. doi: 10.1021/es3000905 PMID: 22432789
9. Kawata K, Osawa M, Okabe S. In vitro toxicity of silver nanoparticles at noncytotoxic doses to HepG2 human hepatoma cells. Environ Sci Technol. 2009; 43: 6046–6051. doi: 10.1021/es900754q PMID: 19731716
10. Park MVDZ, Neigh AM, Vermeulen JP, de la Fonteyne LJJ, Verharen HW, Briedé JJ, et al. The effect of particle size on the cytotoxicity, inflammation, developmental toxicity and genotoxicity of silver nanoparticles. Biomaterials. Elsevier Ltd; 2011; 32: 9810–9817. doi: 10.1016/j.biomaterials.2011.08.085
11. Coutris C, Hertel-Aas T, Lapied E, Joner EJ, Oughton DH. Bioavailability of cobalt and silver nanoparticles to the earthworm Eisenia fetida. Nanotoxicology. 2012; 6: 186–95. doi: 10.3109/17435390.2011.569094 PMID: 21486186
12. Shoults-Wilson WA, Zhurbich OI, McNear DH, Tsyusko O V., Bertsch PM, Unrine JM. Evidence for avoidance of Ag nanoparticles by earthworms (Eisenia fetida). Ecotoxicology. 2011; 20: 385–396. doi: 10.1007/s10646-010-0590-0 PMID: 21229389
13. Shoults-Wilson WA, Reinsch BC, Tsyusko O V, Bertsch PM, Lowry G V, Unrine JM. Effect of silver nanoparticle surface coating on bioaccumulation and reproductive toxicity in earthworms (Eisenia fetida). Nanotoxicology. 2011; 5: 432–444. doi: 10.3109/17435390.2010.537382 PMID: 21142839
14. Edgington AJ, Roberts AP, Taylor LM, Alloy MM, Reppert J, Rao AM, et al. The influence of natural organic matter on the toxicity of multiwalled carbon nanotubes. Environ Toxicol Chem. 2010; 29: 2511–2518. doi: 10.1002/etc.309 PMID: 20865699
15. Alloy MM, Roberts AP. Effects of suspended multi-walled carbon nanotubes on daphnid growth and reproduction. Ecotoxicol Environ Saf. Elsevier; 2011; 74: 1839–1843. doi: 10.1016/j.ecoenv.2011.06.020
16. Kennedy AJ, Gunter JC, Chappell MA, Goss JD, Hull MS, Kirgan RA, et al. Influence of nanotube preparation in aquatic bioassays. Environ Toxicol Chem. 2009; 28: 1930–1938. doi: 10.1897/09-024.1 PMID: 19388791

17. Roberts AP, Mount AS, Seda B, Souther J, Qiao R, Lin S, et al. In vivo biomodification of lipid-coated carbon nanotubes by Daphnia magna. Environ Sci Technol. 2007; 41: 3028–3029. doi: 10.1021/es062572a

18. Funahashi S, Okazaki Y, Ito D, Asakawa A, Nagai H, Tajima M, et al. Asbestos and multi-walled carbon nanotubes generate distinct oxidative responses in inflammatory cells. J Clin Biochem Nutr. 2015; 56: 111–117. doi: 10.3164/jcbn.14-92 PMID: 25759516

19. Di Giorgio ML, Bucchianico Di S, Ragnelli AM, Aimola P, Santucci S, Poma A. Effects of single and multi walled carbon nanotubes on macrophages: Cyto and genotoxicity and electron microscopy. Mutat Res—Genet Toxicol Environ Mutagen. Elsevier B.V.; 2011; 722: 20–31. doi: 10.1016/j.mrgentox.2011.02.008

20. Pulskamp K, Diabaté S, Krug HF. Carbon nanotubes show no sign of acute toxicity but induce intracellular reactive oxygen species in dependence on contaminants. Toxicol Lett. 2007; 168: 58–74. doi: 10.1016/j.toxlet.2006.11.001 PMID: 17141434

21. De Eguileor M, Tettamanti G, Grimaldi a, Boselli a, Scarì G, Valvassori R, et al. Histopathological changes after induced injury in leeches. J Invertebr Pathol. 1999; 74: 14–28. PMID: 10388543

22. De Eguileor M, Grimaldi a, Tettamanti G, Valvassori R, Cooper EL, Lanzavecchia G. Lipopolysaccharide-dependent induction of leech leukocytes that cross-react with vertebrate cellular differentiation markers. Tissue Cell. 2000; 32: 437–445. doi: 10.1054/tice.2000.0132 PMID: 11201283

23. De Eguileor M, Grimaldi a, Tettamanti G, Valvassori R, Cooper EL, Lanzavecchia G. Different types of response to foreign antigens by leech leukocytes. Tissue Cell. 2000; 32: 40–48. doi: 10.1054/tice.1999.0085 PMID: 10798316

24. Grimaldi a, Tettamanti G, Perletti G, Valvassori R, de Eguileor M. Hematopoietic cell formation in leech wound healing. Curr Pharm Des. 2006; 12: 3033–3041. doi: 10.2174/138161206777947443 PMID: 16918432

25. Tettamanti G, Grimaldi A, Rinaldi L, Arnaboldi F, Congiu T, Valvassori R, et al. The multifunctional role of fibroblasts during wound healing in Hirudo medicinalis (Annelida, Hirudinea). Biol Cell. 2004; 96: 443–455. doi: 10.1016/j.biolcel.2004.04.008 PMID: 15325073

26. Schorn T, Drago F, Tettamanti G, Valvassori R, de Eguileor M, Vizioli J, et al. Homolog of allograft inflammatory factor-1 induces macrophage migration during innate immune response in leech. Cell Tissue Res. 2015; 359: 853–864. PMID: 25435328

27. Grimaldi a, Tettamanti G, Rinaldi L, Perletti G, Valvassori R, Eguileor De M. Role of cathepsin B in leech wound healing. ISJ. 2004; 38–46.

28. Macagno ER, Gaasterland T, Edsall L, Bafna V, Soares MB, Scheetz T, et al. Construction of a medicinal leech transcriptome database and its application to the identification of leech homologs of neural and innate immune genes. BMC Genomics. 2010; 11: 407. doi: 10.1186/1471-2164-11-407 PMID: 20579359

29. Ma-Hock L, Treumann S, Strauss V, Brill S, Luizi F, Mertler M, et al. Inhalation toxicity of multiwall carbon nanotubes in rats exposed for 3 months. Toxicol Sci. 2009; 112: 468–81. doi: 10.1093/toxsci/kfp146 PMID: 19584127

30. Zhang L, Hu C, Wang W, Ji F, Cui Y, Li M. Acute toxicity of multi-walled carbon nanotubes, sodium pentachlorophenate, and their complex on earthworm Eisenia fetida. Ecotoxicol Environ Saf. Elsevier; 2014; 103: 29–35. doi: 10.1016/j.ecoenv.2014.01.041

31. Moore RD, Mumaw V, Schoenberg MD. Optical microscopy of ultrathin tissue sections. J Ultrastruct Res. 1960; 4: 113–116. doi: 10.1016/S0022-5320(60)90047-2 PMID: 13772346

32. De Eguileor M, Tettamanti G, Grimaldi A, Congiu T, Ferrarese R, Perletti G, et al. Leeches: immune response, angiogenesis and biomedical applications. Curr Pharm Des. 2003; 9: 133–147. doi: 10.2174/1381612033392198 PMID: 12570664

33. Grimaldi A, Girardello R, Malagoli D, Falabella P, Tettamanti G, Valvassori R, et al. Amyloid / Melanin distinctive mark in invertebrate immunity. ISJ. 2012; 9: 153–162.

34. Sipe JD, Cohen a S. Review: history of the amyloid fibril. J Struct Biol. 2000; 130: 88–98. doi: 10.1006/jsbi.2000.4221 PMID: 10940217

35. Girardello R, Drago F, de Eguileor M, Valvassori R, Vizioli J, Tettamanti G, et al. Cytokine impregnated biomatrix: a new tool to study multi-wall carbon nanotubes effects on invertebrate immune cells. J nanomedicine Nanotechnol. 2015; 6: 323. doi: 10.4172/2157-7439.1000323

36. Trowbridge IS, Thomas ML. CD45: an emerging role as a protein tyrosine phosphatase required for lymphocyte activation and development. Annu Rev Immunol. 1994; 12: 85–116. doi: 10.1146/annurev.iy.12.040194.000505 PMID: 8011300

37. Alboni S, Cervia D, Sugama S, Conti B. Interleukin 18 in the CNS. J Neuroinflammation. 2010; 7: 9. doi: 10.1186/1742-2094-7-9 PMID: 20113500

38. Alboni S, Montanari C, Benatti C, Blom JMC, Simone ML, Brunello N, et al. Constitutive and LPS-regulated expression of interleukin-18 receptor beta variants in the mouse brain. Brain Behav Immun. Elsevier Inc.; 2011; 25: 483–493. doi: 10.1016/j.bbi.2010.11.011

39. Grimaldi A, Tettamanti G, Congiu T, Girardello R, Malagoli D, Falabella P, et al. The main actors involved in parasitization of Heliothis virescens larva. Cell Tissue Res. 2012; 350: 491–502. doi: 10.1007/s00441-012-1503-8 PMID: 23053052

40. Fleeger JW, Gust KA, Marlborough SJ, Tita G. Mixtures of metals and polynuclear aromatic hydrocarbons elicit complex, nonadditive toxicological interactions in meiobenthic copepods. Environ Toxicol Chem. 2007; 26: 1677–1685. doi: 10.1897/06-397r.1 PMID: 17702342

41. Maria VL, Bebianno MJ. Antioxidant and lipid peroxidation responses in Mytilus galloprovincialis exposed to mixtures of benzo(a)pyrene and copper. Comp Biochem Physiol—C Toxicol Pharmacol. 2011; 154: 56–63. doi: 10.1016/j.cbpc.2011.02.004 PMID: 21354328

42. Bouraoui Z, Banni M, Ghedira J, Clerandeau C, Narbonne JF, Boussetta H. Evaluation of enzymatic biomarkers and lipoperoxidation level in Hediste diversicolor exposed to copper and benzo[a]pyrene. Ecotoxicol Environ Saf. 2009; 72: 1893–1898. doi: 10.1016/j.ecoenv.2009.05.011 PMID: 19501399

43. Dondero F, Banni M, Negri A, Boatti L, Dagnino A, Viarengo A. Interactions of a pesticide/heavy metal mixture in marine bivalves: a transcriptomic assessment. BMC Genomics. BioMed Central Ltd; 2011; 12: 195. doi: 10.1186/1471-2164-12-195

44. Banni M, Bouraoui Z, Clerandeau C, Narbonne JF, Boussetta H. Mixture toxicity assessment of cadmium and benzo[a]pyrene in the sea worm Hediste diversicolor. Chemosphere. Elsevier Ltd; 2009; 77: 902–906. doi: 10.1016/j.chemosphere.2009.08.041

45. Benedetti M, Martuccio G, Fattorini D, Canapa A, Barucca M, Nigro M, et al. Oxidative and modulatory effects of trace metals on metabolism of polycyclic aromatic hydrocarbons in the Antarctic fish Trematomus bernacchii. Aquat Toxicol. 2007; 85: 167–175. doi: 10.1016/j.aquatox.2007.08.009 PMID: 17923160

46. Chang X, Ji G, Sui Q, Huang J, Yu G. Rapid photocatalytic degradation of PCP-Na over NaBiO3 driven by visible light irradiation. J Hazard Mater. 2009; 166: 728–733. doi: 10.1016/j.jhazmat.2008.11.126 PMID: 19150748

47. Du J, Wang S, You H, Zhao X. Understanding the toxicity of carbon nanotubes in the environment is crucial to the control of nanomaterials in producing and processing and the assessment of health risk for human: A review. Environ Toxicol Pharmacol. Elsevier B.V.; 2013; 36: 451–462. doi: 10.1016/j.etap.2013.05.007

48. Oberdörster G, Oberdörster E, Oberdörster J. Nanotoxicology: An emerging discipline evolving from studies of ultrafine particles. Environ Health Perspect. 2005; 113: 823–839. PMID: 16002369

49. Tettamanti G, Grimaldi A, Congiu T, Perletti G, Raspanti M, Valvassori R, et al. Collagen reorganization in leech wound healing. Biol Cell. 2005; 97: 557–568. doi: 10.1042/BC20040085 PMID: 15898949

50. Gorchev HG, Ozolins G. WHO guidelines for drinking-water quality. WHO Chron. 2011; 38: 104–108.

51. Albini A, Pagani A, Pulze L, Bruno A P E et al. Environmental impact of multi-wall carbon nanotubes in a novel model of exposure: systemic distribution, macrophage accumulation and amyloid deposition. Int J Nanotechnol. 2015; 10: 1–12.

52. Tettamanti G, Grimaldi A, Ferrarese R, Palazzi M, Perletti G, Valvassori R, et al. Leech responses to tissue transplantation. Tissue Cell. 2003; 35: 199–212. doi: 10.1016/S0040-8166(03)00027-2 PMID: 12798129

53. Tettamanti G, Malagoli D, Benelli R, Albini A, Grimaldi A, Perletti G, et al. Growth factors and chemokines: a comparative functional approach between invertebrates and vertebrates. Curr Med Chem. 2006; 13: 2737–2750. doi: 10.2174/092986706778521986 PMID: 17073625

54. Fowler DM, Koulov A V., Alory-Jost C, Marks MS, Balch WE, Kelly JW. Functional amyloid formation within mammalian tissue. PLoS Biol. 2006; 4: 0100–0107. doi: 10.1371/journal.pbio.0040006

55. Falabella P, Riviello L, Pascale M, Di Lelio I, Tettamanti G, Grimaldi A, et al. Functional amyloids in insect immune response. Insect Biochem Mol Biol. Elsevier Ltd; 2012; 42: 203–211. doi: 10.1016/j.ibmb.2011.11.011

Nanomedicine & Nanotechnology

Girardello et al., J Nanomed Nanotechnol 2015, 6:5
http://dx.doi.org/10.4172/2157-7439.1000323

Research Article Open Access

# Cytokine Impregnated Biomatrix: A New Tool to Study Multi-Wall Carbon Nanotubes Effects on Invertebrate Immune Cells

**Rossana Girardello[1], Francesco Drago[2], Magda de Eguileor[1], Roberto Valvassori[1], Jacopo Vizioli[2], Gianluca Tettamanti[1] and Annalisa Grimaldi[1]***

[1]*Department of Biotechnology and Life Sciences, University of Insubria, Via J. H. Dunant 3, 21100 Varese, Italy*
[2]*Inserm U1192, Laboratoire de Protéomique, Réponse Inflammatoire, Spectrométrie de Masse (PRISM), Université Lille 1, Cité Scientifique, 59655 Villeneuve D'Ascq, France*

## Abstract

The novel features of engineered nanoparticles, such as multi-wall carbon nanotubes (MWCNTs) are impressive and attractive for technology, however they dissolved in water and accumulate in soils through the application of sewage sludge, accidental spills, and deposition from the air, agrochemicals or soil remediation. Given that several studies have revealed that chronic exposure to these nanomaterials products through the ingestion of drinking water, inhalation and dermal contact may harbour potential risks to human health, risk assessment of this nanomaterials in the aquatic environment are becoming essential. Here we propose a freshwater invertebrate, the leech *Hirudo medicinalis*, as a model to assess the effects MWCNTs on the immune system by means of *in vivo* and *in vitro* experiments. For this study, we used a consolidated experimental approach based on injection in the body wall of the leech of the biomatrice Matrigel (MG), added with a specific macrophage chemoattractant, the cytokine Allograft inflammatory factor-1 (AIF-1) and/or with MWCNTs. MG sponges analysis show the presence of a larger number of cells positive for both CD68 and HmAIF-1, specific monocyte-macrophage markers. Ultrastructural analysis suggests that MWCNTs may be internalized by phagocytosis but they seem also to be able to pierce cell membranes during cells migration.

Cells extracted from MG were also used for *in vitro* treatment with MWCNTs at different concentration (2.5, 5, 10, 25, 50 and 100 µg/ml) for 24 h to study cell morphology changes and production of amyloid fibrils in order to encapsulate the foreign bodies. Our results, not only confirm the ability of MWCNTs in inducing a potent inflammatory response, but highlight rapid colorimetric assays that can be successfully used as sensitive tools for aquatic pollution biomonitoring.

**Keywords:** Multi-wall carbon nanotubes (MWCNTs); *Hirudo medicinalis*; Macrophages; Matrigel; Innate immune response; Amyloid fibrils

## Introduction

The rapid development of nanotechnology and nanoscience during the last decade has led to the discovery of nanomaterials such as carbon nanotubes, classified into single-walled (SWCNTs) and multi-walled (MWCNTs) carbon nanotubes, which have several potential applications. The former are mainly used in biology and medicine [1], while the latter are widely used in industry, and their applications are increasing constantly in particular in waste water treatment [2]. Due to their massive production and in the light of the most recent studies, which emphasize the potential toxicity of nanotubes, it is more than ever necessary to take into account their impact on the environment [3]. Aquatic ecosystems seem to be particularly susceptible to contamination by MWCNTs and other pollutants with harmful consequences for the organisms that inhabit them. Several studies, in fact, demonstrate MWCNTs toxicity and bio-persistence within tissues and cells [4-6]. The bioaccumulation of MWCNTs in aquatic animals may as well represent a risk to humans, who may be exposed to this nanomaterial through many pathways, such as inhalation, injection, penetration but also ingestion [7]. In particular several studies revealed that the physical dimension of MWCNTs are critical factors in mesothelial injury and carcinogenesis [8] and are associated with phagocytosis [9] that leads to the production of pro-inflammatory cytokines and reactive oxygen species (ROS) [10]. Although the literature abounds with studies on MWCNTs toxicity, the existing toxicological data are still fragmentary and their biological interactions with cells, proteins and tissues have not yet been fully understood [3].

The aim of this work is to develop and optimize approaches to suggest an invertebrate animal model able to give rapid and sensitive responses upon the presence of pollutions in water, such as nanoparticles, even if at low concentration. Immune system of organisms represents a sensitive physiological indicator that may be affected even at low concentrations of nanomaterial exposure; however the animal models usually employed in ecotoxicological studies are not suitable due to their immune responses strictly linked to their bauplan.

The model organism chosen in this study is the leech *Hirudo medicinalis.* This aquatic invertebrate is suitable for experimental manipulation, economic, easily treated and without significant ethical considerations related to use and regulatory restrictions. Leech is a new interesting animal model for several reasons: i) its immune response processes includes the same steps described for vertebrate [11-15], involving similar cellular mechanisms and key molecules that play pivotal roles for guiding and regulating the hematopoietic cells activation and differentiation, revealing a conserved regulation immune response processes; ii) any response evoked by different stimuli are activated within a short period of time (6, 24 hours) and clear and easily detectable due to their small size and anatomical

***Corresponding author:** Annalisa Grimaldi, Department of Biotechnology and Life Sciences, University of Insubria, Via J. H. Dunant, 3, 21100 Varese, Italy, Tel: +390332421325; Fax: +390332421300; E-mail: annalisa.grimaldi@uninsubria.it

**Received** June 24, 2015; **Accepted** August 16, 2015; **Published** October 01, 2015

**Citation:** Girardello R, Drago F, de Eguileor M, Valvassori R, Vizioli J, et al. (2015) Cytokine Impregnated Biomatrix: A New Tool to Study Multi-Wall Carbon Nanotubes Effects on Invertebrate Immune Cells. J Nanomed Nanotechnol 6: 323. doi:10.4172/2157-7439.1000323

simplicity; iii) it shows an added value related to a novel developed assay based on the use of a biomatrix (MATRIGEL) [16-18] to obtain *in vitro* expansion of macrophages primary leech cells implicated in immune response process that could be used to test the effect of the nanomaterial on immune cells.

Our combined experimental approaches, based on high sensitive inflammatory response and rapid colorimetric tests, can highlight adverse effects of MWCNTs on immune system cells, even at low concentration, and could be used as quick sensitive tools for aquatic pollution bio-monitoring.

## Materials and Methods

### Animals and treatment

Leeches (*H. medicinalis*, Annelida, Hirudinea, from Ricarimpex, Eysines, France) measuring 10 cm were kept in water at 19–20°C in aerated tanks. Animals were fed weekly with calf blood. Animals were randomly divided into separate experimental groups according to different protocols and treatments. Each treatment was performed at the level of the 20$^{th}$ metamere. Before each experiment, leeches were anaesthetized with a 10% ethanol solution.

**Group 1:** Leeches injected with 300 µl of liquid MG (an extract of the murine Engelbreth–Holm–Swarm (EHS) tumor produced as previous described [19]) served as controls.

**Group 2:** Leeches (five animals/condition) injected with 300 µl of liquid MG supplemented with 100, 150 and 300 ng of the recombinant protein r*Hm*AIF-1 (kindly donated by Jacopo Vizioli and Francesco Drago, University of Lille, France), were used to selectively isolate the macrophages cells migrating under the influence of *Hm*AIF-1. The best concentration of r*Hm*AIF-1 required to induce significant cell migration was 300 ng and was used for the next experiments.

**Group 3:** Leeches injected with 300 µl of liquid MG supplemented with 20 µg of Multi-walled commercially available and industrially employed Carbon Nanotubes (MWCNTs), NANOCYL™ NC7000 (Belgium NANOCYL, Sambreville; average 9.5 nm diameter by 1.5 µm mean length with surface area of 250-300 m$^2$/g, not functionalized, manufactured by catalytic carbon vapour deposition (CCVD) process, with a purity of 90%). For these experiments, the pristine MWCNTs were used directly without any chemical processing before use. This concentration of MWCNTs was necessary to obtain visible aggregates in the Matrigel pellet.

**Group 4:** Leeches injected with 300 µl of liquid MG supplemented with 300 ng r*Hm*AIF-1 and 20 µg of MWCNTs.

Animals were sacrificed after 1 week. MG implants were removed from the animal and processed in different ways depending on the type of analyses.

### Transmission electron microscopy (TEM)

MG implants for routine transmission electron microscopy (TEM) were fixed in 2% glutaraldehyde in 0.1 M sodium cacodylate buffer (pH 7,2) for 1 hour at room temperature. Specimens were washed in the same buffer and then post-fixed for 1h with 1% osmium tetroxide in cacodylate buffer at room temperature. After standard dehydration in ethanol series, specimens were treated with propylene oxide/ Epon-Araldite (1:1) for 1 hour and then embedded in an Epon-Araldite 812 mixture. Sections were obtained with a Reichert Ultracut S ultratome (Leica, Nussloch, Germany). Thin sections (80-90 nm) were stained by uranyl acetate and lead citrate and observed with a Jeol 1010 EX electron microscope (Jeol, Tokyo, Japan). Images were acquired with digital camera Morada, Olympus (Tokyo, Japan).

### Colorimetric and indirect immunofluorescence staining

MG implants were embedded in Polyfreeze tissue freezing medium (Polysciences, Eppelheim, Germany) and immediately frozen in liquid nitrogen. Cryosections (7 µm) were obtained with a Leica CM1850 cryotome and slides were immediately used or stored at -20°C.

For colorimetric assays, cryosections were immersed in distilled water and incubated with May Grunwald Giemsa differential staining (Bio Optica, Milano, Italy), which permits identification of hematopoietic cells based upon their cytoplasmic pH properties.

For Thioflavin-S method, samples were treated with Mayer's hemalum for 2 minutes. After washings with water samples were stained with 1% Thioflavin-S in aqueous solution. After further washing, they were treated with 1% acetic acid for 20 minutes. This method stains the amyloid fibrils in green/yellow fluorescence.

For indirect immunofluorescence, samples washed with PBS were pre-incubated for 30 min with PBS containing 2% bovine serum albumin (BSA) before the primary antibody incubation for 1 hour at room temperature. The primary antibodies (diluted 1:200) used were: rabbit anti-human CD45 (GenScript, USA), which reacts with leech hematopoietic precursors cells, rabbit anti-human CD68 (Santa Cruz Biotechnology, USA), which reacts with leech macrophages, as previously demonstrated [14], and rabbit anti-*Hm*-AIF-1 (kindly donated by Jacopo Vizioli and Francesco Drago, University of Lille). The washed specimens were incubated for 1 h at room temperature with an anti-rabbit secondary antibody (Jackson Immuno Research Laboratories, USA) Cy3 conjugated (dilution 1:200). After further washing with PBS, cryosections were incubated for 10 minutes with the nuclear marker DAPI (4',6-diamidino-2-phenylindole). The slides were mounted in Citifluor (Citifluor Ltd, London, UK) with coverslips and observed by light and fluorescence microscopy Nikon Eclipse Ni (Nikon, Japan).

The staining was visualized using excitation/emission filters of 490/525 nm for Thioflavin-S, 550/580nm for Cy3 and 360/420 nm for DAPI. Data were recorded with Nikon Digital Sight DS-SM (Nikon, Japan) digital camera. Images were combined with Adobe Photoshop (Adobe Systems, Inc.). In control samples, primary antibodies were omitted and sections were treated with BSA-containing PBS.

### *In vitro* matrigel assays

After 1 week *in vivo* (corresponding to a suitable cell concentration for seeding) r*Hm*AIF-1 supplemented MG implants were harvested and cultured. Each implant was minced in small pieces using sterilized razor blades and plated in wells of 60 mm in diameter in DMEM medium (Celbio, Milan, Italy) modified by dilution (1:4) to reach iso-osmolality and supplemented with 1% glutamine, 10% fetal bovine serum and 1% gentamicin [16]. Cells were maintained at 20°C and histologically and immunocytochemically examined 1 days and 1 week after seeding.

All cultures were performed in triplicate and scored at 1 week from seeding with an inverted Olympus microscope (Tokyo, Japan). Data were recorded with a DS-5M-L1 digital camera system (Nikon).

### Assessment of cell viability with trypan blue

Cell viability was assessed using the vital dye Trypan blue, which is incorporated only in dying or dead cells. The cells were incubated at

room temperature for 5 min with 0.4% trypan blue solution (diluted 1:1 in basal medium) and directly observed using an inverted optical microscope (Olympus).

### *In vitro* MWCNTs treatment

Cells were cultured on a round coverslip in 24 wells plate for 1 week before MWCNTs treatment. MWCNTs powder was weighed re-suspended in culture medium and then sonicated 15 min for 2 cycles in an ultrasonic bath (starsonic 35, Liarre, Italy) to avoid particles aggregation. MWCNTs were administrated at 2.5, 5, 10, 25, 50 and 100 µg/ml for 24 h. Particle exposure concentrations were chosen upon assessment of existing literature concerning exposure of vertebrate macrophages cell lines to MWCNTs and SWCNTs [3]. Cells were then fixed with paraformaldehyde 3% for 10 minutes and washed in PBS before proceeding with immunocytochemical and colorimetric assays described above.

### Statistical analysis

Cells extracted from matrigel pellet were plated out in 60 mm diameter at a density of 1000 cells/well and counted after one week from seeding, using the Image J software package. Five fields for each time lapse (1 day and 1 week) were analyzed and the number of counted cells is referred to the total area of the well. Statistical significance was assessed by an unpaired Student's t test using Origin 5.0 software (Microcal).

## Results

### Morphological, immunocytochemical and colorimetric characterization of cells infiltrating the MG sponge

**Light and trasmission electron microscopy:** First, since MG can be supplemented with different concentrations of cytokines, we sought the best r*Hm*AIF-1 concentration for the macrophages tissue cells recruitment in the biomatrix. We supplemented 300 µl of MG with 100, 150 (data not shown) and 300 ng of r*Hm*AIF1 and the MG pellets, formed following inoculation, were recovered and processed for standard histology one week after injection. While cellular infiltrates were not observed in control MG samples (Figure 1A), the number of cells migrating in the biomatrix increased in relation to the r*Hm*AIF-1 concentration with the highest cell density obtained with 300 ng of r*Hm*AIF-1 in the MG (Figure 1B). In order to assess the interaction between MWCNTs and cells migrated in the MG pellet, we used the biopolymer matrigel supplemented with both r*Hm*AIF-1 and MWCNTs. Numerous migrated cells were visible in the MG sponge,

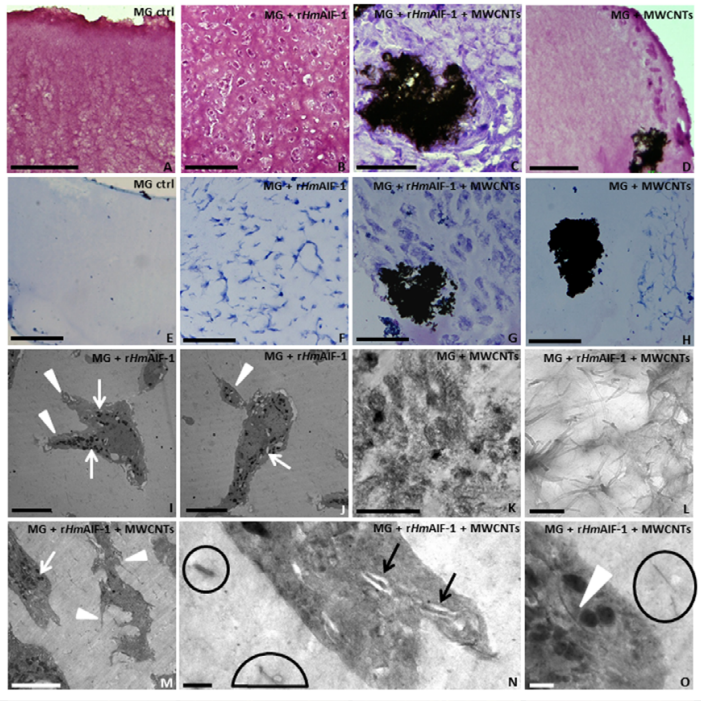


**Figure 1:** Morphological and colorimetric analyses of cells infiltrating the MG removed from the animal 1 week after injection. (A-H) Appearance under the light microscope of the cells infiltrating the gels without (A, E) and with the r*Hm* AIF-1 (B, F). The r*Hm*AIF-1 recruits a large number of cells (B) positively stained by May GrunwaldGiemsa method (E, F). (C, D, G, H) in MG pellet supplemented with both MWCNTs and r*Hm*AIF-1 (C, G) or only with MWCNTs (D, H), migrating cells positive for GrunwaldGiemsa staining (G, H) are visible dispersed in the biomatrix and surrounding the MWCNTs aggregates (arrowheads). (I-O) TEM images. (I, J, M-O) Detail of cells infiltrating the MG pellets characterized by a cytoplasm with numerous highly electron-dense granules (arrows), pseudopodia (arrowheads in I, J) and lamellipodia (arrowheads in M). (K, L, N, O) Detail of MWCNTs dispersed or grouped in aggregates differently sized inside the MG sponge (K, L, encircled in N, O) or in intracellular vesicles (arrows in N) and freely dispersed in the cytoplasm (arrowhead in O). Bars in A-H: 50 µm; Bars in I-K, M: 5 µm; Bars in L: 200 nm; Bars in N, O: 500 nm.

most forming a clot around the large MWCNTs aggregates (Figure 1C). Migrating cells, even if in a reduced number, was present in the MG pellet supplemented only with MWCNTs (Figure 1D). Cells coloured with the May Grunwald Giemsa differential staining showed dark blue nuclei typical of monocyte and macrophages cell lines (Figure 1E-1H).

Ultrastructural analysis at TEM showed that in MG supplemented only with r*Hm*AIF-1 cells appear either round or with an irregular shape with a cytoplasm rich in electron-dense granules, with a pronounced migratory phenotype showing pseudopodia and an active degradation of the surrounding matrix (Figure 1I and 1J). Cells migrated in MG pellet supplemented with MWCNTs, visible dispersed throughout the MG sponge or grouped in aggregates (Figure 1K and 1L), showed increased membrane ruffling and lamellipodia associated with phagocytosis (Figure 1M). Moreover, particulate acquisition was evident as engulfment of particles settled in vesicles or in the cytoplasm (Figure 1N and 1O).

**Immunocytochemical characterization:** In order to better characterize the cells infiltrating the MG and surrounding the MWCNTs aggregates, the Matrigel pellets were removed from the leech after one week from injection and sections of the biopolymer were immunostained with antibodies to macrophage cell markers. The cells infiltrating the Matrigel sponge, either supplemented with only the r*Hm*AIF-1 protein, with both r*Hm*AIF-1 and MWCNTs or with only MWCNTs, were strongly positive for the antibodies anti-CD68 (Figure 2A-2C) and anti-*Hm*AIF-1 (Figure 2D-2F). In particular, in the MG containing MWCNTs, numerous infiltrating $CD68^{+}$/*Hm*AIF-$1^{+}$ macrophages reached and surrounded the MWCNTs aggregates (Figure 2 B, 2C, 2E and 2F). No signal was detected in negative control experiments where primary antibodies were omitted (Figure 2G).

**Thioflavin-S staining for amyloid fibrils detection:** Since recently has been demonstrated that MWCNTs aggregates induce macrophage recruitment, tissue inflammation and amyloid deposition in mice [20], we performed a Thioflavin-S staining on MWCNTs supplemented MG sponges to reveal the presence of amyloid fibrillar material. Thioflavin-S positivity was found in the macrophages surrounding the aggregates of MWCNTs, indicating that these cells were implicated in the production and deposition of amyloid fibrils (Figure 2H and 2I).

## Cultured Cells and MWCNTs *in vitro* treatment

In order to obtain primary cultures of leech macrophages cells, the MG polymers supplemented with r*Hm*AIF-1 was removed from the leeches after 1 week *in vivo* and the cells placed in culture. Starting from day 1 after seeding, cultured cells were present as clusters (Figure 3A and 3B). One week after seeding, cultures were formed by an increased number of cells (Figure 3C). To determine the growth and viability characteristics of the cultured cells, the cells from the matrigel polymers that had been removed from the leeches after 1 week *in vivo*, were plated at a density of 1000 cells for each well, and the number of

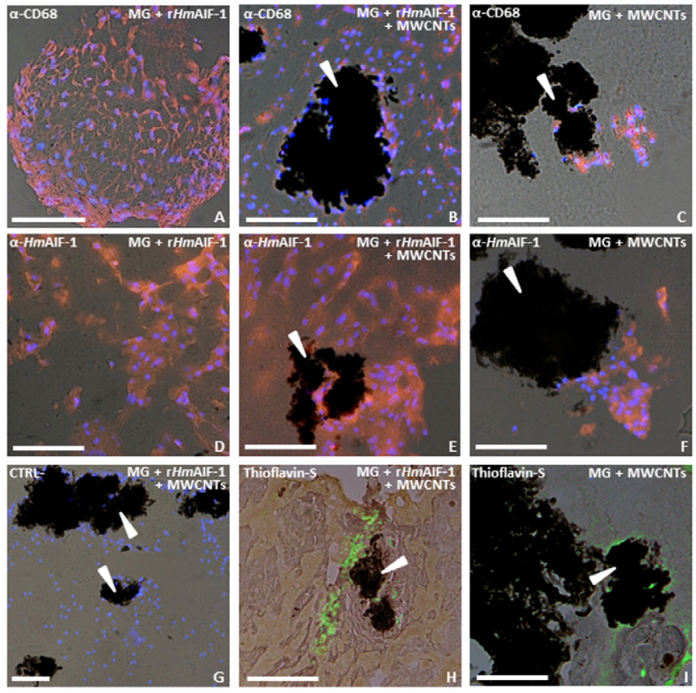


**Figure 2:** Immunocyto chemical characterization of macrophage cells recruited into the matrigel sponges by r*Hm*AIF-1 and MWCNTs and removed 1 week after injection. Combined fluorescence/transmission images of MG implants cryosections shows that the numerous cells α-CD68 (red in A-C) and α-*Hm*AIF-1 (red in D-F) infiltrate the biomatrix and surround the MWCNTs aggregates (arrowheads in B, C, E, F). Nuclei are counterstained with DAPI (blue). (G) Negative control. (H-I) Thioflavin-S staining recognizes amyloid structures (yellow in H, I) associated to macrophages infiltrating the MWCNTs supplemented MG sponge or forming a scaffold around the MWCNTs aggregates (arrowheads in H, I). Bars in A-I: 50 μm.

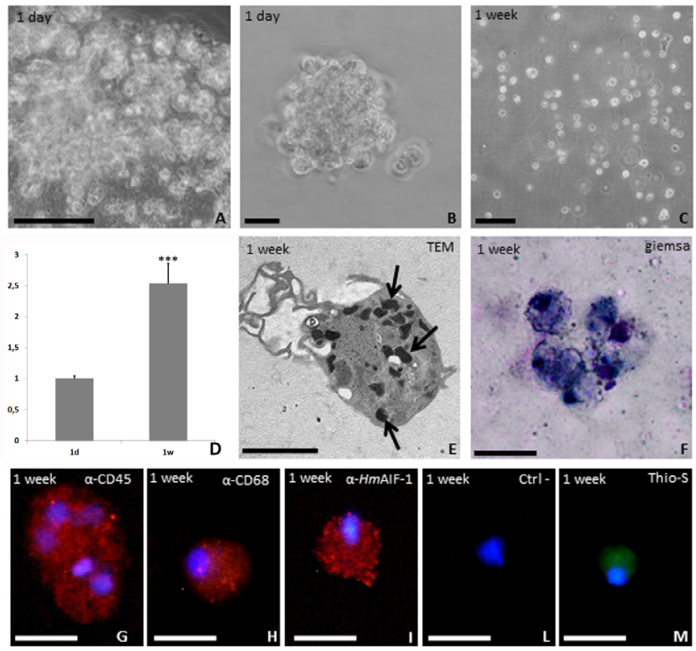


**Figure 3:** Culture of cells recruited into the matrigel sponges by r*Hm* AIF-1. After 1 week *in vivo* the MG was removed and the cells infiltrating the matrigel sponge were plated out. Phase contrast image of cultured cells 1 day (A, B) and 1 week after seeding (C). (D) Quantitative evaluation of cell numbers. Column 1: cells cultured for 1 day Column 2: cells cultured for 1 week. *p<0.01. These cells are ultra structurally similar to macrophages with a cytoplasm filled with electron-dense granules (arrows in E), are Giemsa positive cells (F) and immuno-stained with CD45 (G), CD68 (H) and *Hm* AIF-1 (J) antibodies, markers of macrophages cells. (L) Negative control in which the primary antibody was omitted. These cells show also a weak positivity to Thioflavin-S staining (yellow in M). Nuclei are counterstained with DAPI (blue in G-M). Bars in A, C: 50 µm; bars in B, D, F-M: 10 µm; bar in E: 2 µm.

cells were counted after one week from seeding. As shown by statistical analysis the number of cells increased by 2.5 times (Figure 3D). Trypan blue exclusion demonstrated that these cells were still viable (data not shown), exhibited the same morphological aspects described for the cells within the MG *in vivo* (Figure 3E), were positive for May Grunwald Giemsa differential staining (Figure 3F) and expressed the leukocyte-specific marker CD45 (Figure 3G), and the macrophage markers CD68 (Figure 3H) and *Hm*AIF-1 (Figure 3I). No signal was visible in negative control sample (Figure 3L). Moreover these cells showed a weak positivity for Thioflavin-S dye (Figure 3M).

After obtaining primary culture of macrophages, we evaluated their ability to produce amyloid fibrils after MWCNTs exposure (Figure 4A-4X). $CD45^+$ (Figure 4A-4F) and *Hm*$AIF\text{-}1^+$ (Figure 4G-4L) macrophages incubated for 24 h with increasing concentrations of MWCNTs (2.5, 5, 10, 25, 50 and 100 µg/ml) were highly positive for Thioflavin-S staining. The amyloid fibrils stained in yellow (Figure 4M-4R) were accumulated in large dilated reticulum cisternae filled with spatially organized fibrillar material, as visible by ultrastructural analysis at TEM (Figure 4U) and then released in the extracellular environment (Figure 4T). Combined fluorescence/transmission images clearly showed that *Hm*$AIF\text{-}1^+/CD45^+$ macrophage cells (Figure 4V and 4W), strictly associated to MWCNTs aggregates, produce amyloid fibrils Thioflavin-$S^+$ (Figure 4S and 4T).

## Discussion

The contamination of water by various different pollutants is a serious problem worldwide in terms of human health and agriculture. MWCNTs are currently attracting intense research efforts because of their unique properties, which make them suitable for many industrial developments, applications in biomedicine, nanoelectronics, mechanical engineering, personal care products and textiles. MWCNTs are currently also produced and used in industry on a large-scale, increasing the risk for a widespread human and environmental exposure. Data in literature [21] have demonstrated that these nanoparticles have a very long half-life *in vivo*, could affect cellular functions at molecular levels and are capable of penetrating physiological barriers to reach vital organs inducing chronic inflammation, which it is often associated with insurgence of cancer. The physical dimensions and the biopersistence of MWCNTs were found to be similar to asbestos, and they indeed have revealed asbestos-like pathogenicity [22,23]. In order to avoid making the same mistakes, more research must be done on these new and emerging products in the market to provide a complete understanding of biological properties of MWCNTs, including uptake, distribution, intracellular trajectory, interactions with the immune system.

We have recently observed that *in vivo* treatment of *H. medicinalis* with water dispersed MWCNTs induce toxic effect also at low concentrations and after a short time of exposure. The

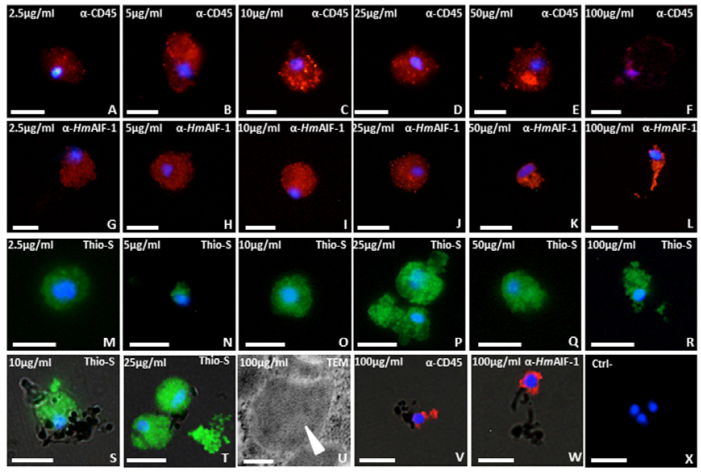


**Figure 4:** Effects of MWCNTs treatment on cultured macrophages. Cells extracted from MG after 1 week from injection and treated for 24 h with increasing concentration of MWCNTs (2.5, 5, 10, 25, 50 and 100 µg/ml) are CD45$^+$ (red in A-F), *Hm* AIF-1$^+$ (red in G-L) and show an increasing positivity for Thioflavin-S staining (yellow in M-R). Combined fluorescence/transmission (S, T) and TEM images clearly show the amyloid fibril deposition (yellow in S, T) and organized fibrillar material (arrowhead in U) by CD45$^+$/*Hm* AIF-1$^+$ macrophages (V-W) strictly associated with MWCNTs aggregates. Nuclei in blue are stained with DAPI. No signal is detected in negative control experiments (X). Bars in A-T, V-X: 10 µm; bar in U: 500 nm

uptake of MWCNTs by leeches is associated with the induction of an inflammatory process, inducing a massive angiogenesis and migration of CD45$^+$ and CD68$^+$ macrophages throughout the animal body wall (Unpublished data, submitted to Plosone). These results suggest a novel entry mechanisms and toxicity profiles of MWCNTs, in fact, immunity is an essential function to retain organism's well-being, and represents a sensitive physiological indicator that may be affected even at low concentrations of nanomaterials exposure [24].

In order to better understand this point, we focused our attention on leech macrophages observing the behaviour of these cells *in vivo* and *in vitro* toward the nanomaterial. For this purpose we use a consolidated experimental approach based on a novel developed assay that allows the isolation of a specific cell population using the biomatrix Matrigel injected in the body wall of the leech [16-18].

We observe that aggregates of nanotubes are able to induce the migration of macrophages into the MG sponges. To increase the number of recruited cells in MG, allowing us to better analyze the internalization process of this nanomaterial, we loaded MG with both MWCNTs and the cytokine r*Hm*AIF-1, which has been recently demonstrated to be a powerful chemo attractant for leech macrophages [25,26]. One week from injection, r*Hm*AIF-1 invokes within the Matrigel a larger number of cells which are positive for the markers CD45, CD68 and *Hm*AIF-1 which has been already demonstrated to be expressed by the monocyte/macrophage lineage both in leech and in vertebrates [14,26-28]. Ultrastructural analysis at TEM revealed that in leech macrophages MWCNTs are both internalized in vesicles and freely dispersed in the cytoplasm.

These data suggest that curled MWCNTs are internalized by phagocytosis or during the process of matrix degradation, while straight and rigid MWNCTs seem to be able to pierce cell membranes during cells migration and are then found free in the cytosol. These findings corroborate the observations of other authors on vertebrate macrophages [29-31]. Moreover, since recent experimental studies show that carbon nanotubes influence the aggregation process of proteins associated with neurodegenerative diseases like amyloid fibril production, we evaluate, by using the colorimetric methods of Thioflavin-S [32], the MWCNTs ability to induce amyloid deposits in correspondence of MWCNTs/macrophages associations [20]. Several studies demonstrated in fact that nanoparticles that enter cells by diffusing through cell membranes or by active uptake, such as endocytosis [33], cause toxic effects such as the formation of reactive oxygen species (ROS) [5,8,34]. Oxidative stress can induce proteins to adopt an insoluble beta-pleated sheet conformation [35], and according to numerous authors [36-40] oxidative damage appears to be the earliest events preceding amyloid fibril formation. Thus, we evaluate the amyloid fibril production from macrophage in relation to MWCNTs exposure. As expected, we found a massive accumulation of fibrils Thioflavin-S$^+$, associated to the macrophages forming a scaffold around the MWCNTs aggregates. The presence of these fibrils in MWCNTs and r*Hm*AIF-1 supplemented MG confirms the strong reaction of macrophages to the nanomaterial.

Starting from these results, the next target of our work was to obtain *in vitro* expansion of macrophages primary leech cells that could be used as a sensitive method to evaluate the presence of the nanomaterial in contaminated water. We used the biopolymer MG supplemented with r*Hm*-AIF-1 as a vector to isolate these cells *in vivo* and then culture them obtaining an *in vitro* expansion of macrophages primary leech cells. Seven days after seeding cells cultured in a normal medium expressed the same specific macrophage markers (CD45, CD68, *Hm*AIF-1) as that already observed *in vivo*. The ability of MWCNTs to induce amyloid fibrils generation were assessed by measuring Thioflavin-S fluorescence as a reporter of amyloid fibrils generation. As compared with control unexposed cells, a significant increase in Thioflavin-S staining was observed in exposed macrophage cell in concentration independent manner and the amyloid fibrils formed

a scaffold around the MWCNTs aggregates, indicating that amyloid deposition might be a barrier to contain non-self-material.

Recent data on murine model [20] showed inflammatory responses generated by commercially available nanotubes that are inhaled. Moreover, literature is beginning to show data concerning the potential risks to public health and the aquatic environment when these nanomaterials are dispersed in water. Our data on leeches confirmed the toxicological effects of nanotubes. The use of annelids to implement the data so far produced is in order to demonstrate the reliability and reproducibility of the new model in respect to those commonly utilized by eco-toxicologists. In fact, unlike other invertebrates, *H. medicinalis* use the same strategies and the same molecules of vertebrates in response to different stimuli. For these reasons, it is critical to investigate the question of the nanomaterial safety utilizing new models and methods for assessing the environmental risks of these possible toxic particles.

The data produced by this project will be a cornerstone in determining the potential toxicity of MWCNTs and the eventual precautions needed in the wastewater discharge. Our results also provide critical information to regulatory agencies and industry to determine the need for monitoring and regulation regarding MWCNTs.

### Acknowledgement

Dr. Rossana Girardello is a student of the Ph.D. program in Biotechnology, Biosciences and Surgical Technologies, School in Biological and Medical Sciences, University of Insubria. This work was supported by CARIPLO foundation 2012 to VR. The authors wish to thank the Centro Grandi Attrezzature (CGA) of the University of Insubria.

### References

1. Ji Z, Zhang D, Li L, Shen X, Deng X, et al. (2009) The hepatotoxicity of multi-walled carbon nanotubes in mice. Nanotechnology 20: 445101.
2. Theron J, Walker JA, Cloete TE (2008) Nanotechnology and water treatment: Applications and emerging opportunities. Crit Rev Microbiol 34: 43-69.
3. Du J, Wang S, You H, Zhao X (2013) Understanding the toxicity of carbon nanotubes in the environment is crucial to the control of nanomaterials in producing and processing and the assessment of health risk for human: A review. Environ Toxicol Pharmacol 36: 451-462.
4. Saria R, Mouchet F, Perrault A, Flahaut E, Laplanche C, et al. (2014) Short term exposure to multi-walled carbon nanotubes induce oxidative stress and DNA damage in *Xenopus laevis* tadpoles. Ecotoxicol Environ Saf 107: 22-29.
5. Pereira MM, Mouton L, Yepremian C, Coute A, Lo J, et al. (2014) Ecotoxicological effects of carbon nanotubes and cellulose nanofibers in *Chlorella vulgaris*. J Nanobiotechnology 12: 1-13.
6. Velzeboer I, Peeters ETHM, Koelmans AA (2013) Multiwalled carbon nanotubes at environmentally relevant concentrations affect the composition of benthic communities. Environ Sci Technol 47: 7475-7482.
7. Teow Y, Asharani PV, Hande MP, Valiyaveettil S (2011) Health impact and safety of engineered nanomaterials. Chem Commun (Camb) 47: 7025-7038.
8. Funahashi S, Okazaki Y, Ito D, Asakawa A, Nagai H, et al. (2015) Asbestos and multi-walled carbon nanotubes generate distinct oxidative responses in inflammatory cells. J Clin Biochem Nutr 56: 111-117.
9. Dörger M, Münzing S, Allmeling AM, Messmer K, Krombach F (2001) Differential responses of rat alveolar and peritoneal macrophages to man-made vitreous fibers in vitro. Environ Res 85: 207-214.
10. Boyles MSP, Young L, Brown DM, MacCalman L, Cowie H, et al. (2015) Multi-walled carbon nanotube induced frustrated phagocytosis, cytotoxicity and pro-inflammatory conditions in macrophages are length dependent and greater than that of asbestos. Toxicol Vitr 29: 1513-1528.
11. De Eguileor M, Tettamanti G, Grimaldi A, Congiu T, Ferrarese R, et al. (2003) Leeches: Immune response, angiogenesis and biomedical applications. Curr Pharm Des 9: 133-147.
12. De Eguileor M, Grimaldi A, Tettamanti G, Valvassori R, Cooper EL, et al. (2000) Different types of response to foreign antigens by leech leukocytes. Tissue Cell 32: 40-48.
13. Grimaldi A, Tettamanti G, Rinaldi L, Perletti G, Valvassori R, et al. (2004) Role of cathepsin B in leech wound healing. ISJ: 38-46.
14. Grimaldi A, Tettamanti G, Perletti G, Valvassori R, de Eguileor M (2006) Hematopoietic cell formation in leech wound healing. Curr Pharm Des 12: 3033-3041.
15. Tettamanti G, Malagoli D, Benelli R, Albini A, Grimaldi A, et al. (2006) Growth factors and chemokines: A comparative functional approach between invertebrates and vertebrates. Curr Med Chem 13: 2737-2750.
16. Grimaldi A, Bianchi C, Greco G, Tettamanti G, Noonan DM, et al. (2008) In vivo isolation and characterization of stem cells with diverse phenotypes using growth factor impregnated biomatrices. PLoS One 3.
17. Grimaldi A, Banfi S, Gerosa L, Tettamanti G, Noonan DM, et al. (2009) Identification, isolation and expansion of myoendothelial cells involved in leech muscle regeneration. PLoS One 4.
18. Grimaldi A, Banfi S, Vizioli J, Tettamanti G, Noonan DM, et al. (2011) Cytokine Loaded Biopolymers as a Novel Strategy to Study Stem Cells during Wound-Healing Processes. Macromol Biosci 11: 1008-1019.
19. Kibbey MC (1994) Maintenance of the EHS sarcoma and Matrigel preparation. J Tissue Cult Methods 16: 227-230.
20. Albini A, Pagani A, Pulze L, Bruno APE (2015) Environmental impact of multi-wall carbon nanotubes in a novel model of exposure: Systemic distribution, macrophage accumulation and amyloid deposition. Int J Nanotechnol in press.
21. Oberdörster G, Oberdörster E, Oberdörster J (2005) Nanotoxicology: An emerging discipline evolving from studies of ultrafine particles. Environ Health Perspect 113: 823-839.
22. Poland CA, Duffin R, Kinloch I, Maynard A, Wallace W a H, et al. (2008) Carbon nanotubes introduced into the abdominal cavity of mice show asbestos-like pathogenicity in a pilot study. Nat Nanotechnol 3: 423-428.
23. Murphy FA, Schinwald A, Poland CA, Donaldson K (2012) The mechanism of pleural inflammation by long carbon nanotubes: Interaction of long fibres with macrophages stimulates them to amplify pro-inflammatory responses in mesothelial cells. Part Fibre Toxicol 9: 8.
24. Hayashi Y, Engelmann P (2013) Earthworm's immunity in the nanomaterial world : New room , future challenges. Invertebr Surviv J 10: 69-76.
25. Drago F, Sautière PE, Le Marrec-Croq F, Accorsi A, Van Camp C, et al. (2014) Microglia of medicinal leech (*Hirudo medicinalis*) express a specific activation marker homologous to vertebrate ionized calcium-binding adapter molecule 1 (Iba1/alias aif-1). Dev Neurobiol 1.
26. Schorn T, Drago F, Tettamanti G, Valvassori R, de Eguileor M, et al. (2015) Homolog of allograft inflammatory factor-1 induces macrophage migration during innate immune response in leech. Cell Tissue Res 359: 853-864.
27. Yang ZF, Ho DW, Lau CK, Lam CT, Lum CT, et al. (2005) Allograft inflammatory factor-1 (AIF-1) is crucial for the survival and pro-inflammatory activity of macrophages. Int Immunol 17: 1391-1397.
28. Tian Y, Kelemen SE, Autieri M V (2006) Inhibition of AIF-1 expression by constitutive siRNA expression reduces macrophage migration, proliferation, and signal transduction initiated by atherogenic stimuli. Am J Physiol Cell Physiol 290: C1083-C1091.
29. Pulskamp K, Diabaté S, Krug HF (2007) Carbon nanotubes show no sign of acute toxicity but induce intracellular reactive oxygen species in dependence on contaminants. Toxicol Lett 168: 58-74.
30. Di Giorgio ML, Bucchianico S Di, Ragnelli AM, Aimola P, Santucci S, et al. (2011) Effects of single and multi walled carbon nanotubes on macrophages: Cyto and genotoxicity and electron microscopy. Mutat Res - Genet Toxicol Environ Mutagen 722: 20-31.
31. Nagai H, Toyokuni S (2012) Differences and similarities between carbon nanotubes and asbestos fibers during mesothelial carcinogenesis: Shedding light on fiber entry mechanism. Cancer Sci 103: 1378-1390.
32. Grimaldi A, Girardello R, Malagoli D, Falabella P, Tettamanti G, et al. (2012) Amyloid / Melanin distinctive mark in invertebrate immunity. ISJ 9: 153-162.
33. Johnston HJ, Hutchison GR, Christensen FM, Aschberger K, Stone V (2009)

The biological mechanisms and physicochemical characteristics responsible for driving fullerene toxicity. Toxicol Sci 114: 162-182.

34. Li N, Xia T, Nel A (2008) The Role of Oxidative Stress in Ambient Particulate Matter- induced Lung Diseases and Its Implications in the Toxicity of Engineered Nanoparticles. Free Radic Biol Med 44: 1689-1699.
35. Drake J, Link CD, Butterfield DA (2003) Oxidative stress precedes fibrillar deposition of Alzheimer's disease amyloid ??-peptide (1-42) in a transgenic *Caenorhabditis elegans* model. Neurobiol Aging 24: 415-420.
36. Christen Y (2000) Oxidative stress and Alzheimer disease 1, 2. 71.
37. Squier TC (2001) Oxidative stress and protein aggregation during biological aging. Exp Gerontol 36: 1539-1550.
38. Zhu X, Raina AK, Perry G, Smith M a. (2004) Alzheimer's disease: The two-hit hypothesis. Lancet Neurol 3: 219-226.
39. Chen Q, Ding Q, Keller JN (2005) The stationary phase model of aging in yeast for the study of oxidative stress and age-related neurodegeneration. Biogerontology 6: 1-13.
40. Yan HD, SS (2010) Mitochondrial permeability transition pore in Alzheimer's disease: Cyclophilin D and amyloid beta. Biochim Biophys Acta 1802: 198–204.

**Citation:** Girardello R, Drago F, de Eguileor M, Valvassori R, Vizioli J, et al. (2015) Cytokine Impregnated Biomatrix: A New Tool to Study Multi-Wall Carbon Nanotubes Effects on Invertebrate Immune Cells. J Nanomed Nanotechnol 6: 323. doi:10.4172/2157-7439.1000323